UNIVERSITÀ
DEGLI STUDI
DI PADOVA

DIPARTIMENTO DI SCIENZE MEDICO-DIAGNOSTICHE E TERAPIE SPECIALI

SCUOLA DI DOTTORATO DI RICERCA IN SCIENZE MEDICHE, CLINICHE E SPERIMENTALI

INDIRIZZO: SCIENZE CARDIOVASCOLARI

CICLO: 26°

Age- and Gender-specific Reference Values for Cardiac Chamber Geometry and Function Using Three-dimensional Echocardiography

Direttore della Scuola: Chiar.mo Prof. Gaetano Thiene

Coordinatore d'indirizzo: Chiar.mo Prof. Gaetano Thiene

Supervisore: Chiar.mo Prof. Sabino Iliceto

Dottorando: Dott. Luigi Paolo Badano

Publication: January 2014

Address for Correspondence:
Luigi P. Badano, MD, FESC, FACC
Dpt of Cardiac, Thoracic and Vascular Sciences, University of Padua
Via Giustiniani 2, 35128, Padua, Italy
Tel. +39 049 8218640
Fax +39 049 8211802
Mobile +39 329 8324847
E-mail lpbadano@gmail.com

INTRODUCTION

In order to diagnose any disease, a standard of reference is required. This standard is the state of health or normality. In clinical practice, because previous measurements from the same patients during health are rarely available, it is customary to compare the test results of patients who are supposed or known to have a disease with the test results of healthy persons who serve as the control or normal range.

Normative reference values for cardiac chamber anatomy and function are important for the accurate identification of xardiac chamber remodeling and/or dysfunction , risk stratification and selection of therapy. Three-dimensional echocardiography (3DE) allows accurate, unbiased measurement of cardiac chamber size and function without geometric assumptions regarding their shape. (1-3) It is widely available, cost-effective and does not expose patients to potentially harmful ionizing radiations, being ideal for serial assessment. Reference values for cardiac chamber geometry and function derived using two-dimensional echocardiography (2DE) may not be appropriate for values measured from 3DE data sets. (4,5) Age- and gender-appropriate reference values are particularly important for an earlier identification of cardiovascular diseases(6-8). Moreover, since 3DE is increasingly used in clinical practice to assess size and function of cardiac chambers, specific 3DE-derived reference values are desirable.

Using a series of clinical studies in healthy subjects, this research project aims to: (i) determine the normative values for left ventricular (LV, Chapter 5),(9) right ventricular (RV, chapter 6), (10) left atrial (LA, Chapter 7) and right atrial (RA, Chapter 8)(5) volumes and

function indexes using 3DE in a large cohort of healthy subjects; (ii) compare the cardiac chamber parameters measured by 3DE with the same values calculated using 2DE; (iii) analyze the effects of age, body size and gender on these parameters.

The experimental part of the thesis (Chapters 4-9) is preceeded by a general first part aiming to provide a comprehensive review about the concept of normality in medicine and the development of reference values (Chapter 1), the history and technological evolution of three-dimensional echocardiography (Chapter 2) and the description of current 3DE technology implemented in clinical and research practice to analyze cardiac chamber geometry and function (Chapter 3). Finally, study project limitations and its clinical implications are discussed in Chapter 9.

PART I

GENERAL SECTION

THE CONCEPT OF REFERENCE RANGES IN MEDICINE AND THE EVOLUTION OF THREE_DIMENSIONAL ECHOCARDIOGRAPHY

CHAPTER 1

The concept of normality in biology and medicine

1.1 Introduction

The main task of a cardiologist performing echocardiography is to aid in the investigation of patients by supplying quantitative information about the geometry and function of cardiac structures in the beating heart. However, isolated results are of scant interest. A meaningful evaluation requires comparison with other results concerning the same measurement (e.g. LV ejection fraction) from the same individual or from comparable individuals . Such values are usually called "*normal values*", but this term implies a state of normality, which is hopeless to define in an useful way, especially since the term "*normal*" is ambiguous in itself. (11)

1.2 Definition of "normality"

Inherent with the concept of "*normal range*" is the concept of "*normality*". The main issue with the concept of normality in clinical practice derives from the ambiguity among its medical connotation (where it is used as a synonim for "health"), its statistical connotation (where it is used as a synonim for "Gaussian distribution"), and its popular connotation (where it is used as a synonim for "ideal, usual or conventional").

The term "health" is said to be the "*state of being hale, sound , or whole, in body, mind, or soul; especially the state of being free from physical disease or pain*" (*Merriam-Webster Online Dictionary*, http://www.webster-dictionary.org/definition/health). By using this definition, a person who is in good health may indulge in physical and mental activities without distress , and he/she is

free from diseases that may threaten his or her well-being or life. Similarly, the orthodox medical definition of normal "*denotes the absence of infection, disease, or malformation , or the absence of experimental or therapeutic manipulations*" (Webster's New International Dictionary of the English Language, second edition, unabridged, 1960). However, considering the term "normal" as a synonim of "health" implies that every value which falls outside the "normal range" for that measurement will be automatically labeled as "disease". This concept is obviously unacceptable in clinical practice

Conventionally, a value/measurement compatible with health is called "normal", a term that has led to confusion because of its biological and statistical uses. We cannot consider as "normal" only those measurements which follow a Gaussian distribution (i.e. distribute them in a nicely symmetrical, bell shaped curve around the mean value, presumably the true value) simply because measurements between "normal" individuals do not regularly follow a normal or Gaussian distribution pattern. (12) Application of statistics of normal distribution in such istances can lead to absurd conclusions. For example, Kaku et al. (13), examined LV geometry and function with three-dimensional echocardiography (3DE) a large cohort of normal subjects and in the age group 1-19 years the lower normal limits (mean value – 2 standard deviations) of the LV stroke volume was 2 ml and 6 ml in males and females, respectively.

In the early days of the 19th centrury, the German mathematician, physicist and astronomer Johann Carl F. Gauss , proposed the "law of errors". This law states that if repeated measures are made on the same physical object, the distribution of the random component of the errors can be well approximated by the Gaussian, or normal, distribution. This law implies that repeated measurements of the length of the same stick would follow the normal distribution; but the law certainly does not imply that measurements of the lengths of all the sticks to be found in a walking stick store will follow the same normal distribution.

Even today, many scientists are strongly convinced that if a sample is large enough, the distribution will be "normal" regardless of the measurement under study, and that 95% of the measurements will be included in mean value ± 2 standard deviations (SD). A famous quotations says "*Everybody believes in the law of errors, the experimenters because they think it is a mathematical theorem and the mathematicians because they think it is an experimental fact*". (14) There is a mathematical theorem, but, as already stated, it refers to the random component of the errors made in repeated measurements of the same object. The experimental fact is that for most physiologic variables the distribution is smooth, unimodal and skewed, and that "mean value ± 2 standard deviations" does not cut off the desired central 95%.

Often, "*normal*" has been used as a synonim for "ideal". Homer Smith H. (15) suggested that this confusion between normal and ideal originated with Plato and Platonic idealism, with its strong sense of the absolute: "*The Ideal Circle is not inherent in the substantive circle which we draw, but in the mind; but not in my mind or yours, or of any particular man, for particular men come and go; since the Ideal Circle endures everywhere and forever, it must be inherent in some universal unchanging mind which can only be the mind of God… The Ideal Billygoat existed in the divine mind before the first actual billygoat was, or smelled, and will continue to exist and smell when the last actual billygoat , imperfect in form and odor, has ceased to be*". In this quotation there are similarities with our frequently unquestioning, nearly mystic, respect for the "normal range" in this kind of idealism (e.g. the use of cardiac troponin in the screening of patients with acute chest pain). Normal ranges, no matter how imperfectly derived, attain through long use a patina of authority making them descriptive of a mystical ideal.

The logical fallacy of confusing the "normal" with "ideal" is that "ideal persons" are theoretical beings, the mathematical combination of all ideal or perfect human attributes,

"*existing only in the mind of God*". If our normal ranges were truly representative of such ideal persons, we would find "abnormalities" in every individual patient we examine. It is quite obvious that clinical "normal ranges" can not be based on such concepts and it is likewise logical that we do not want to use reference standards of this preciseness, similar to National Bureau of Standards reference standards of weight and measure.

1.3 The concept of reference values

Difficulty in defining "normality" in medicine has led some scientists to propos to abandon the terms "normal values and normal ranges" to adopt the more realistic terms "reference values/ranges". The concept of reference values was introduced in 1969 by Grasbeck and Saris to describe fluctuation of blood analyte concentrations in well-characterized groups of individuals. (16) Reference values, first introduced as a philosophy, have gained universal acceptance as one of the most powerful tools in laboratory medicine and clinical testing to aid in the clinical decision making process.

The change from "normal values" to "reference values" is not just a semantic issue not related to the establishment of the scientific bases to interpret quantitative data obtained by the diagnostic modalities. Looking at the definition of reference values/ranges (e.g. ranges of values which include a series of quantitative measurements of a certain parameter obtained either from a single individual or from cohorts of individuals who fulfill well-defined inclusion and exclusion criteria. Inclusion and exclusion criteria should be available for others who would like to use the same reference ranges. Several reference sample groups will be available for each measured parameter in order to take into account the effects of age, gender, body size, etc.) it is clear that this concept is more realistic and closer to the clinical practice than the concept of "normal values".

The concept of reference ranges imply that: (i). "*Absolute health*" as it has been outlined in the World Health Organization Consitution ("*a state of complete physical, mental and social well-being and not merely the absence of disease or infirmity*") does not exist. (17) Some

element of structural or functional, somatic, psychic or social "pathology" (however defined) is probably present in everyone (just like entropy is a characteristic of any thermodynamic system). Therefore, when reference values are derived from a population of heathy subjects, the level of "health" of enrolled subjects should be defined according to clear inclusion and exclusion criteria; (ii) Since health may be conceptually different in different countries, in the same country at different times, and in the same individual at different ages, reference values are not absolute but they change according to the population being examined; (iii) reference values cannot be obtained retrospectively from cohorts of patients who underwent the clinical test/measurement of what we want to define the reference values for clinical reasons and have subsequently been found normal on the basis of previous reference values. Conversely, the *reference population* from which the reference values will be obtained should be enrolled prospectively according to well *a-priori* defined inclusion and exclusion criteria.

The function of the normal range is to provide a base line for the interpretation of test results by the physician. Since health is the only possible base line to determine the alterations produced by disease, it follows that the normal range first should be established on healthy subjects. Ideally, the best way to establish reference values would be to obtain several measurements of the parameter to be tested while the subject under examination was healthy and to use the results as a comparison when a disease is suspected. This will eliminate the inter-individual variability of measurements which is always significantly higher than the intra-individual variability. However, this approach (*subject-based* reference values) is only rarely available in clinical practice (e.g. measurement of LV ejection fraction before chemotherapy) and reference values are usually obtained from measurements performed on large cohorts of healthy subjects from which the upper and lower reference limits are calculated (e.g. an interval of the distribution of measurements comprising the central 95% of them) . However, the inference that these values actually represent 95% of the reference

measurements is based on three assumptions: (i). The cohort is large enough that the degree of freedom can be ignored; (ii). The selection of the cohort has been adequate to be representative of the population from which our patients come; (iii). The distribution of measurements is normal (Gaussian).

CHAPTER 2

The evolution of three-dimensional echocardiography

2.1 Introduction

Since the early days of cardiovascular imaging, the concept of 3D imaging was indisputably perceived as a need based on the recognition that depicting the complex shape of the cardiovascular system in less than three dimensions severely limited the diagnostic value of the information obtained from medical imaging. During the last half of the twentieth century, we have witnessed an impressive technological progress driven by strong demand from the cardiology community that moved from fuzzy single-projection X-ray films to multi-slices high spatial resolution tomographic images depicting anatomical details previously seen only in anatomy atlases. The possibility to visualize these details in living patients changed completely the way cardiologists understand disease processes and resulted in new standards in the diagnosis of diseases and patients' management. Currently, the diagnosis of most cardiovascular disease states heavily relies on information obtained by noninvasive imaging.

However, 3D imaging of the beating heart remained a challenge because of its constant motion. While 3D imaging of stationary organs was conceptually easy to solve by collecting information from different parts or from different angles consecutively, imaging of the beating heart required data collection to occur virtually in real time. This was a real challenge for

engineers and physicists. In fact, it can be read in textbooks from the early 1970's explanations why real-time two-dimensional (2D) imaging of the beating heart is an enormous technological advancement that is unsurpasssable because of the limitations imposed by the constant speed at which ultrasound waves travel inside the human body.

Neverteless, despite the fact that the speed of sound has not changed since then, the combination of the exponential rise of computational power of computers with ingenious engineering solutions that increased the efficiency of the process of image formation from ultrasound reflections has meant that, during the last decade, 3DE has completed its transition from a predominant research tool to an imaging technique employed in everyday clinical practice. (1,2,18)

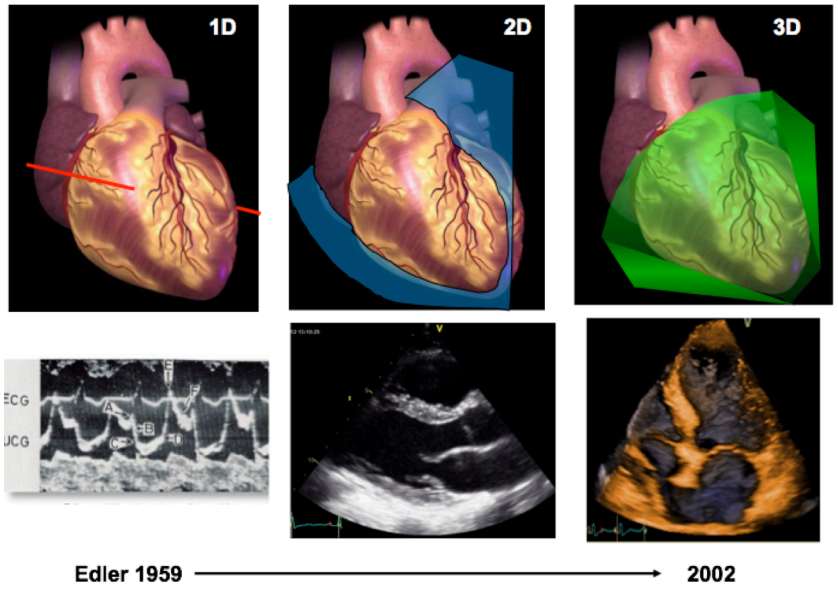

Figure 2.1. Progress in ultrasound technology. From the early M-mode (1D), when one single ultrasound beam produced a time-depth display of cardiac structures, through two-dimensional echocardiography (2D), when a real-time tomographic display of the beating heart was made available, to current three-dimensional technology (3D), with which a real-time pyramidal acquisition of data is available.

This transition began in 2002 with the release of a reasonable user-friendly version of a matrix array transducer capable of real-time 3D imaging together with software which allows rapid slicing and quantification of 3DE data sets.

Before these technological achievements, attempts to develop 3DE imaging had relied in using a 2DE transducer (either tracking it in space or moving it in a prespecified pattern) to acquire multiple 2D views. This required spatial information about the ultrasound probe itself with the aid of cardiac and, in some technological solutions, respiratory gating to be assembled into a 3D reconstructed image using dedicated software. The ultrasound probe has been tracked via a variety of means either extrinsic and intrinsic to the probe. More recent systems obviate the need for these spatial tracking methods. In the following paragraphs, I will review the evolution of 3DE and describe the milestones this technology has gone through on its way to its current technological evolution.

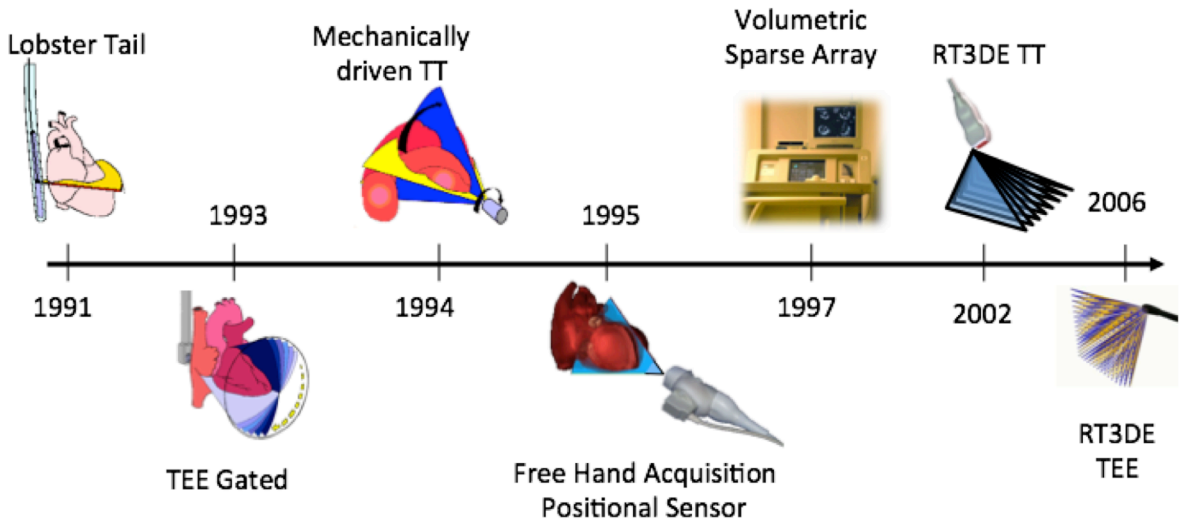

Figure 2.2. **Temporal evolution of three-dimensional echocardiography technology** (see text for details). Abbreviations: RT3DE, real-time three-dimensional echocardiography; TEE, transesophageal; TT, transthoracic.

2.2 Extrinsic tracking ("positional" and "free-hand" scanning)

The first attempt in imaging the human heart in 3D by ultrasound was made by Dekker et al.(19) in 1974, who used a mechanical articulated arm that measured probe displacement during the acquisition of multiple 2DE views to perform freehand transthoracic scanning. This marked the birth of static surface rendering, the earliest 3D echocardiographic technique.

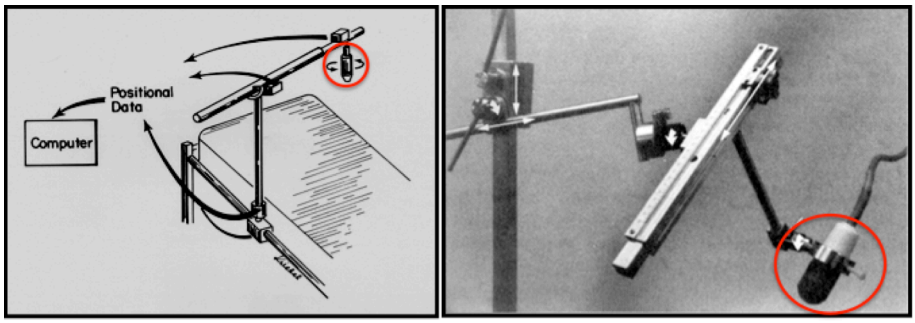

Figure 2.3. **The mechanical arm**. Schematic drawing of the scanning bed and the device (*left panel*) and actual picture of the arm with the probe (*right panel*). A large external beam device gives spatial data regarding an ultrasound probe to enable three-dimensional reconstruction. The ultrasound probe is highlighted by a red circle.

This work demonstrated the possibility of producing a 3D data set, but the technology was impractical for clinical use.

Trying to improve the tracking method, Moritz and Shreve(20) developed an acoustic locator (the so.called "spark-gap) whereby an acoustic element was attached to the ultrasoud probe and sent regular audio pulses that were detected by a fixed antenna to be included in a Cartesian locator grid.

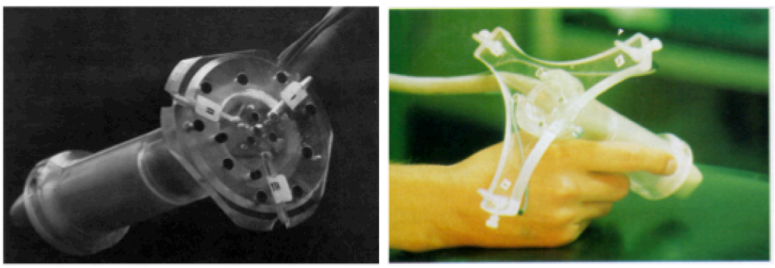

Figure 2.4. **Acoustic locators or "spark-gaps"**. The ultrasound probe position is tracked by a means similar to radar technology.

In 1977, Raab et al. (21) reported about an electromagnetic sensor which could be attached to the ultrasound probe allowing continuous monitoring of its position in space. Although this technique was quite advanced for 1977, it was not used systematically until the mid 1990s (Figure 2.5). Several other Authors published early attempts to produce 3DE data sets during this time period. (22-24) Further development of these techniques led to what has been termed "*free-hand scanning*". With this modality, a highly developed magnetic-field system orients sequentially acquired 2DE imaging planes by tracking the movement of the ultrasound probe as it is manipulated by the operator.

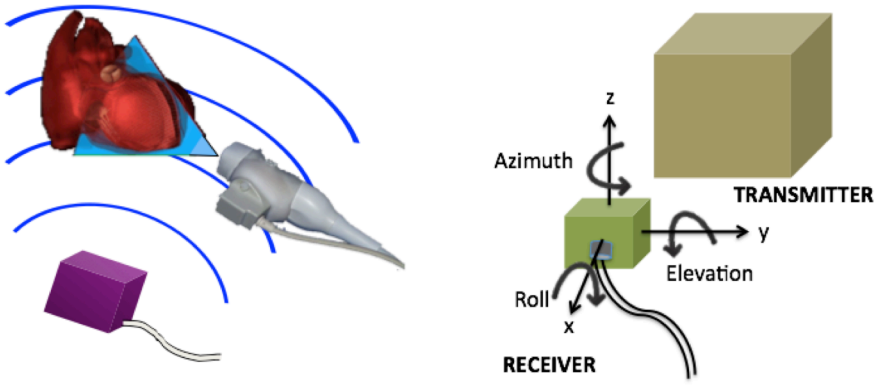

Figure 2.5. Freehand scanning. A modified ultrasound probe is tracked in 3D space using an electromagnetic locator system (*left panel*). Schematic drawing of the receiver and transmitting device and the Cartesian coordinate system for tracking the location of the trasnducer (*right panel*). Images then may be reconstructed off-line to create 3D data sets.

2.3 Gated sequential acquisition

One crucial developmental aspect for the success of 3D reconstruction from multiplane acquisition was the registration of the different planes, so that they could be combined together to create a 3D image of the heart. This was achieved by sequential gated acquisition, wherein different cut planes were acquired one-by-one with gating designed to minimize artifacts. To minimize spatial misalignment of slices because of respiration, respiratory gating was used, such that only cardiac cycles coinciding with a certain phase of the respiratory cycle were captured. Similarly, to minimize temporal misalignment because of heart rate variability, ECG gating was used, such that only cardiac cycles within preset limits of R-R

interval were included. This methodology became standard in both transthoracic and transesophageal multiplane imaging aimed at 3D reconstruction and was widely used until real-time 3D imaging became possible.

To achieve effective multiplane acquisition, new techniques were developed that operated under the assumption that both the patient and the housing of the ultrasound probe remained in a relatively fixed position. The ultrasound probe was held by a device that moved the probe in a specified, preprogrammed fashion within the housing of a mechanical device. Examples were linear, fan-like and rotational acquisition methods.

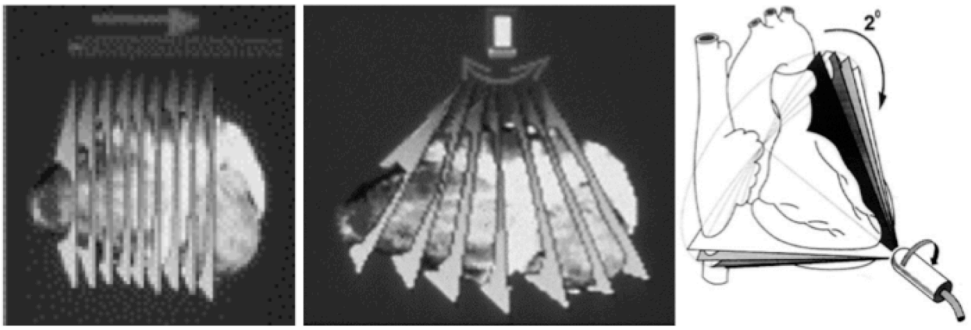

Figure 2.6. Gated sequential imaging. Transducer motion modalities to generate 3DE images using gated sequential imaging. **Linear** (*left panel*): multiple parallel equi-distantly spaced 2D images can be obtained by progressive computer-controlled linear motion of the transducer in prespecified depths. **Fan-like** (*central panel*): multiple two-dimensional images are obtained in a fan-like array by tilting the transducer in specified arc angles to create a pyramidal data set. **Rotational** (*right panel*): multiple two-dimensional images are obtained by rotating the transducer 180° and obtaining images at pedetermined intervals (e.g. every 3° or 6°) to create a conical data set.

In the early 1990s, the use of linear step-by-step motion acquisition, wherein the transducer was mechanically advanced between acquisitions using a motorized driving device become commercially available. (25)

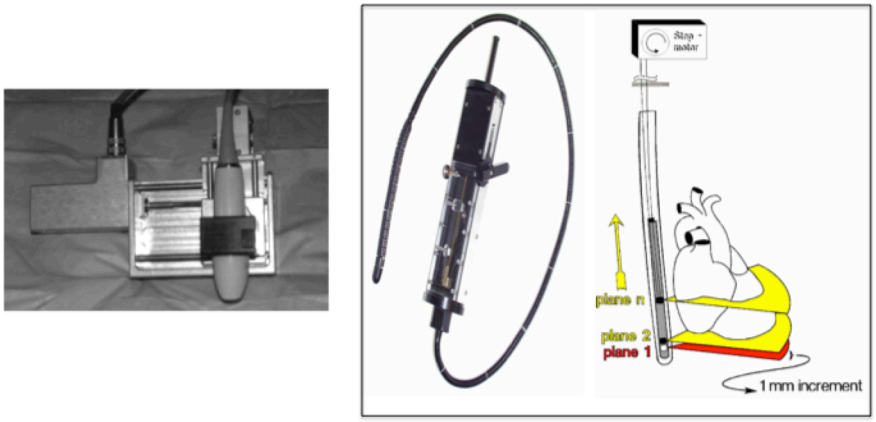

Figure 2.7. Motorized linear-motion device used to acquire parallel cut planes for reconstructing 3D images using linear step-by-step transducer motion (*left panel*). Pull back transoesophageal probe that employed the same approach of linear motion (*right panel*)

However, this simple solution was not applicable for transthoracic echocardiography, because of the need to find intercostal acoustic windows for each acquisition step. This approach was implemented in a pull-back transesophageal echocardiography transducer, known as "lobster tail" probe (Figure 2.7, *Right panel*). In the handle of the transducer there was a motorized unit that incrementally pulled crystals in a parallel fashion at 1 mm increments gated to electrocardiogram (ECG) and respiration. The first transesophageal 3DE study was performed in the early 90's using this device. (26)

2.3.1 Transoesophageal rotational imaging

An alternative approach to linear scanning was to keep the transducer in a fixed position corresponding to an optimal acoustic window, and rotate the imaging plane by internally steering the imaging element in different direction This concept of rotational scanning in combination with gated sequential scanning was implemented into transoesophageal technology and resulted in a probe that has subsequently become the main source of multiplane images used for 3D reconstruction, both for research and clinical practice. (27,28)

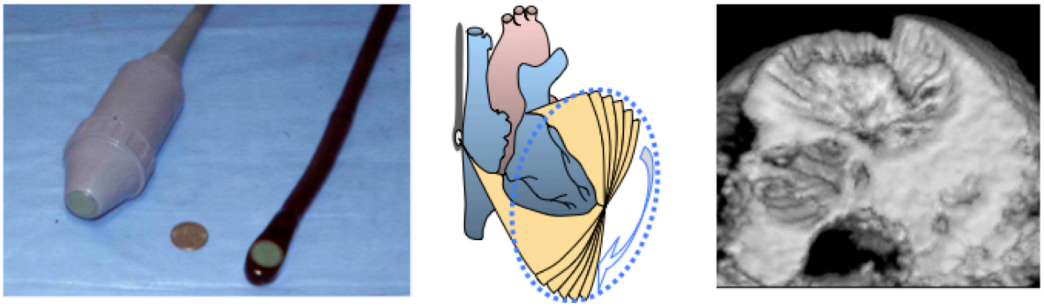

Figure 2.8. Rotational approach implemented into a transoesophageal multiplane transducer (*left panel*). Schematic drawing of sequential ultrasound images obtained by progressive rotation of the transducer in a prespecified fashion (*central panel*). Example of a 3D image of the mitral valve with anterior leaflet prolapse from multiplane images acquired using this transducer (*right panel*)

This approach provided 3D reconstructions of reasonably good quality due to the high quality of the original 2D images and the fact that the transoesophageal probe is relatively well "anchored" in its position throughout image acquisition, especially in sedated patients. Nevertheless, cardiac structures, such as valve leaflets appeared jagged as a result of stitch artifacts (Figure 2.8, *right panel*), reflecting the contributions of individual imaging planes that could not be perfectly aligned during reconstruction, despite the ECG and respiratory gating. Multiple studies demonstrated the clinical usefulness of this approach mostly in the context of the evaluation of valvular heart disease.

2.3.2 Transthoracic rotational imaging

An early transthoracic implementation of rotational approach consisted of a motorized device that contained a conventional transducer, which was mechanically rotated several degrees at a time, resulting in first transthoracic gated sequential multiplane acquisitions suitable for 3D reconstruction of the heart. (29-31)

Figure 2.9. Motorized device that housed an external stepper motor that mechanically rotated a built-in transthoracic transducer.

Despite the previously unseen transthoracic 3DE images that excited so many, it quickly became clear that this methodology was destined to remain limited to the research arena because image acquisition was too time-consuming and tedious for clinical use. In addition, the quality of the reconstructed images was limited.

With each of these methods, once the numerous 2D "planes" have been obtained according to prescribed transducer movements, the images had to be realigned and digitally reformatted into rectangular pixels that were then stacked. Gaps between adjacent images were filled by interpolation. A cubic volume of "voxels" was then derived from the stacked images that could then be volume rendered or "sliced" in any plane of interest.

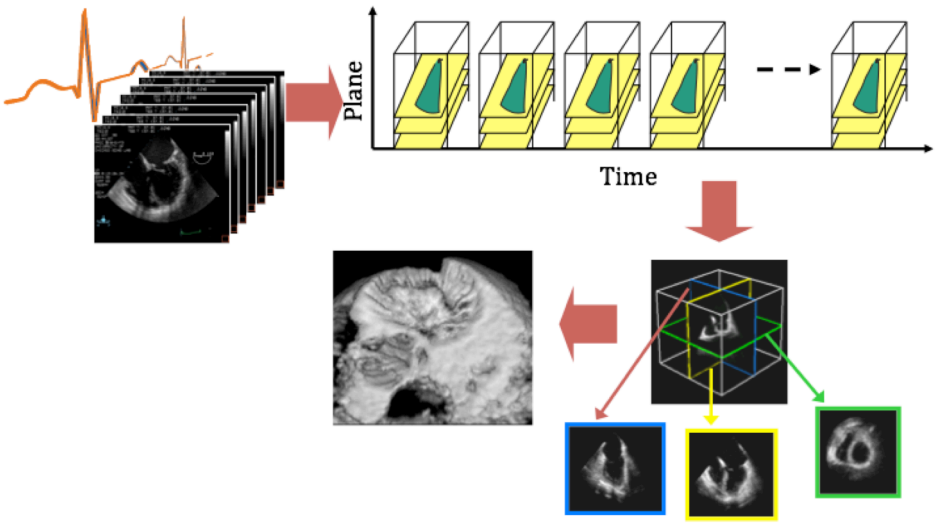

Figure 2.10. Reconstruction of a 3D data set from multiple 2D images. The collection of images (typically 15 to 60 cardiac cycles, with 10 to 15 frames/heart beat) were re-sampled in a cubical data set and ultimately rendered into a 3D image or sliced according to planes of interest

A profound limitation to each of these techniques was that they fundamentally relied on the acquisition of multiple 2D images. Image quality was therefore highly dependent on concordance between adjacent images. The inherent need to interpolate data became problematic if the adjacent images were themselves discordant due to voluntary or involuntary patient movement. Problems inherent to irregular heart rate and lung artifact were minimized by using cardiac and respiratory gating to prespecified heart rates and

phases of the respiratory cycle. Images were therefore acquired over a varying period of time, often up to 2 to 3 minutes, and even longer in the presence of atrial fibrillation. This was because, from a practical standpoint, the image mismatch was too profound if the R-R gating was set to vary by more than roughly 150 msec. If a patient with atrial fibrillation was gated at 150-msec variation, the acquisition could take up to 10 minutes. In this setting, it was unlikely that either the patient or the physician obtaining the data could remain stationary for this length of time. Actually, to obtain a satisfactory 3D reconstruction with this technology, it was required a very skilled operator, a very cooperative patient, an operatorr skilled with 3D reconstruction and a bit of luck. If succesful, although image quality was suboptimal for small discrete structure like valve morphology analysis, even at this time, data sets were useful for ventricular volume assessment.

However, the presence of the locator device, which, limited significantly the portability of the ultrasound system, the need of avoiding any metallic close to the system and the patient, the long reconstrunction times and the unpredictability of the final results have further hindered more widespread use of this technique in clinical practice.

2.4 Early transthoracic real-time 3D imaging

The collective experience and the limitations of the gated sequential acquisition and offline 3D reconstruction gradually led developers to the understanding that scanning volumes rather than isolated cut planes would intrinsically address many of the previous issues. This revolutionary idea led von Ramm et al.(32,33) to develop the first real-time 3DE system at Duke university. This system was equipped with a phased-array transducer, in which piezoelectric elements were arranged in multiple rows, rather than one row, allowing fast sequential scanning of multiple planes. The phased array technology, that has been an integral part of the 2D transducers for decades, was modified to electronically change the direction of the beam not only within a single plane to create a fan-shaped scan, but also in the

lateral direction to generate a series of such scans. Importantly this was achieved without any mechanical motion, allowing the speeds necessary for volumetric real-time imaging.

The first generation of real-time 3D transducers was bulky due to unprecedented number of electrical connections to the individual crystals, despite the relatively small number of elements in each row. This sparse array matrix transducer consisted of 256 non-simultaneously firing elements and had large footprint, which did not allow good coupling with the chest wall for optimal acoustic windows, and produced 3D images that were suboptimal in any selected plane, when compared to the quality of standard at the time 2D echocardiographic images. Nevertheless, the mere fact of successful real-time 3D imaging of an entire volume of heart using one cardiac cycle was a huge technological breakthrough.

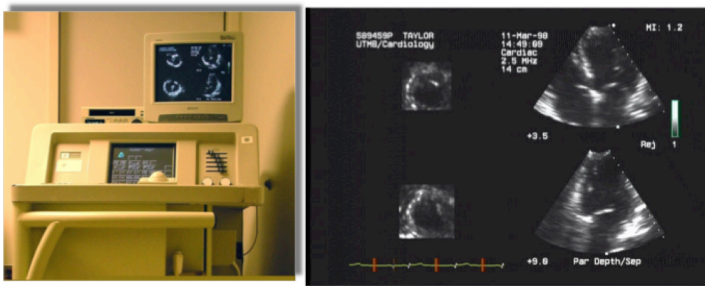

Figure 2.11. The first real-time 3D echocardiography system (C-scan, Volumetrics, Inc) equipped with a sparse matrix array transducer (*left panel*). In the right panel the images which can be obtained with that system are shown: apical views of the heart on the right (4-chamber on top, and 2-chamber of the left ventricle on the bottom), and short axis, or C scans, of the LV derived from perpendicular cuts through the apical views on the left.

This represented a major transition from the thin slice sector imaging obtainable with 2DE. Despite volumetric acquisition was a very positive development, the images were displayed as 2D (Figure 2.11). The 2D images were derived from the 3D data set but were displayed as 2D orthogonal cut planes.

However, the road was paved and in November 2002, at the time of the American Heart Association meeting, Philips released the first generation of real-time 3DE.

CHAPTER 3

Current three-dimensional echocardiography technology

3.1 Introduction

The milestone in the development of current 3DE technology has been the development of fully-sampled matrix array transthoracic transducers based on advanced digital processing and improved image formation algorithms which allowed the operators to obtain on cart transthoracic real-time volumetric imaging with short acquisition time, high spatial and temporal resolution. Further technological developments (i.e. advances in miniaturization of the electronics and in element interconnection technology) made possible to insert a full matrix array into the tip of a transoesophageal probe and provide transoesophageal real-time volumetric imaging.

In addition to transducer engineering, improved computer processing power and the availability of dedicated software packages for both on- and off-line analysis have allowed 3DE to become a practical clinical tool.

3.2 Comparison between 2DE and 3DE ultrasound transducers

The backbone of the 3DE technology is the transducer. (34) A conventional 2DE phased array transducer is composed by 128 piezoelectric elements, electrically isolated from each other, arranged in a single row.

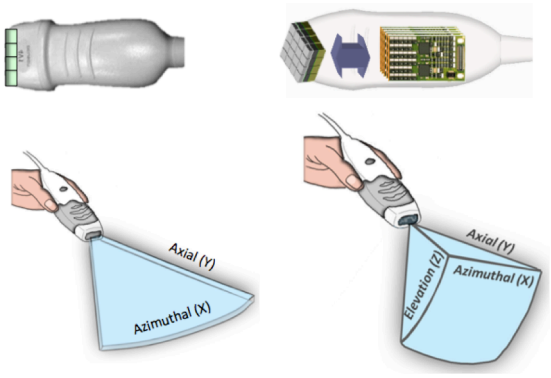

Figure 3.1. Two- and three-dimensional transducers. Schematic drawing showing the differences between a two- (*left panel*) and a three-dimensional (*right panel*) transducer

Each ultrasound wave front is generated by firing individual elements in a specific sequence with a delay in phase with respect to the transmit initiation time. Each element adds and subtracts pulses to generate a single ultrasound wave with a specific direction that constitutes a radially propagating scan line.

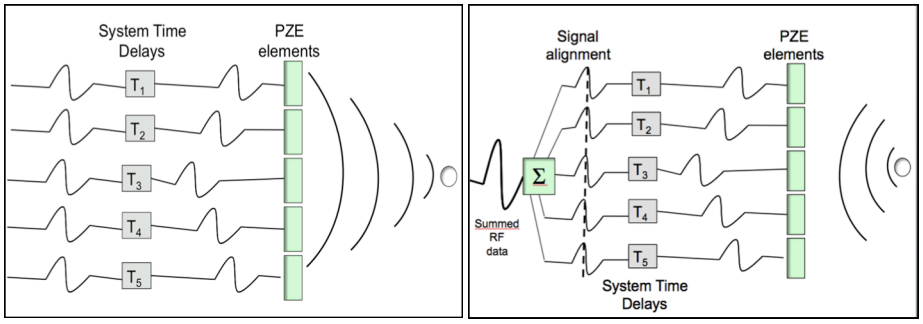

Figure 3.2. **Two-dimensional beamforming**. Schematic drawing of beamforming using a conventional 2DE phased array transducer. During transmission (*left panel*), focused beams of ultrasound are produced by pulsing each piezoelectric element with pre-calculated time delays (i.e. phasing). During reception (*right panel*), focusing is achieved by applying selective delays at echo signals received by the different piezoelectric elements in order to create isophase signals that will be summed in a coherent way.

Since the piezoelectric elements area arranged in a single row, the ultrasound beam can be steered in two dimensions - vertical (axial) and lateral (azimuthal) - while resolution in the z axis (elevation) is fixed by the thickness of the tomographic slice (Figure 3.2, left panel), which, in turn, is related to the vertical dimension of piezoelectric elements.

Currently, 3DE matrix-array transducers are composed of about 3000 individually

connected and simultaneously active (fully sampled) piezoelectric elements with operating frequencies ranging from 2 to 4 MHz and 5 to 7 MHz for transthoracic and transoesophageal transducers, respectively. To steer the ultrasound beam in 3D, a 3D array of piezoelectric elements needs to be used in the probe, therefore piezoelectric elements are arranged in rows and columns to form of a rectangular grid (matrix configuration) within the transducer (Figure 3.2, right panel). The electronically controlled phasic firing of the elements in that matrix generates a scan line that propagates radially (y or axial direction) and can be steered both laterally (x or azimuthal direction) and in elevation (z direction) in order to acquire a volumetric pyramid of data (Figure 3.2, right panel). Matrix array probes can also provide real-time multiple simultaneous 2D views, at high frame rate, oriented in predefined or user-selected plane orientations.

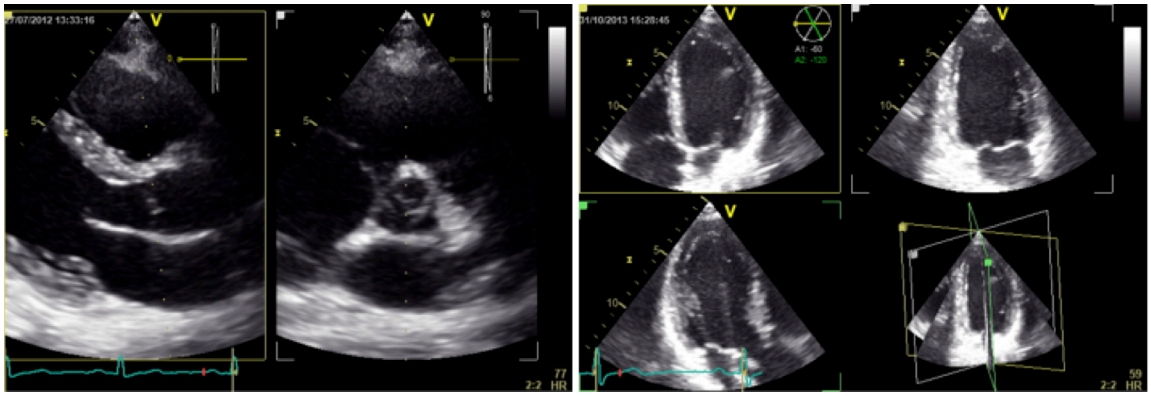

Figure 3.3. **Multiplane acquisition using the matrix array transducer**. Bi-plane acquisition showing a parasternal long-axis view (reference view) and a simultaneous short axis view taken at the level of the dotted yellow line on the reference view (*left panel*). Tri-plane acquisition (*right panel*) showing simultaneously a 4- (left upper corner), 2-camber (right upper corner) views and an apical long-axis view (left lower corner). The angles of the 2-chamber and the long-axis views are adjustable during the acquisition to optimize the views.

The main technological breakthrough which allowed manufacturers to develop fully sampled matrix transducers has been the miniaturization of electronics that allowed the development of individual electrical interconnections for every piezoelectric element which could be independently controlled, both in transmission and in reception.

Beamforming is a technique used to process signals in order to produce directionally or

spatially selected signals sent or received from arrays of sensors. In 2DE, all the electronic components for the beamforming (high-voltage transmitters, low-noise receivers, analog-to-digital converter, digital controllers, digital delay lines) are in the system and consume a lot of power (around 100W and 1,500 cm^2 of personal computer electronics board area). If the same beamforming approach would have been used for matrix array transducers used in 3DE, it would require around 4kW power consumption and a huge PC board area to accommodate all the needed electronics. To reduce both power consumption and the size of the connecting cable, several miniaturized circuit boards are incorporated into the transducer, allowing partial beamforming to be performed in the probe.

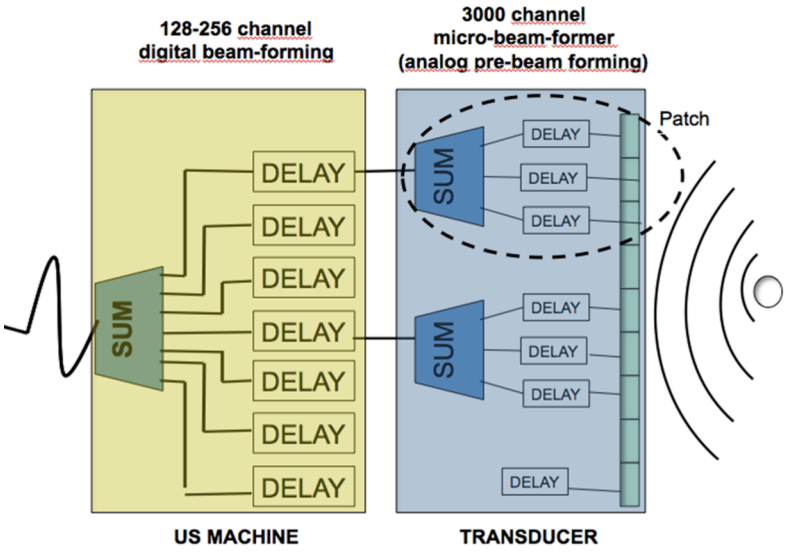

Figure 3.4. **Three-dimensional beamforming**. Beamforming with 3D matrix array transducers has been splitted in two: the transducer and the ultrasound machine levels. At the transducer level, interconnection technology and integrated analog circuits (DELAY) control transmit and receive signals using different subsection of the matrix (patches) to perform analog pre-beamforming and fine steering. Signals from each patch are summed to reduce the number of digital lines in the coaxial cable that connects the transducer to the ultrasound system from 3000 to the conventional 128-256 channels. At the ultrasound machine level, analog-to-digital (A/D) convertors amplify, filter and digitize the elements signals which are then focused (coarse steering) using digital delay (DELAY) circuitry and summed together (SUM) to form the received signal from a desired object.

This unique circuit design results in an active probe which allows microbeamforming of the signal with low power consumption (<1 W) and avoids to connect every piezoelectric element to the ultrasound machine. The 3000 channel circuit boards within the transducer

control the fine steering by delaying and summing signals within subsections of the matrix, known as patches (Figure 3.4). This microbeamforming allows to reduce the number of the digital channels to be put into the cable that connects the probe to the ultrasound system from 3000 (which would make the cabling too heavy for practical use) to the conventional 128-256 allowing the same size of the 2D cable to be used with 3D probes. Coarse steering is controlled by the ultrasound system where the analog-to-digital conversion occurs using digital delay lines (Figure 3.4).

However, the electronics inside the probe produce heat whose amount is directly proportional to mechanical index used during imaging, therefore the engineering of active 3DE transducer should include thermal management.

Finally, new and advanced crystal manufacturing processes allows production of single crystal materials with homogeneous solid state technology and unique piezoelectric properties. These new transducers result in reduced heating production by increasing the efficiency of the transduction process which improves the conversion of transmit power into ultrasound energy and of received ultrasound energy into electrical power. Increased efficiency of the transduction process together with a wider bandwidth result in increased ultrasound penetration and resolution which improve image quality with the additional benefits of reducing artifacts, lowering power consumption and increase Doppler sensitivity.

Further developments in transducer technology have resulted in a reduced transducer footprint, improved side-lobe suppression, increased sensitivity and penetration, and the implementation of harmonic capabilities that can be used for both gray-scale and contrast imaging. The last generation of matrix transducers are significantly smaller than the previous ones and the quality of 2D and 3D imaging has improved significantly, allowing a single transducer to acquire both 2D and 3DE studies, as well as of acquiring the whole LV cavity in a single beat.

3.2 Three-dimensional echocardiography physics

3DE is an ultrasound technique and the physical limitation of the constant speed of ultrasounds in human body tissues (approximately 1,540 m/s in myocardial tissue and blood) cannot be overcome. The speed of sound in human tissues divided by the distance a single pulse has to travel forth and back (determined by the image depth) results in the maximum number of pulses that can be fired each second without producing interferences. Based on the acquired pyramidal angular width and the desired beam spacing in each dimension (spatial resolution), this number is related to the volumes per second that can be imaged (temporal resolution). Therefore, similar to 2DE imaging, in 3DE imaging there is an inverse relationship between volume rate (temporal resolution), acquisition volume size and the number of scan lines (spatial resolution). Any increase in one of these factors will cause a decrease in the other two.

The relation between volume rate, number of parallel receive beams, sector width, depth, and line density can be described by the following equation:

$$\text{Volume rate} = \frac{1{,}540 \times \text{No. of parallel received beams}}{2 \times \text{Volume width}^2 \times \text{Lateral resolution}^2 \times \text{Volume depth}}$$

therefore the volume rate can be adjusted to the specific needs by either changing the volume width or depth. The 3D system allows the user to control the lateral resolution by changing the density of the scan lines in the pyramidal sector too. However, a decrease in spatial resolution also affects the contrast of the image. Volume rate can also be increased by increasing the number of parallel receive beams, but in this way the signal-to-noise ratio and the image quality will be affected.

To put all this in perspective let us assume that we want to image up to 16 cm depth in the body and acquire a 60° x 60° degrees pyramidal volume. Since the speed of sound is

approximately 1540 m/s and each pulse has to propagate 16 cm x 2 (to go forth and come back to the transducer), 1540/0.32= 4812 pulses may be fired per second without getting interference between the pulses. Assuming that 1° beam spacing in both X and Z dimension is a sufficient spatial resolution we would need 3600 beams (60 x 60) to spatially resolve the 60° x 60° pyramidal volume. As a result we will get a temporal resolution (volume rate) of 4812/3600= 1.3 Hz, which is practically useless in clinical echocardiography.

The example above shows how the fixed speed of sound in body tissues has been a major challenge to the development of 3DE imaging. Manufacturers have developed several techniques such as parallel receive beamforming, multibeat imaging and real-time zoom acquisition to cope with this challenge but in practice this is usually achieved by selecting the appropriate acquisition modality for different imaging purposes (see sub-chapter 3.4 Image acquisition and display).

Parallel receive beamforming or multiline acquisition is a technique where the system transmits one wide beam and receives multiple narrow beams in parallel. In this way the volume rate (temporal resolution) is increased by a factor equal to the number of the received beams. Each beamformer focuses along a slightly different direction that was insonated by the broad transmit pulse. As an example, to obtain a 90° x 90°, 16-cm depth pyramidal volume at 25 vps, the system needs to receive 200,000 lines/s. Since the emission rate is around 5000 pulsed/s, the system should receive 42 beams in parallel for each emitted pulse. However, increasing the number of parallel beams to increase temporal resolution leads to an increase in size, costs and power consumption of the beamforming electronics, and deterioration in the signal-to-noise ratio and contrast resolution. With this technique of processing the received data, multiple scan lines can be sampled in the amount of time a conventional scanner would take for a single line, at the expense of reduced signal strength and resolution, as the receive beam are steered farther and farther away from the center of the transmit beam.

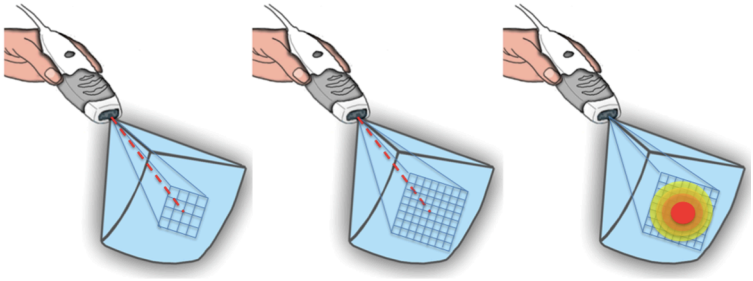

Figure 3.5. Parallel receive beamforming. Schematic representation of the parallel receive or multiline beamforming technique receiving 16 (left panel) or 64 (central panel) beams for each transmit pulse (dashed red line). The right panel shows the degradation of the power and resolution of the signal (from red maximal to bright yellow minimal) from the parallel receiving beams steered farther away from the center of the transmit beam.

Another technique to increase the size of the pyramidal volume and maintain the volume rate (or the reverse, e.g. maintain volume rate and increase the pyramidal volume) is the multibeat acquisition. With this technique, a number of ECG-gated subvolumes acquired from consecutive cardiac cycles are stitched together to build up the final pyramidal volume.

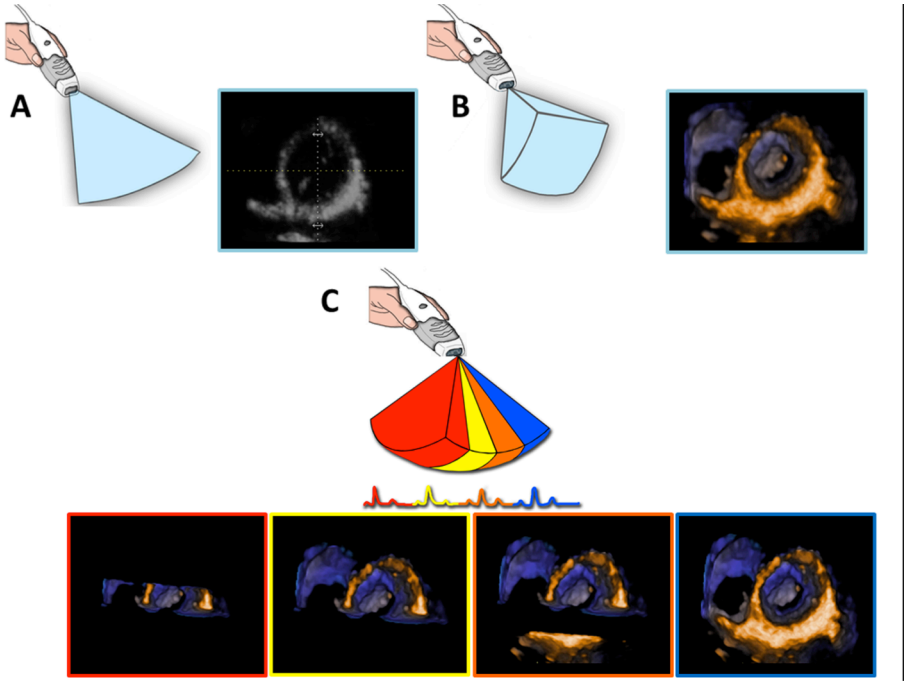

Figure 3.6. Multibeat acquisition. Two- (panel A) and three-dimensional volume rendered (panel B) imaging of the mitral valve from the ventricular perspective. The latter has been obtained from a 4-beat full-volume acquisition illustrated in panel C. The 4 pyramidal subvolumes (the colors show the relationships between the pyramidal subvolumes, the ECG beats and the way the 3D data set has been built up in the lower part of the figure.

Multibeat acquisition will be effective only if the different subvolumes will be constant in position and size, therefore any transducer movement, cardiac translation motion due to respiration, change in cardiac cycle length will create subvolume malalignment and stitching artifacts.

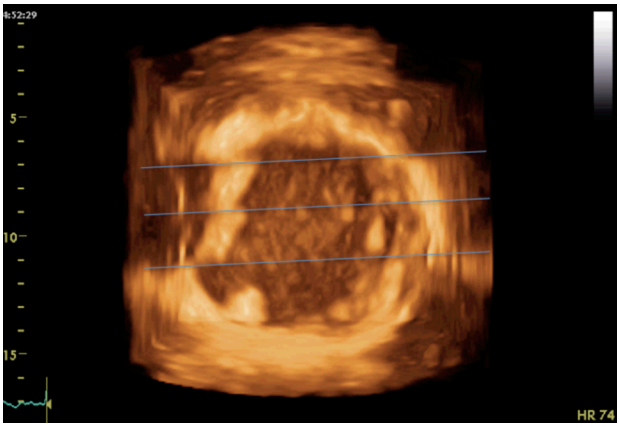

Figure 3.7. Stitching artifacts. Volume-rendered image displayed with respiratory gating artifacts. The blue lines highlight the misalignment of the pyramidal subvolumes

Finally, the quality of the images of the cardiac structures which can be obtained by a 3DE data set will be affected by the point spread function of the system. The point spread function describes the imaging system response to a point input. A point input, represented as a single pixel in the "ideal" image, will be reproduced as something other than a single pixel in the "real" image.

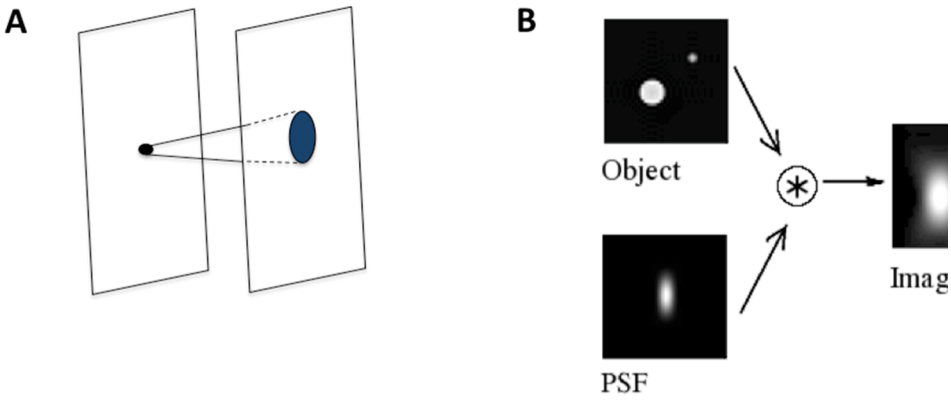

Figure 3.8. Point spread function. A. Graphical representation of the extent of degradation (blur) of a point passing through a optical system. B. Effect of the point spread function on the final image of a circular object

The degree of spreading (blurring) of any point object varies according to the dimension employed. In current 3DE systems it will be around 0.5 mm in the axial (y) dimension, around 2.5 mm in the lateral (x) dimension, and around 3 mm in the elevation (z) dimension. As a result we will obtain the best images (less degree of blurring, i.e. distortion) when using the axial dimension and the worst (greatest degree of spreading) when we use the elevation dimension.

These concepts have an immediate practical application in the choice of the best approach to image a cardiac structure. According to the point spread function of 3DE the best results is expected to be obtained by using the parasternal approach because structures are mostly imaged by the axial and lateral dimensions. Conversely, the worst result is expected to be obtained by the apical approach which mostly uses the lateral and elevation dimensions.

3.3 Image acquisition and display

Currently, 3D data set acquisition can be easily implemented into standard echocardiographic examination by either switching among 2D and 3D probes or, with newest all-in-one-probes, by switching between 2D and 3D modalities available in the same probe. The latter probes are also capable to provide single-beat full-volume acquisition, as well as real-time 3D color Doppler imaging.

At present, three different methods for 3D data set acquisition are available: (2)

- multiplane imaging
- “real-time” (or “live”) 3D imaging
- multi-beat ECG-gated imaging

In the multiplane mode, multiple, simultaneous 2D views can be acquired at high frame rate using predefined or user-selected plane orientations and displayed using the split screen option (Figure 3.3). The first view on the left is usually the reference plane that is

orientated by adjusting the probe position while the other views represents views obtained from the reference view by simply tilting and/or rotating the imaging planes. Multiplane imaging is a real time acquisition and secondary imaging planes orientation can only be adjusted during acquisition. Doppler colour flow can be superimposed on 2D images and in some systems both tissue Doppler and speckle tracking analysis can be performed. Although strictly not a 3D acquisition, this imaging mode is useful in situations where assessment of multiple views from the same cardiac cycle is useful (e.g. atrial fibrillation or other irregular arrhythmias, stress echo, evaluation of intervenricular dyssynchrony)

In the real-time mode, a pyramidal 3D volumetric data set is obtained from each cardiac cycle and visualized live, beat after beat as during 2D scanning. As the data set is updated in real-time, image orientation and plane can be changed by rotating or tilting the probe. Analysis can be done with limited post-processing and the data set can be rotated (independent of the transducer position) to view the heart from different orientations. Heart dynamics is shown in a realistic way, with instantaneous on-line volume rendered reconstruction. It allows fast acquisition of dynamic pyramidal data structures from a single acoustic view that can encompass the entire heart without the need of reference system, ECG and respiratory gating. Real-time imaging is time-saving both for data acquisition and analysis. Although this acquisition mode overcomes rhythm disturbances or respiratory motion limitations, it still suffers of relatively poor temporal and spatial resolution. Real-time imaging can be acquired in the following modes:

i. Live 3D. Once the desired cardiac structure has been imaged in 2DE it can be converted to a 3D image by pressing a specific button in the control panel of the ultrasound system. The 3D system automatically switch to a narrow sector acquisition (approximately 30° x 60° pyramidal volume) to preserve spatial and

temporal resolution. The size of the pyramidal volume can be increased to visualize larger structures, but both scan line density (spatial resolution) and volume rate (temporal resolution) will drop down. 3D live imaging mode is used to: (i). Guide full-volume acquisition; (ii). Visualize small structures (aortic valve, masses etc); (iii). Record short-lived events (i.e. bubble passage); (iv). Acquire full volume data sets in patients with irregular cardiac rhythm/dyspnea; (v). monitor interventional procedures.

ii. Live 3D colour. Colour flow can be superimposed on a live 3D data set to visualize blood flow in real time. Temporal resolution is usually very low.

iii. 3D zoom. This imaging mode is an extension of live 3D and allows a focussed real time view of a structure of interest. A crop box is placed on a 2D single- or multiplane image to allow the operator to adjust lateral and elevation width to include the structure of interest in the final data set, then the system automatically crops the adjacent structures to provide a real time display of the structure of interest with high spatial and temporal resolution. The draw-back of the 3D zoom mode is that the operator loses the relationships of the structure of interest with surrounding structures. Mainly used during transoesophageal studies for detailed anatomical analysis of the structure of interest

iv. Full-volume. The full-volume mode has the largest acquisition volume possible (usually 90° x 90° degrees). Real-time (or "single-beat") full-volume acquisition is affected by low spatial and temporal resolution and it is used for quantification of cardiac chambers when multibeat ECG gated acquisition is not possible (e.g irregular cardiac rhythm, patient unable to cooperate for breath-holding)

In contrast to real-time/live 3D imaging, multi-beat acquisition is realized through sequential acquisitions of narrow smaller volumes obtained from several ECG-gated

consecutive heart cycles (from 2 to 6) that are subsequently stitched together to create a single volumetric data set (Figure 3.6). Once acquired, the data set cannot be changed by manipulating the probe like in live 3D imaging and analysis requires off-line slicing, rotation and cropping of the acquired data set. It provides large data sets with high temporal and spatial resolution that can be used for quantitating cardiac chamber size and function or to assess spatial relationships among cardiac structures. However, this 3D imaging mode has the disadvantage of the ECG-gating, as the images are acquired over several cardiac cycles and the final data set is available to be visualized by the operator only after the last cardiac cycle has been acquired, it is a "*near real-time*" imaging, and it is prone to artifacts due to patient or respiratory motion or irregular cardiac rhythms. Multibeat imaging can be acquired with or without color flow mapping and usually more cardiac cycles are required for 3D color data sets.

3D data sets can be sectioned in several planes and rotated in order to visualize the cardiac structure of interest from any desired perspective, irrespective of its orientation and position within the heart. This allows the operator to easily obtain unique visualizations, that may be difficult or impossible to achieve using conventional 2DE (e.g. en-face views of the tricuspid valve or cardiac defects). Three main actions are undertaken by the operator to obtain the desired view from a 3D volumetric data set: cropping, slicing and rotating. Similarly to what the anatomists or the surgeons do to expose an anatomic structure within a 3DE data set, the operator should remove the surrounding chamber walls. This process of virtually removing the irrelevant neighbouring tissue is called cropping, and can be performed either during or after acquisition.

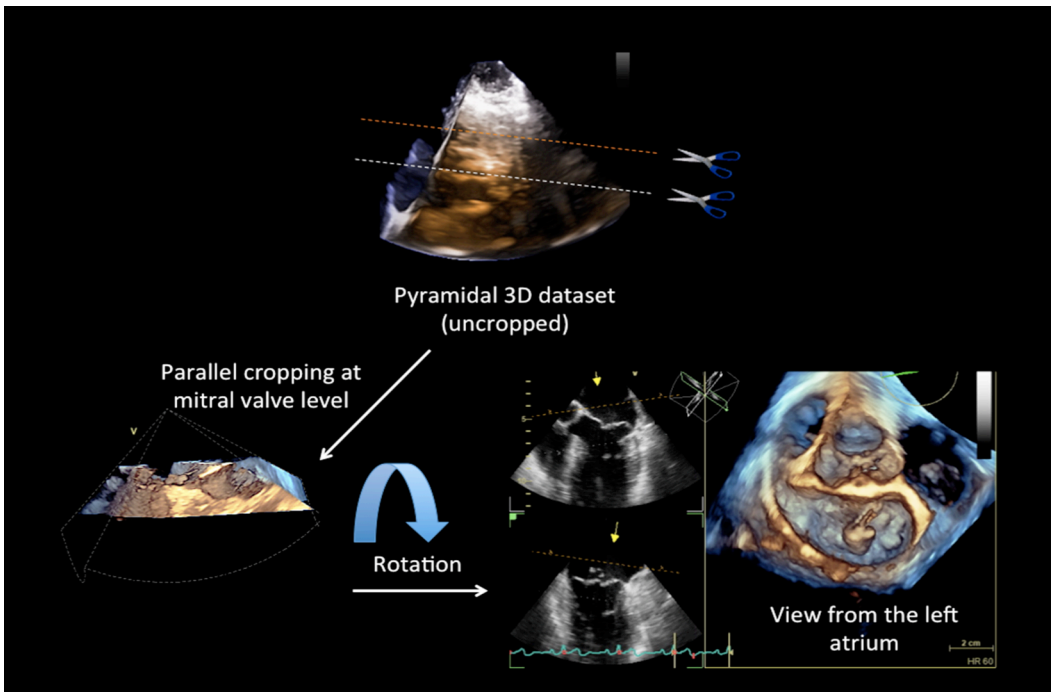

Figure 3.9. Data set cropping and rotation. To display the mitral valve from the left atrial perspective (surgical view) a full-volume pyramidal data set has been cropped to remove part of the left ventricle from above and part of the left atrium from below. Then, remaining data set has been rotated to the desired perspective and to put the cardiac structures in an anatomical sound position

In contrast with 2DE images, displaying a cropped image requires also data set rotation (Figure 3.9) and the definition of the viewing perspective (i.e. since the same 3D structure can be visualized *en face* either from above or below, as well as from any desired view angle)(2). Slicing refers to a virtual "cutting" of the 3D data set into one or more (up to twelve) 2D (tomographic) grey-scale images.

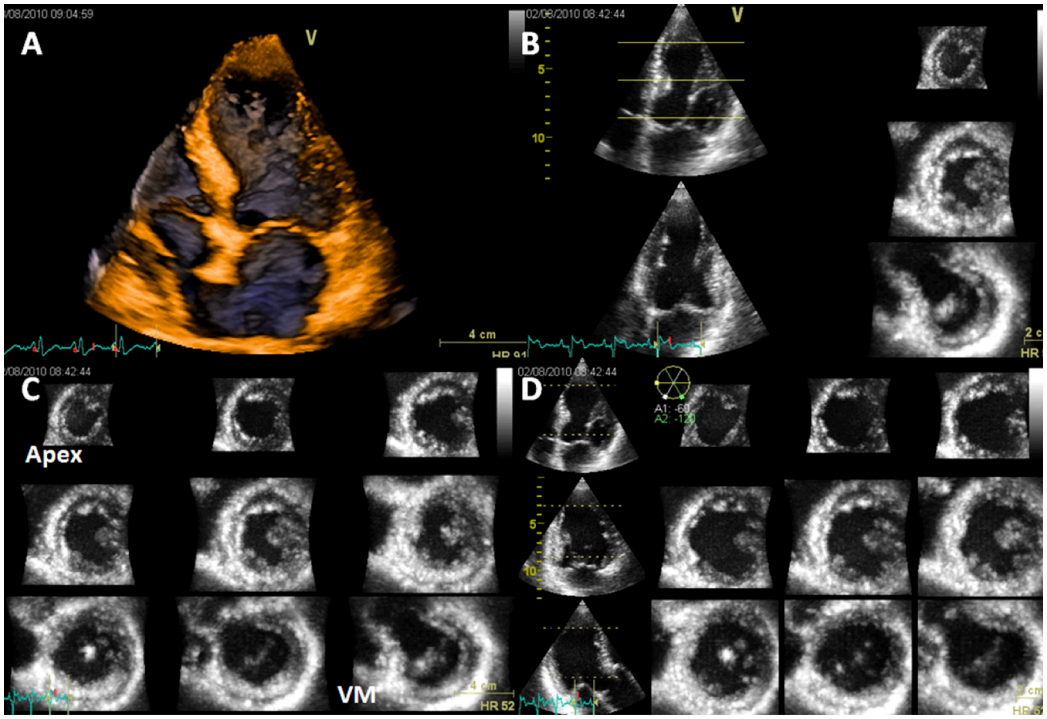

Figure 3.10 Data set slicing. A full-volume data set (*Panel A*) can be sliced in several ways. Two longitudinal (4-chamber and the orthogonal view) plus 3 transversal slices at different levels of the left ventricle (yellow lines) (*Panel B*). Nine transversal slices of the left ventricle from the mitral valve (MV) to the apical (Apex) level (Panel C). Three longitudinal slices (4- and 2-chamber plus the long-axis apical views) and nine transversal views (Panel D). The position of the lowest and the highest transversal planes are adjustable by the operator and the slices in between are automatically repositioned to be equidistant. The position of longitudinal planes are adjustable as well both during acquisition and post processing.

Finally, irrespective of its acquisition window, a cropped or a sliced image should be displayed according to the anatomical orientation of the heart within the human body and this is usually obtained by rotating the selected images.

Acquisition of volumetric images generates the technical problem of rendering the depth perception on a flat, 2D monitor. 3D graphic reproduction has been made possible using computer graphics techniques. First, data are segmented to delineate the 3D surface of structures of interest. Data segmentation algorithms separate, within the 3D data set, the object to be rendered from the surrounding structures: blood, pericardial fluid, air. Since these structures have different physical properties and different ability to reflect ultrasounds, segmentation is obtained by setting a threshold of echo intensity (For example, any voxel with echo intensity equal or lower than blood will not be processed further). Once segmented, the

3D data set can be displayed using three rendering techniques: wireframe rendering, surface rendering and volume rendering.

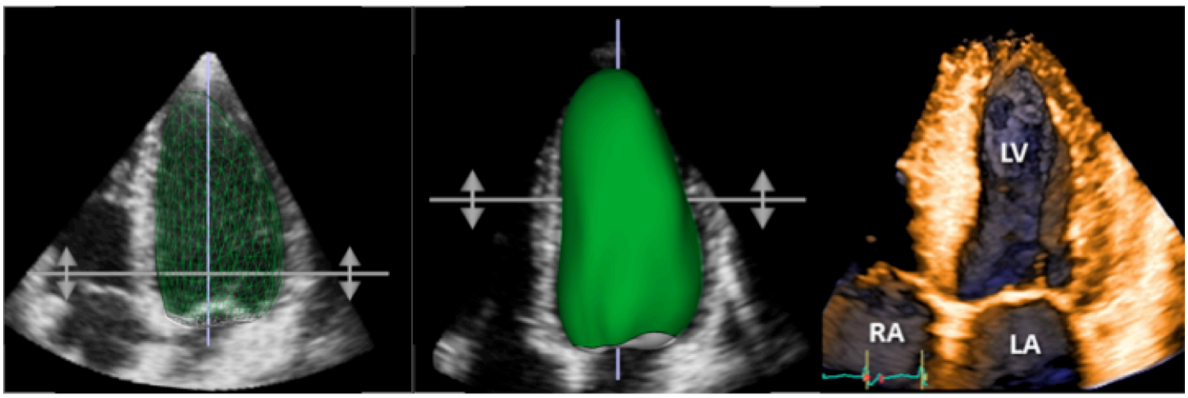

Figure 4.11. 3D display techniques of the left ventricle. Wireframe (*left panel*), surface (*central panel*) and volume (*right panel*) rendering (see text for details).

For the purposes of cardiac chamber quantification only the wireframe and surface rendering are relevant. Volume rendering is used to visualized structures with complex morphology like the heart valves which require greater anatomical detail for clinically meaningful imaging. In the volume rendering modality, various color maps are applied to convey the depth perception to the observer. Generally, lighter shades (e.g. bronze,) are used for structures closer to the observer, while darker shades (e.g. blue) are used for deeper structures (Figure 3.11, right panel).

Surface rendering modality (Figure 3.11, central panel) displays the 3D surface of cardiac structures, identified either by manual tracing or by using automated border detection algorithms on multiple 2D cross-sectional images of the structure/cavity of interest. This stereoscopic approach is useful for the assessment of shape and for a better appreciation of geometry and dynamic function during the cardiac cycle.

Wireframe rendering (Figure 4.11, left panel) is the simplest of the available techniques. It identifies equidistant points on the surface of a 3D object obtained from manual tracing, or using semiautomatic border detection algorithms, to trace the endocardial contour in cross-sectional images and then connect these points using lines (wires) to create a mesh of little

polygonal tiles. Smoothing algorithms are used to smooth angles and give a realistic appearance to the structure of interest. This rendering technique processes a relatively low amount of data and it is used for relatively flat endocardial boundaries such as the cardiac chamber walls. This stereoscopic approach is useful for the assessment of shape and for better visualization of chambers volume and function during the cardiac cycle.

The surface-rendering technique is very similar to the wireframe technique but identifies many more points on the surface of the structure of interest and the lines joining the points become indistinguishable. It displays in detail the surfaces of the analyzed object facing the observer as a solid structure (Figure 3.11, central panel).

PART II

EXPERIMENTAL SECTION

DEVELOPMENT OF AGE- AND GENDER-SPECIFIC REFERENCE VALUES FOR CARDIAC CHAMBER GEOMETRY AND FUNCTION USING THREE_DIMENSIONAL ECHOCARDIOGRAPHY

CHAPTER 4

Research project overview

4.1 Background

Correct quantification of cardiac chamber size and geometry coupled with the assessment of ventricular mass and function are critically important for patient evaluation and represent the most frequent indication for an echocardiographic study.

2DE assessment of cardiac chamber volumes and function relies on geometric assumptions and is subject to plane positioning errors, leading to chamber foreshortening and subsequent underestimation of volumes. Moreover, since cardiac chambers like the RV has a complex asymmetric geometry which cannot be fitted into simple geometric models, and separate inflow and outflow which cannot be adequately visualized with any single 2D view, its volumes and ejection fraction cannot be reliably calculated with conventional 2DE. All these reasons may explain why standardization of measures with 2DE has been less successful compared to other imaging techniques and echocardiography is sometimes perceived as less reliable and an excessively operator-dependent technique. (35)

The advent of 3DE represents a major innovation in cardiovascular ultrasound(1). 3DE is the only imaging technique based on volumetric scanning able to show moving structures in the beating heart, in contrast to cardiac magnetic resonance (CMR) and computed tomography, which are based on post-acquisition 3D reconstruction from multiple tomographic images and displaying only 3D rendered snapshots. Presently, 3D data set

acquisition can be easily implemented into standard echocardiographic examination by either switching among 2D and 3D probes or, with newest all-in-one-probes, by switching between the 2D and 3D modes available in the same probe. 3DE overcomes geometric assumptions and enables an accurate quantitative and reproducible evaluation of cardiac chambers thus offering solid elements for patient management. Multiple studies have shown that 3DE measurements of cardiac chamber volumes and function are significantly more accurate and reliable than 2DE when compared with CMR imaging as the reference technique. (1) Recently, joint European Association of Echocardiography (EAE)/American Society of Echocardiography (ASE) recommendations have been published, aiming to provide clinicians with a systematic approach to 3D image acquisition and analysis. (2)

However, the implementation of 3DE for cardiac chamber volume and function measurements in the routine of the echocardiographic laboratories requires the availability of reliable reference values. (2) At present, normative data about 3DE cardiac chamber volumes and function parameter are very limited. (1,3)

Accordingly, we designed this prospective, observational study to: (i) determine the normative values for cardiac chamber volumes and function parameters using 3DE in a large cohort of healthy subjects; (ii) compare the cardiac chamber parameters measured by 3DE with the same values calculated using 2DE; (iii) analyze the effects of age, body size and gender on these parameters.

4.2 Methods

5.2.1 Study population

Between October 2011 and September 2013, 263 healthy volunteers with a wide age range were prospectively recruited among hospital employees, fellows in training, their parents, and people who underwent medical visits for driving or working license and met the inclusion criteria. The size of the study has been chosen according to Altman et al.(36) who

set at 200 the minimum number of subjects to enrol in a study aimed at assessing the reference values for biological variables. Prospective criteria for recruitment included: age > 18 years; no previous history of cardiovascular or lung disease; no symptoms; absence of cardiovascular risk factors (i.e. systemic arterial hypertension, smoking, diabetes, hypercholesterolemia and familial history of cardiovascular disease); normal electrocardiogram; physical examination; and no cardio-active treatment. Exclusion criteria included: trained athletes; pregnancy; body mass index > 30 kg/m^2. The study was approved by the University of Padua Ethics Committee (protocol #2380P, approved on 06/10/2011) and all volunteers signed an informed consent before undergoing physical examination, blood pressure and anthropometric measurement, and echocardiography. Body surface area (BSA) was calculated according to the formula by DuBois and DuBois. (37)

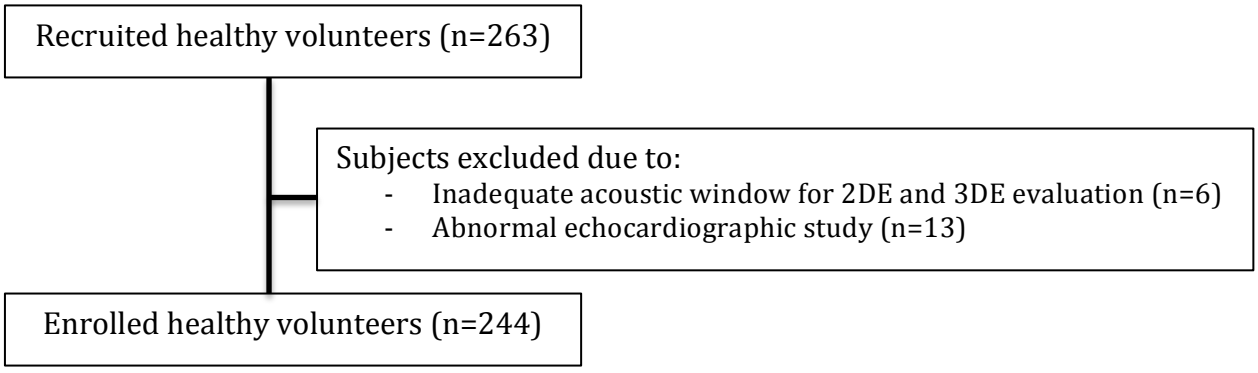

Figure 4.1. Enrollment flow chart. 2DE: two-dimensional echocardiography; 3DE: three-dimensional echocardiography.

TABLE 4.1 – Demographic Characteristics of the enrolled healthy volunteers

	All (n=244)	**Men** (n=103)	**Women** (n=141)	p Value
Age (years)	43 ± 14	42 ± 14	44 ± 14	NS
Age range (years)	18 - 75	18 – 74	18 - 75	NS
Heart rate (bpm)	68 ± 12	67 ± 12	69 ± 11	NS
Height (cm)	170 ± 9	178 ± 6	165 ± 7	< 0.001
Weight (kg)	67 ± 11	76 ± 9	61 ± 8	< 0.001
Body mass index (kg/m^2)	23.1 ± 2.8	24.1 ± 2.4	22.3 ± 2.8	< 0.001
Body surface area (m^2)	1.78 ± 0.18	1.93 ± 0.13	1.67 ± 0.13	< 0.001
Systolic blood pressure (mmHg)	121 ± 13	126 ± 11	117 ± 14	< 0.001
Diastolic blood pressure (mmHg)	74 ± 8	77 ± 8	71 ± 8	< 0.001

* p values refer to gender differences

For the development of the reference values for the RV, data collected at the University of Padua were merged with those prospectively collected in 2 Italian tertiary centers (Centro Cardiologico Monzino, Milan; University Federico II, Naples) having a large expertise in 3DE for RV quantification (>400 studies/year/center for both clinical and research purposes). Participating centers were asked to provide samples with a fairly uniform distribution among genders and age (from 18 to 90 years).

4.2.2 Data set acquisition.

Using a standardized protocol, all examinations were perfomed by three cardiologists with experience in research echocardiography (DM, LDB, LPB)[1] using a commercially-available Vivid E9 ultrasound machine (GE Vingmed Ultrasound, Norway) equipped with M5S and 4V probes for 2D and 3DE, respectively. All patients were examined in the left lateral position

[1] DM= dott.ssa Denisa Muraru, LDB = dott.ssa Lucia Dal Bianco, LPB= dott. Luigi Paolo Badano

using grey scale second-harmonic 2D imaging technique, with the adjustment of image contrast, frequency, depth, and sector size for adequate frame rate and optimal endocardial border visualization. Care was taken to avoid cardiac chamber foreshortening in both apical views, and image acquisition was done during breath holding to minimize respiratory movements.

Conventional transthoracic echocardiography included: (i). 2D guided M-mode tracings of LV wall thickness and cavity diameter to calculate LV mass; (ii). Zoom imaging of LV outflow tract obtained from parasternal 2D long-axis view; (iii). Spectral recordings of LV outflow tract flow sampled using a pulsed-wave Doppler sample volume positioned just proximal to the aortic valve so that the location of the velocity recording could match the LV outflow tract measurement; (iv). Apical 4- and 2-chamber view recordings for LV volumes, taking care of maximising LV length and obtaining the highest frame rate by reducing depth in order to exclude atria; (v). Apical 4- and 2-chamber view recordings for LA volumes, taking care of maximising LA length and obtaining the highest frame rate by reducing the scanning sector angle in order to exclude the right atrium; (vi). RV focused 4-chamber apical view, taking care of maximising RV area and length; and (vii). RA focused 4-chamber view taking care of maximising RA length and area. (38) All tracings and recordings contained at least 3 cardiac cycles to allow averaging of measurements.

Separate 3DE full-volume LV, LA, RV and RA data sets obtained by stitching together 4 or 6 consecutive ECG-gated subvolumes were acquired by the same examiner at the end of the conventional 2DE and Doppler study. Using multi-slice display of the 3D data set, special care was taken to visualize all cardiac chamber segments and to exclude any stitching artifacts between subvolumes. Data sets were stored digitally in raw-data format and exported to a separate workstation for analysis.

4.2.3 Data set post-processing and quantitative analyses

Image quality check, post-processing and analysis were performed by 2 independent observers (DM, LPB)[2], having a 3-year long experience with the software packages used in this project.

*4.2.3.1 Left ventricular data set analysis***.** LV mass was calculated using measurement performed on 2DE guided M-mode tracings(39) according to the ASE leading-edge convention(40). To calculate LV stroke volume (SV), LV outflow tract diameter was measured in the zoom parasternal long-axis view in mid-systole from the white-black interface of the septal endocardium to the anterior mitral leaflet, parallel to the aortic valve plane and within 0.5-1.0 cm of the valve orifice. End-diastole and end-systole were identified from 2DE cine-loops using frame-by-frame analysis of the apical 4- and 2-chamber LV views as the largest and smallest cavity during the cardiac cycle, respectively. Then, manual tracing of endocardial border was performed in both frames, paying attention to include the papillary muscles within the LV cavity. LV end-diastolic (EDV) and end-systolic (ESV) volumes were calculated using the biplane disc-summation algorithm (modified Simpson's rule) and ejection fraction (EF) was calculated as 1- ESV/EDV. 2DE end-diastolic sphericity index was calculated from LV EDV and LV longitudinal axis (calculated as the average between LV longitudinal axes in 4- and 2-chamber views), by applying the same formula as with 3DE (see below).

Quantification of 3D LV volumes and EF was performed using a commercially-available software (4D AutoLVQ, GE Vingmed, Norway), previously validated against CMR, (41) by completing the following steps:

(i) Automatic slicing of LV full-volume data set. The end-diastolic frames needed for contour detection were automatically displayed in quad-view: apical four-, two-chamber, long-axis views and LV short-axis plane. Each longitudinal view was colour- coded and

[2] DM= dott. Denisa Muraru; LPB= dott. Luigi P. Badano

indicated on the short-axis image at 60° between each plane. Both reference frames in the end-systole and end- diastole could be also manually selected, if necessary.

(ii) Alignment. Rapid manual alignment by pivoting and translating the four-chamber plane was first performed in order that the corresponding intersection line of all planes was placed in the middle of the LV cavity, crossing the LV apex and the centre of mitral valve opening in each view. Aligning one plane automatically changed the others. Once LV central longitudinal axis was identified, accurate orientation of LV views was ensured by manual refinement of the angles between the LV planes on the LV short-axis view, in order to correspond to the defining anatomical landmarks of each view.

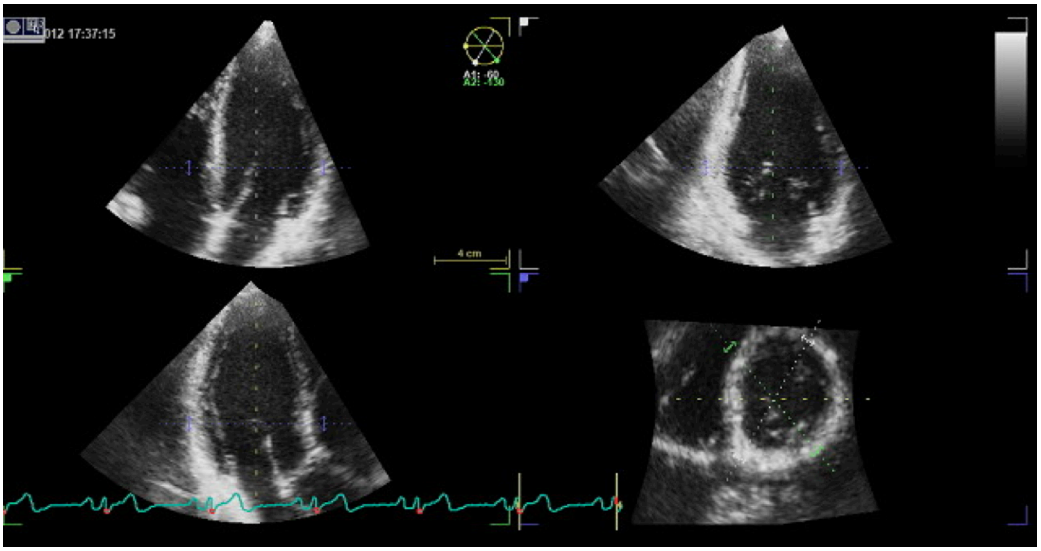

Figure 4.2 Left ventricular data set alignment. The 3 longitudinal planes (e.g. 4-, 2-chamber and long-axis views) are manual aligned by pivoting and translating the respective plane in order that the corresponding intersection line of all planes was placed in the middle of the LV cavity, crossing the LV apex and the centre of mitral valve opening in each view. The spatial orientation of each longitudinal plane is visualized on the short axis plane on the roght lower panel and can be readjusted to optimize it.

(iii) LV reference point identification. To subsequently identify a fitting geometric model, the software required manual input of only three single points for each of the three LV apical planes (two points at mitral annulus borders, and one at the apex showed as green dots in Figure 4.3) first in end-diastolic frames, and then for corresponding end-systolic frames. Manual positioning of the points was simultaneously shown on the LV short-axis view for

guidance in LV endocardial border identification. Furthermore, the apex reference point previously identified on LV longitudinal planes was displayed before adding the apical landmark into the next plane.

(iv) Automated identification of endocardial border. The software automatically detected LV cavity endocardial border in 3D and provided the measured EDV. Three additional short-axis views at different levels were displayed in order to facilitate verification of the accuracy of endocardial surface detection both in cross- section and in long-axis by rotating and translating active view plane. At this stage, LV borders could be manually adjusted, if unsatisfactory, by (dis)placing as many additional points as needed (manually corrected AutoLVQ), with secondary immediate automated refinement of boundary detection accordingly. This could be done on each of the six simultaneously displayed LV views, but also possible in between reference planes for LV with distorted shape.

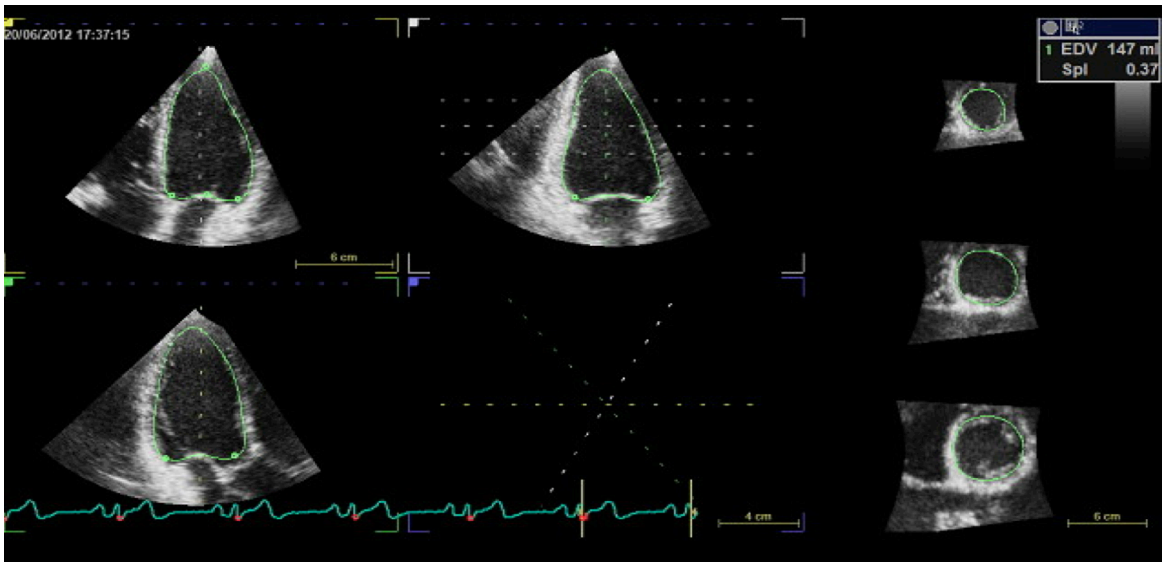

Figure 4.3 Identification of reference point and of endocardial border. Reference points at mitral annulus and LV apex (green dots on the left upper panel) are manually identified to allow the software to provide an automatic identification of the endocardial border (green line).

After completing steps 1 – 4 for end-diastolic views, only 3 – 4 sequence was required for end-systolic frames, since adjustments done in steps 1 – 2 were automatically carried out subsequently in end-systolic views.

(v) Final quantitative analysis and data display. Using the initial contours in both end-systole and end-diastole, a corresponding dynamic surface-rendered LV cast was derived. Final data panel automatically displayed LVEDV, LVESV, LVEF, stroke volume, cardiac output, and heart rate values. A volume – time plot was also provided.

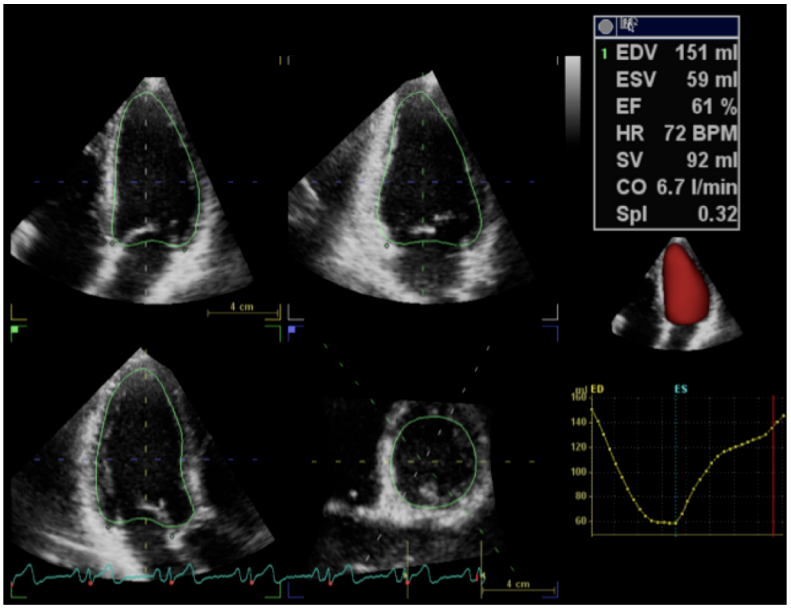

Figure 4.4. Measurement of left ventricular volumes by 3D echocardiography. Left ventricular beutel size is generated through semi-automated identification of endocardial surface and volume measurement is based on beutel voxel count .

Manual editing of the semi-automatically generated endocardial contours was routinely applied in order to include the LV outflow, as well as papillary muscles and trabeculae within the LV cavity since this approach was found to reduce the bias in comparison with CMR. (41,42)

In addition, this software enabled automatic calculation of LV sphericity index and LV mass measurements. LV sphericity index is a quantitative parameter reflecting LV shape and it is calculated as the ratio between the LV EDV divided by the volume of a sphere, whose diameter is equal to the longitudinal LV axis measured at end-diastole(43).

For LV mass calculation, after LV endocavitary volume quantitation the software automatically detected also the epicardial LV contours in end-diastole and in end-systole. Both endo- and epicardial contours were verified by the operator and manually adjusted to fit

the regional differences in LV wall thickness.

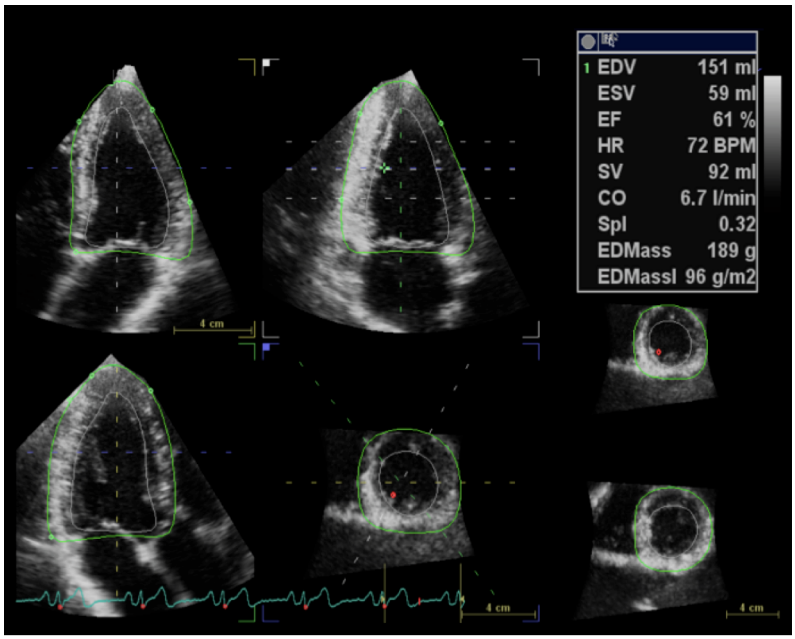

Figure 4.5. Measurement of left ventricular mass by 3D echocardiography. Semi-automated identification of endocardial and epicardial surfaces allows measurement of endo- and epi-cardial volumes. Then, LV mass was automatically computed by multiplying myocardial volume (epicardial volume - endocardial volume) multiplied by the specific weigth of the myocardial tissue (1.05 g/ml).

4.2.3.2 Right ventricular data set analysis. Offline analyses of all RV data sets were carried out using a single commercially-available software package (TomTec 4D RV Analysis, Unterschleissheim, D) by one experienced investigator in each center. This vendor-independent software was validated against CMR and its workflow has been extensively described elsewhere. (44-46) This software uses border-detection algorithms to obtain a dynamic surface-rendered RV cast (beutel) which enables the evaluation of RV geometry and contraction from any perspective.

Adequate identification of 3 pre-defined RV planes is required in order to proceed with RV quantitative analysis workflow: RV apical 4-chamber plane (RV inflow), saggital plane (the plane orthogonal to the 4-chamber plain, that includes the RV outflow tract) and coronal plane (transversal plane displaying the crescentic RV cavity in short-axis).

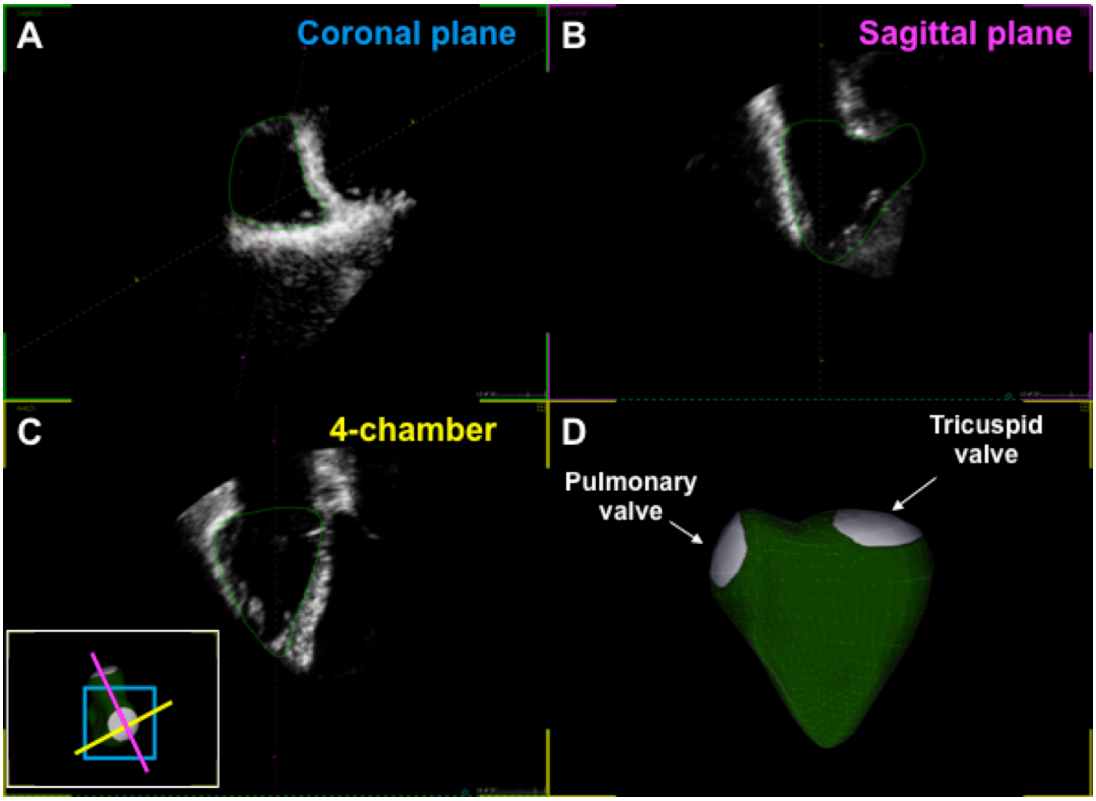

Figure 4.5. Three-dimensional analysis of the right ventricle. Semi-automated dedicated software for right ventricular volumes and function quantitation based of 3D data set. After manual initialization on standard 2D views of the right ventricle (coronal, *A*; sagittal, *B*; 4-chamber, *C*), the software identifies the cavity contour in three dimensions and provides a surface reconstruction of the right ventricular cavity (cast, *D)*.

Endocardial border is manually traced in end-diastolic and end-systolic frames for the three selected RV planes to initialize the automated border detection algorithm. Manual editing of the generated RV surface contour and changes in software sensitivity for border detection may be applied if needed, to optimize the border tracking to fit the irregularities of RV contour and to include trabeculae or papillary muscles in the RV cavity (as recommended and usually performed during CMR quantitative analysis).(47) The 3D RV cast in motion that represents changes inthe RV cavity over the cardiac cycle, a time-volume curve and a panel of quantitative data derived from actual volumetric measurements and not simple calculations are finally obtained.

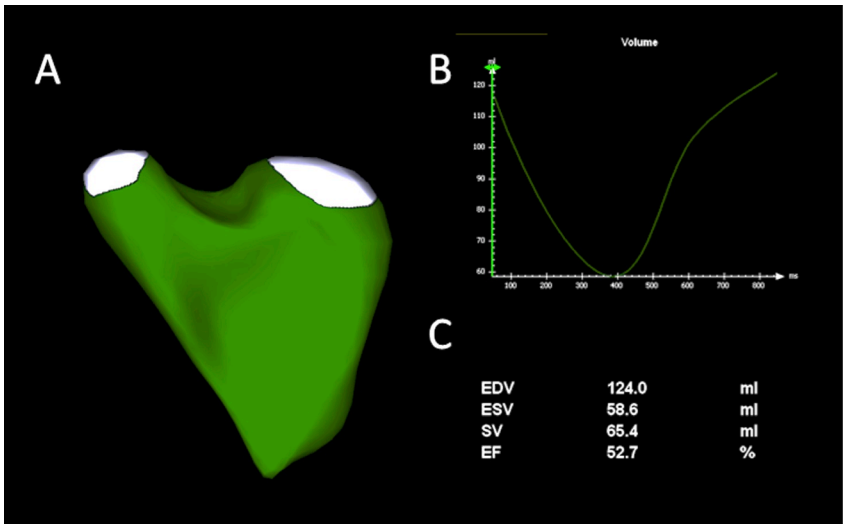

Figure 4.6. **Results of right ventricular quantitative analysis**. Surface rendering of the right ventricle obtained by transthoracic three-dimensional echocardiography (*Panel A*). Time-volume curve showing right volume changes during cardiac cycle (*Panel B*). Results of the quantitative analysis are shown in Panel C.

*4.2.3.3 Left atrial data set analysis***.** 2DE LA images were analyzed using EchoPAC v112.1.3, (GE Vingmed, Horten, Norway). The LV end-systolic frame corresponding to the largest LA area, just before the mitral valve opening, was identified in the dedicated 4CH and 2CH views. Then, endocardial border was manually traced in the same frames paying attention to exclude the area between the mitral leaflets and annulus, pulmonary veins and atrial appendix to obtain LA area.

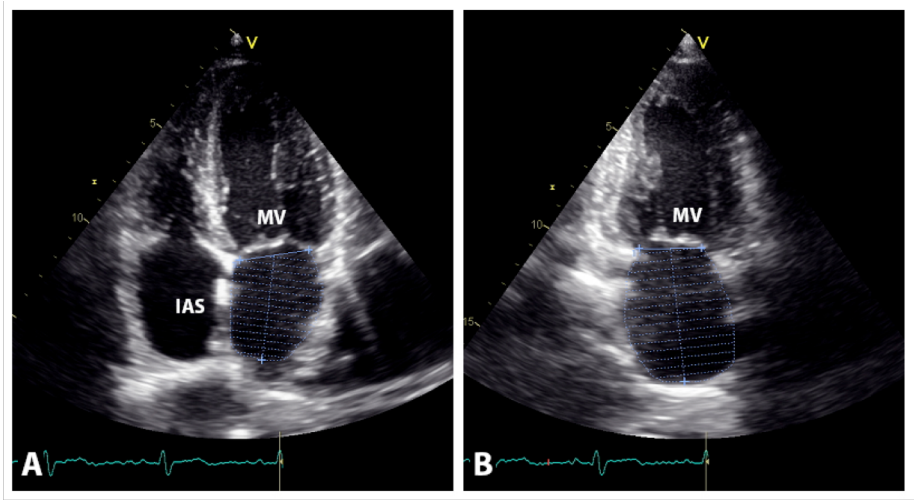

Figure 4.7. Two-dimensional echocardiography assessment of left atrial size. A) Dedicated 4-chamber view; B) Dedicated 2-chamber view. IAS: interatrial septum; MV: mitral valve.

Maximal LA volume (Vmax) was automatically calculated by the software, considering both 4- and 2-chamber analyses, using the biplane discs' summation method.(38) The same process was used to calculate the minimum LA volume (Vmin) and pre A volume (VpreA), corresponding to the end-diastolic frame, just after mitral valve closure, and to the peack of P wave frame, respectively.

3DE LA analysis was performed using a dedicated software designed for volumetric analysis of the LA (LA analysis, Tomtec Imaging Systems, Unterschleissheim, Germany) and recently validated against CMR.(48) At the beginning of the 3DE analysis workflow, LA data set was automatically sliced 4-, 2-chamber and long-axis apical planes, and a short-axis plane. The end-systolic, pre A and end-diastolic frames were marked in the corresponding cardiac cycle. Then, rapid manual data set alignment was performed by translating and rotating the 4-chamber plane in order to obtain orthogonal non-foreshortened planes of the LA in all 3 apical planes. In each apical plane, the LA blood-tissue interface was manually initialized on 2 frames identifying LA Vmax, and Vmin. These initialized LA endocardial boundaries were used to reconstruct the LA endocardial surface. A 3DE surface of the LA volume was then generated for each frame throughout the cardiac cycle resulting in a dynamic cast of the LA cavity .

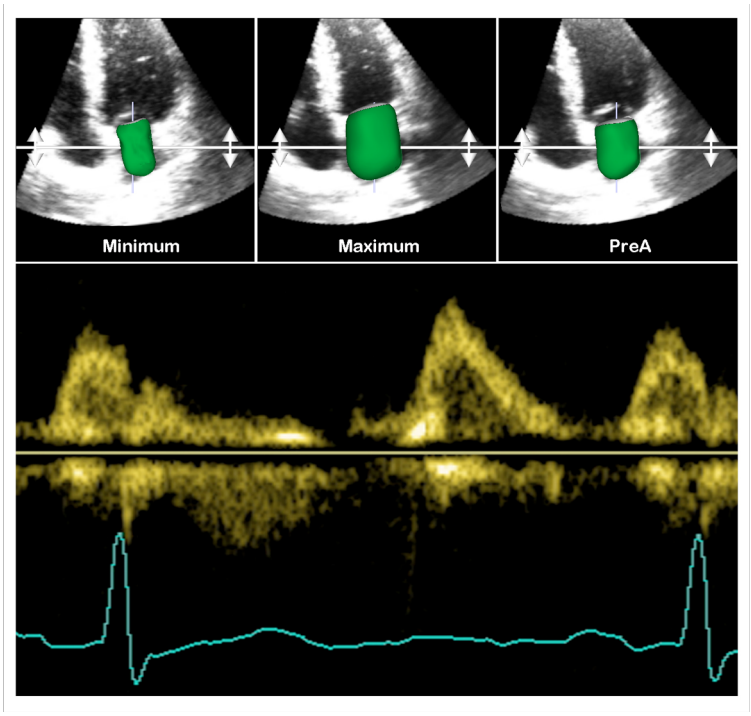

Figure 4.8. Three-dimensional echocardiography quantification of left atrial volumes and function. The 3D LA surface is displayed at 3 different phases of the cardiac cycle, namely the minimum, maximum and pre A LA volumes, along with the electrocardiogram and mitral valve inflow pulsed Doppler to show temporization of LA volume changes. 3D: three-dimensional; LA: left atrium.

For each consecutive frame, the voxel count inside the 3DE LA surface was used to measure LA volume, resulting in a smooth interpolated time-volume curve from which Vmax, Vmin and VpreA can be easily obtained.

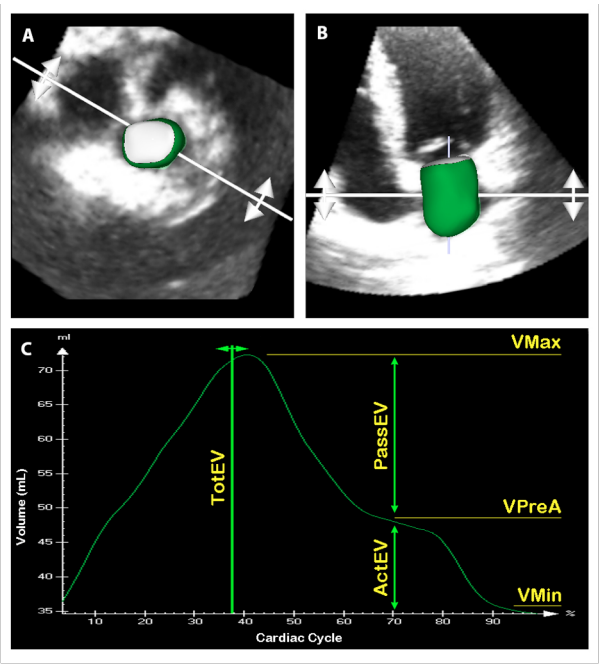

Figure 4.9. Three-dimensional echocardiography (3DE) assessment of left atrial size (LA) and function. Transversal (A) and longitudinal (B) visualization of 3D LA surface superimposed on gray scale 3DE data set, and time-volume curve depicting LA volume changes during the cardiac cycle (C). From this time-volume curve curve the values from maximal (Vmax), minimal (Vmin) and pre-A (VpreA) LA volumes can be obtained, from which passive (PassEV), active (ActEV) and total (TotEV) emptying volumes has been calculated (see text).

From LA volumes we calculated: total emptying volume (EV), which represents the LA reservoir function, as the difference between Vmax and Vmin; passive EV, which represents conduit function, as the difference between Vmax and VpreA; and active EV, which corresponds to LA booster function, as the difference between VpreA and Vmin.(49) Accordingly, total emptying fraction (EmptFr) was total EV/Vmax, passive EmptFr was passive EV/Vmax and active EmptFr was active EV/VpreA. In addition, we calculated the LA expansion index as $[(V_{max}-V_{min})/V_{min}]$ x100% as an index of LV filling pressure

4.2.3.4 Right atrial data set analysis. 2DE images were analyzed using EchoPAC v110.1.3, (GE-Healthcare, Horten, Norway). The RV end-systolic frame corresponding to the largest RA area, just before the tricuspid valve opening, was identified in the dedicated apical 4-chamber view. Supero-inferior and medio-lateral diameters were measured according to current guidelines. (50) Then endocardial border was manually traced in the same frame paying attention to exclude the area between the tricuspid leaflets and annulus to obtain RA area.

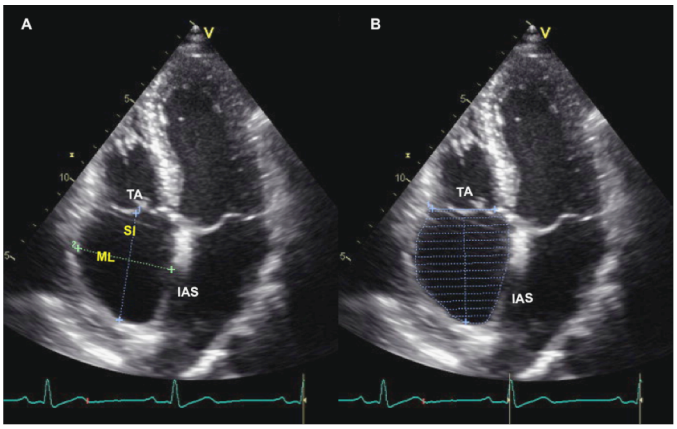

Figure 4.10. Two-dimensional echocardiography (2DE) assessment of right atrial (RA) size. A. RA supero-inferior (SI) and medio-lateral (ML) diameters measured on a dedicated 4-chamber view. B. RA area tracing. IAS, interatrial septum; TA, tricuspid annulus.

Maximal RA volume (Vmax) was automatically calculated by the software using the area-length method. (38) Using the same procedure we also measured the minimal RA volume (Vmin) as the smallest RA cavity during the cardiac cycle, just before tricuspid valve closure,

and pre A volume (VpreA) as the RA volume corresponding at P wave peak on the ECG tracing.

3DE RA analysis was performed using a dedicated software designed for volumetric analysis of the left atrium (LA analysis, Tomtec Imaging Systems, Unterschleissheim, Germany) and recently validated against CMR. (48) At the beginning of the 3D analysis workflow, RA data set was automatically sliced 4-, 2-chamber, and long-axis apical planes and a short-axis plane. Rapid manual data set alignment was performed by translating and rotating the 4-chamber plane in order to obtain orthogonal non-foreshortened planes of the RA in all 3 apical views. In each apical view, the RA blood-tissue interface was manually initialized on 2 frames identifying RA Vmax, and Vmin. These initialized RA endocardial boundaries were used to reconstruct the RA endocardial surface. A surface rendered 3D beutel of the RA volume was then generated for each frame throughout the cardiac cycle resulting in a dynamic cast of the RA cavity.

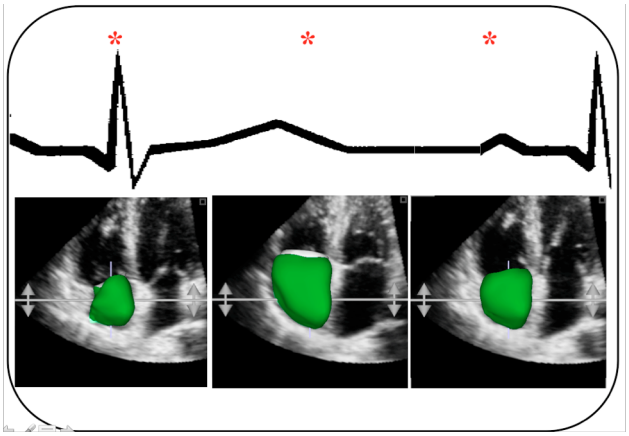

Figure 4.11. 3DE dynamic quantitation of right atrial (RA) volumes and function. The RA beutel is displayed at 3 different phases of the cardiac cycle, namely the minimum, maximum and preA RA volumes along with the electrocardiogram to show temporization of RA function phases.

For each consecutive frame, the voxel count inside the RA beutel was used to measure RA volume, resulting in a smooth interpolated time-volume curve from which Vmax, Vmin and VpreA can be easily obtained.

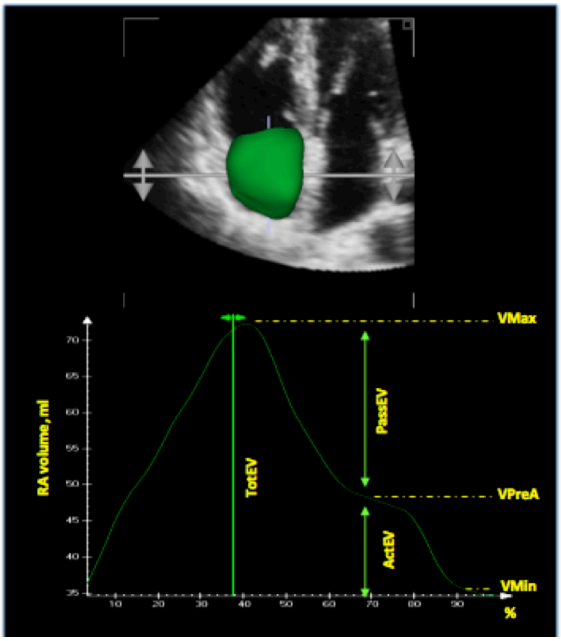

Figure 4.12. **Three-dimensional echocardiography (3DE) assessment of the right atrial (RA) size and function.** Longitudinal visualization of a surface rendered RA beutel superimposed on gray scale 3DE data set (*upper panel*), and time-volume curve depicting RA volume changes during the cardiac cycle (*lower panel*). From this time-volume curve the values for maximal, minimal and pre-A RA volumes can be obtained

Similar to measurements performed for the LA, from RA volumes we calculated total emptying volume (EV), which represents the RA reservoir function, as the difference between Vmax and Vmin; passive EV, which represents conduit function, as the difference between Vmax and VpreA; and active EV¸ which corresponds to RA booster function, as the difference between VpreA and Vmin (49,51). Accordingly, total emptying fraction (EmptFr) was total EV/Vmax, passive EmptFr was passive EV/Vmax and active EmptFr was active EV/VpreA.

4.2.4 Statistical analysis.

Normal distribution of study variables was checked using the Kolmogorov-Smirnov test. Continuous variables were summarized as mean±SD if normally distributed. Variables were compared between men and women using the unpaired t-test. 3DE and 2DE measurements obtained from the same subject were compared using the paired t-test. Pearson correlation was used to analyze the relationships between chamber size size and age and body size.

Inter-observer variablity for 3D LV volumes and mass was analyzed in 15 random subjects by 2 independent observers. Intra-observer variability was analyzed in another group of 15

subjects by the same observer repeating the measurements 1 week later. For each parameter, reproducibility was reported as mean difference and coefficient of repeatability (1.96 SD of the differences between the two measurements) by Bland-Altman analysis, and as intraclass correlation coefficient (ICC).

All analyses were carried out using SPSS 19.0 (SPSS Inc, Chicago, IL, USA) and MedCalc 10.0.1.0 Mariakerke, Belgium). Differences among variables were considered significant at $p<0.05$. Upper and lower limits of normality were computed as the mean value plus or minus 2SD.

CHAPTER 5

Reference values for left ventricular geometry and function by three-dimensional echocardiography

5.1 Background

Noninvasive assessment of LV geometry and function ranks among the principal parameters assessed with echocardiography. Suitability for device implantation, indications to cardiac surgery or to treatment initiation in asymptomatic patients with LV systolic dysfunction are among the most critical decisions that rely on an accurate LV quantification. (52,53)

LV volume measurement by 2DE is highly experience-dependent, uses only partial information contained in few predefined cross-sections to assess global myocardial function, and relies on geometrical assumptions that may not be necessarily valid in all patients. 2DE has also shown limited test-retest reproducibility for LV volumes and EF quantification. (54) Geometric assumptions render the measurements of LV volume and EF particularly inaccurate in those patients in whom these parameters are most needed (i.e. patients with previous myocardial infarction or cardiomyopathies, whose LVs are asymmetric or distorted).

3D LV data set analysis can now be performed using computerized automated or semi-automated endocardial surface detection softwares, which do not rely on geometric assumptions and require only minimal human intervention, therefore improving measurement reproducibility (Figure 4.4). After identification of few anatomical landmarks

(i.e. apex and mitral annulus reference points), the 3D LV cast can be automatically segmented into the standard 16 or 17 segments. The volume of the entire LV cavity, as well as the separate subvolumes corresponding to each of 16 or 17 segments can be measured frame-by-frame and plotted against time .

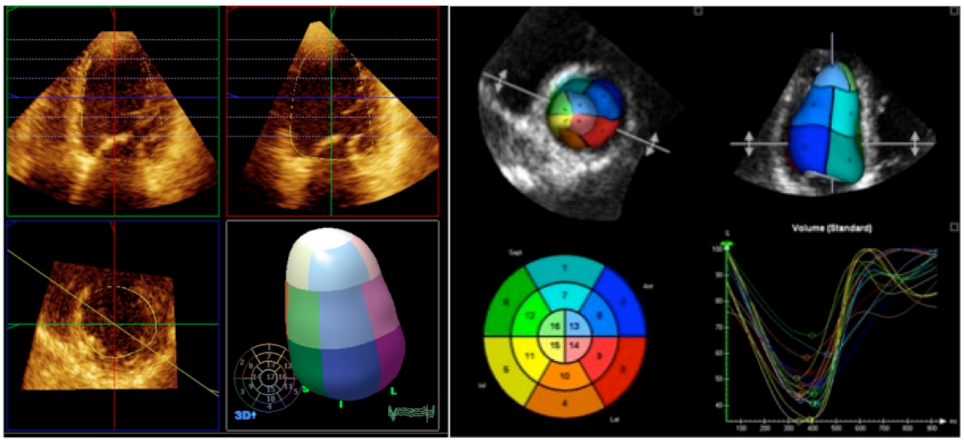

Figure 5.1. **Left ventricular cast segmentation**. The endocardial surface can be subdivided in 16 (*right panel*) or 17 (*left panel*) color-coded areas corresponding to the left ventricular segmentation. Each segment can be assimilated to a pyramid with the base on the endocardium and the apex at the gravity center of the ventricle and time variations of the segmental pyramidal volume can be measured during cardiac cycle and displayed on a volume-time graph. The time to minimal volume of each segment can be measured on the corresponding time-volume curves and the standard deviation of the time to minimal volume of the 16/17 segments has been reported as an index of intraventricular dyssynchrony.

3DE has been extensively validated against CMR (Table 5.1) and has been demonstrated to be more time-saving, reproducible and accurate than conventional 2DE for LV volumes and EF measurement. The possibility of re-aligning planes and optimally adjusting the LV chamber size to its maximum longitudinal axis length is an important advantage offered by 3DE over conventional 2DE. (55) Foreshortening of LV longitudinal axis is a major cause of volume underestimation by 2DE, which accounts for the larger bias observed in comparison with 3DE.

However, despite eliminating LV apical foreshortening and geometric assumptions, 3DE still yields a systematic underestimation of LV volumes as shown in a meta-analysis of 95 studies having CMR as reference. (56) A significant underestimation has been reported for LV ESV (-4.7 ml) and EDV (-9.9 ml), whereas LV EF measurement revealed an excellent accuracy (-0,13%), probably due to a constant underestimation of both volumes.

TABLE 5.1 - Differences between left ventricular volumes and function assessed by three-dimensional echocardiography and conventional two-dimensional echocardiography in comparison with cardiac magnetic resonance.

		Mean difference ±SD from CMR	
Author	**Parameter**	**3DE**	**2DE**
Jenkins et al. (57)	End-diastolic volume (ml) End-systolic volume (ml) Ejection fraction (%)	-4±9 -3±18 0±7	-54±33 -28±28 -1±13
Kuhl et al. (58)	End-diastolic volume (ml) End-systolic volume (ml) Ejection fraction (%)	-13.6±18.9 -12.8±20.5 0.9±4.4	- - -
Caiani et al. (59)	End-diastolic volume (ml) End-systolic volume (ml) Ejection fraction (%)	-4.1±29 -3.5±33 -8 ±14	-23±86 -19±60 +3.7±16
Shiota et al. (60)	End-diastolic volume (ml) End-systolic volume (ml) Ejection fraction (%)	-43±65 -37±67 1±4%	- - -
Zeidan et al. (61)	End-diastolic volume (ml) End-systolic volume (ml) Ejection fraction (%)	-6±11 -4±9 2±5%	- - -
Chan et al. (62)	End-diastolic volume (ml) End-systolic volume (ml)	-10.4±26.4 -0.9±18.8	- -
Corsi et al. (63)	End-diastolic volume (ml) End-systolic volume (ml) Ejection fraction (%)	2.9±12 2.8±7 -1±5	- - -
Sugeng et al. (64)	End-diastolic volume (ml) End-systolic volume (ml) Ejection fraction (%)	-4 -1 2	- - -
Nikitin et al. (65)	End-diastolic volume (ml) End-systolic volume (ml) Ejection fraction (%)	7±28 3±22 -1±10	- - -
Jacobs et al. (66)	End-diastolic volume (ml) End-systolic volume (ml) Ejection fraction (%)	-14±17 -6.5±16 -1±6	-23±29 -15±24 1±9
Gutierrez-Chico et al.(67)	End-diastolic volume (ml) End-systolic volume (ml) Ejection fraction (%)	-3±1 2±7 0±6	- - -
Van den Bosch et al. (68)	End-diastolic volume (ml) End-systolic volume (ml) Ejection fraction (%)	-3±12 -12±31 -1±7	- - -
Pouleur et al. (69)	End-diastolic volume (ml) End-systolic volume (ml) Ejection fraction (%)	-20±31 -12±31 1±11	- - -
Qi et al.(70)	End-diastolic volume (ml) End-systolic volume (ml) Ejection fraction (%)	-22±23 -15±20 5±10	- - -
Bicudo et al.(71)	End-diastolic volume (ml) End-systolic volume (ml) Ejection fraction (%)	-4 0.3 -2	- - -
Shimada et al.(56)	End-diastolic volume (ml) End-systolic volume (ml) Ejection fraction (%)	-9.9 -4.7 -0.13	- - -

Abbreviations: 2DE, two-dimensional echocardiography; 3DE, three-dimensional echocardiography; CMR, cardiac magnetic resonance; SD, standard deviation.

Mor-Avi et al. (42), in a multicenter study comparing 3DE and CMR to assess LV volumes, found that LV volumes were highly correlated with CMR (EDV: r = 0.91; ESV: r = 0.93), but were 26% and 29% smaller consistently across institutions, with the magnitude of the bias being inversely related to the level of experience of the operators. They found that the main reason for this underestimation was the limited spatial resolution of 3DE, which cannot provide clear definition of endocardial trabeculae which are, therefore, included into the myocardium rather being part of the LV as it is done when tracing endocardium with CMR.

Female gender and presence of cardiac disease were associated with a larger extent of underestimation.

As a rule, good image quality is a prerequisite for an accurate quantitation of global LV function using semi- or automated border detection algorithms. A manual editing of the automatically-identified endocardial surface may be required in order to ensure an accurate quantitative analysis, particularly in patients with suboptimal image quality. (41,42,72) Some authors reported that LV volume measurements by 3DE are smaller when less than 60% of the endocardial border is visualized; (73) in this setting, the use of contrast agents may improve the accuracy and reproducibility of measurements. (74,75)

Simultaneous LV shape analysis (i.e. 3D sphericity index) is provided from the endocardial 3D surface reconstruction: as the LV becomes more globular, the sphericity index approaches unity. In patients with acute myocardial infarction, 3DE derived sphericity index has been demonstrated to be an earlier and more accurate predictor of LV remodeling than other clinical, ECG, and echocardiographic variable. (76)

By adding an automated detection of the LV epicardial surface and applying 3D speckle-tracking analysis within the LV myocardial wall delimited between the endocardial and epicardial surfaces, additional parameters can be obtained from the same 3D data set: LV

mass (Figure 4.5), as well as myocardial deformation components (longitudinal, circumferential, radial and area strain). (55)

LV mass calculations by M-mode and 2DE are subject to the same limitations in reproducibility and accuracy affecting LV size and function. Several comparative studies (Table 5.2) have proven that 3DE is more accurate than M-mode or 2DE methods to calculate LV mass when CMR was used as reference standard. Inter-observer and test/re-test reproducibility were also improved by the 3DE approach. (57) More accurate measurements of LV mass may facilitate its use as a surrogate outcome marker in trials involving antihypertensive medications. (77)

TABLE 5.2 - Differences between left ventricular mass calculation by three-dimensional echocardiography and conventional two-dimensional echocardiography in comparison with cardiac magnetic resonance.

	Mean difference ±SD from CMR	
Author	**3DE**	**2DE**
Mor-Avi et al. (78)	-4±17	-39±29
Caiani et al. (79)	-2.1±11.5	-34.9±24.8
Jenkins et al. (57)	0±38	16±57
Qin JX et al. (80)	-9±33	-15±47
Oe H. et al. (81)	-14.1±29.1	-10.7±83.7
van den Bosch et al. (82)	2±20	-
Bicudo et al. (71)	-6	-
Takeuchi et al. (83)	-2	-
Pouleur et al. (69)	1±3	-

Abbreviations as in Table 5.1.

3DE provides new opportunities of assessing regional LV wall motion. Conventional 2DE, being confined to several predefined views, actually shows only a very limited part of the whole LV myocardium.

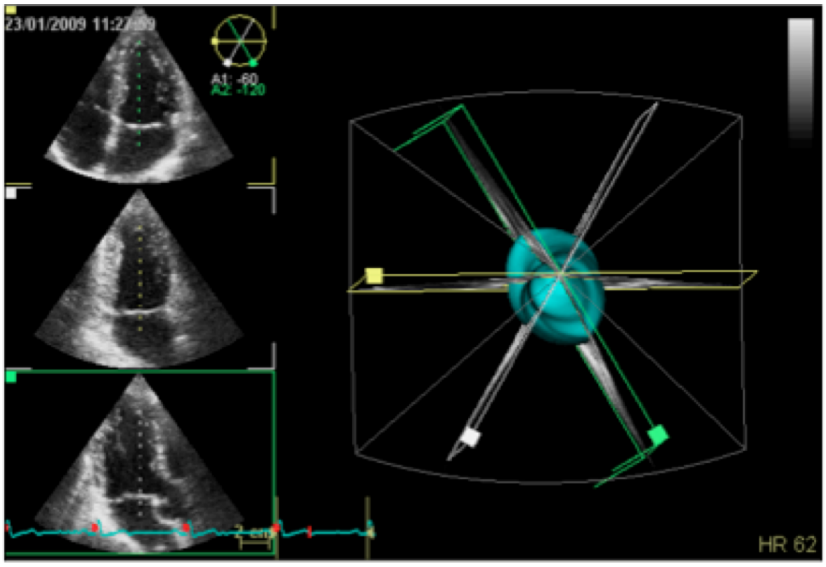

Figure 5.2. Limited actual visualization of left ventricular myocardium with 2DE. Schematic representation of the position of 3 apical views of left ventricle obtainable with conventional 2D echocardiography. As shown, the 3 longitudinal slices cover only a very limited part of left ventricular circumference and cannot be changed anymore once acquired, if proven unsatisfactory or foreshortened.

Conversely, 3DE can display the entire myocardial volume in a multi-slice panel, allowing a comprehensive assessment of the whole LV circumference (Figure 3.10). This display modality can improve the accuracy of visual regional wall motion assessment, because even limited wall motion abnormalities, localized in regions that are not apparent in conventional 2D views, can be visualized. Furthermore, with 3DE, a quantitative analysis of LV regional functional is possible by comparing regional volume variation of each pyramidal-shaped LV segment during the cardiac cycle (Figure 5.1). A good correlation of quantitative 3DE analysis with 2DE regional wall motion score(84) and CMR(85) has been reported. Very recently 3D speckle-tracking technology has been validated for regional wall motion analysis, (86) providing an additional quantitative tool to objectively assess segmental myocardial deformation.

However, despite this impressive amount of data and the fact that both EAE and ASE recommend 3DE, rather than 2DE, for routine clinical assessment of LV geometry and function, (87) the adoption of 3De into routine clinical practice is still limited. The limited availability of reference values, particularly the lack of gender- and anthropometric-based

analysis have hindered the extensive use of 3DE to assess the LV for clinical and research purposes. (87)

5.2 Development of reference values for LV geometry and function by 3DE

Of the 263 healthy volunteers screened for eligibility, 37 (14%) were excluded for: unknown cardiac pathology detected by echocardiography (n=13), obesity (n=4), professional sport activity (n=3), elevated blood pressure levels at enrolment (n=4), premature ventricular contractions (n=2), pregnancy (n=1), right bundle branch block (n=1). Other 7 healthy subjects were excluded due to poor apical acoustic window and 3 due to technical inadequate 3D LV data sets identified during image analysis. Thus, the overall feasibility of LV acquisition and quantitation by 3DE in our study population was 86%.

Temporal resolution of 3D data sets was 34±5 volumes/second, while for 2DE data sets it was 76±7 frames/second. The quality of 3DE data sets for LV quantification was judged subjectively, considering the signal-to-noise ratio, degree of blood-tissue contrast and completeness of LV wall visualization; image quality was excellent in 31%, good in 45%, fair in 20% and poor in 4% of subjects. Manual optimization of endocardial border detection required the addition of a mean of one point (range 0-5) after automatic processing. Manual optimization of epicardial border detection for LV mass measurement required the addition of a mean of 3 points (range 0-7) after automatic processing. The quality of 2D LV data sets for LV quantitation by disc-summation method was verified by calculating the differences in the LV longitudinal axes in 4- vs 2-chamber views; less than 10% difference was found in 96% of subjects at end-diastole and in 90% of them at end-systole.

Table 5.3 summarizes the demographics and the 3DE LV parameters of geometry and function in the study population taken as a whole and separately by gender. Subject age range was 18-76 years, and 45% of enrolled subjects were men. There was no difference in age or heart rate between men and women. However, women showed significantly smaller body size and lower blood pressure levels than men (Table 5.3).

5.2.1 3DE LV volumes and function

LV volumes were larger in men than in women, even after normalization for BSA. Upper reference values (mean + 2 SD) for 3D LV EDV and ESV were 75 ml/m^2 and 34 ml/m^2 in men, and 72 ml/m^2 and 28 ml/m^2 in women, respectively.

TABLE 5.3 - Demographics and parameters of left ventricular geometry and function obtained by three-dimensional echocardiography in the study population.

	All (n=226)	**Men** (n=101)	**Women** (n=125)	p Value
Age (years)	44±14	43±14	44±15	0.584
Height (cm)	170±9	177±7	164±7	<0.0001
Weight (kg)	68±11	76±9	61±8	<0.0001
Body mass index (kg/m^2)	23±3	24±3	22±3	<0.0001
BSA (m^2)	1.78±0.18	1.93±0.13	1.66±0.12	<0.0001
Heart rate (bpm)	67±10	67±11	68±10	0.338
Systolic BP (mmHg)	123±14	128±12	118±14	<0.0001
Diastolic BP (mmHg)	74±8	77±8	71±9	<0.0001
LV EDV (ml)	106±25	123±25	93±16	<0.0001
LV EDV/BSA (ml/m^2)	59±10	63±11	56±8	<0.0001
LV ESV (ml)	39±11	46±10	33±7	<0.0001
LV ESV/BSA (ml/m^2)	22±5	24±5	20±4	<0.0001
LV SV (ml)	68±15	76±16	60±12	<0.0001
LV SV/BSA (ml/ m^2)	38±6	39±7	36±6	0.001
LV EF (%)	64±4	62±4	65±4	<0.0001
LV mass (g)	135±23	150±22	124±16	<0.0001
LV mass/BSA (g/m^2)	76±9	77±10	74±8	0.023
LV end-diastolic sphericity index	0.35±0.07	0.35±0.07	0.34±0.07	0.838
LV mass/EDV (g/ml)	1.30±0.2	1.24±0.18	1.30±0.18	<0.0001

Data is expressed as mean±SD.
Abbreviations: BP, blood pressure; BSA, body surface area; EDV, end-diastolic volume; EF, ejection fraction; ESV, end-systolic; LV, left ventricular; SV, stroke volume.

As expected, LV EDV and ESV calculated on 2DE images were significantly smaller than those measured from 3DE data sets.

TABLE 5.4 - Comparison of parameters of left ventricular geometry and function obtained by three-dimensional echocardiography with those derived from two-dimensional echocardiography.

	3DE	2DE	p Value	3DE upper limit	2DE upper limit
EDV (ml)	107±25	97±25	<0.0001	157	147
ESV (ml)	39±11	35±11	<0.0001	61	57
Sphericity index	0.35±0.07	0.34±0.06	0.35	0.49	0.46
EF (%)	64±4	65±4	<0.0001	56*	57*

*lower limit.

Abbreaviations: 3DE, three-dimensional echocardiography; 2DE, two-dimensional echocardiography. Other abbreviations as in Table 5.3

5.2.2 Relationships with gender, age and body size

LV EF was significantly higher in women (Table 5.3). However, since LV volumes in women were smaller, LV SV in women was also found to be significantly smaller than in men and this difference persisted after normalization for BSA. Lower reference values (mean - 2SD) for LV EF were 54% in men and 57% in women, while for SV were 25 ml/m^2 and 24 ml/m^2 using BSA, respectively. LV EF was significantly smaller with 3DE than with 2DE, but this difference was clinically irrelevant (Table 5.4, Figure 5.3). LV SV measured with 3DE was significantly lower than the LV SV calculated using conventional 2D-Doppler method (76±16 ml vs 94±20 ml in men and 60±12 ml vs 75±12 ml in women, p<0.0001 for both) (Figure 5.3).

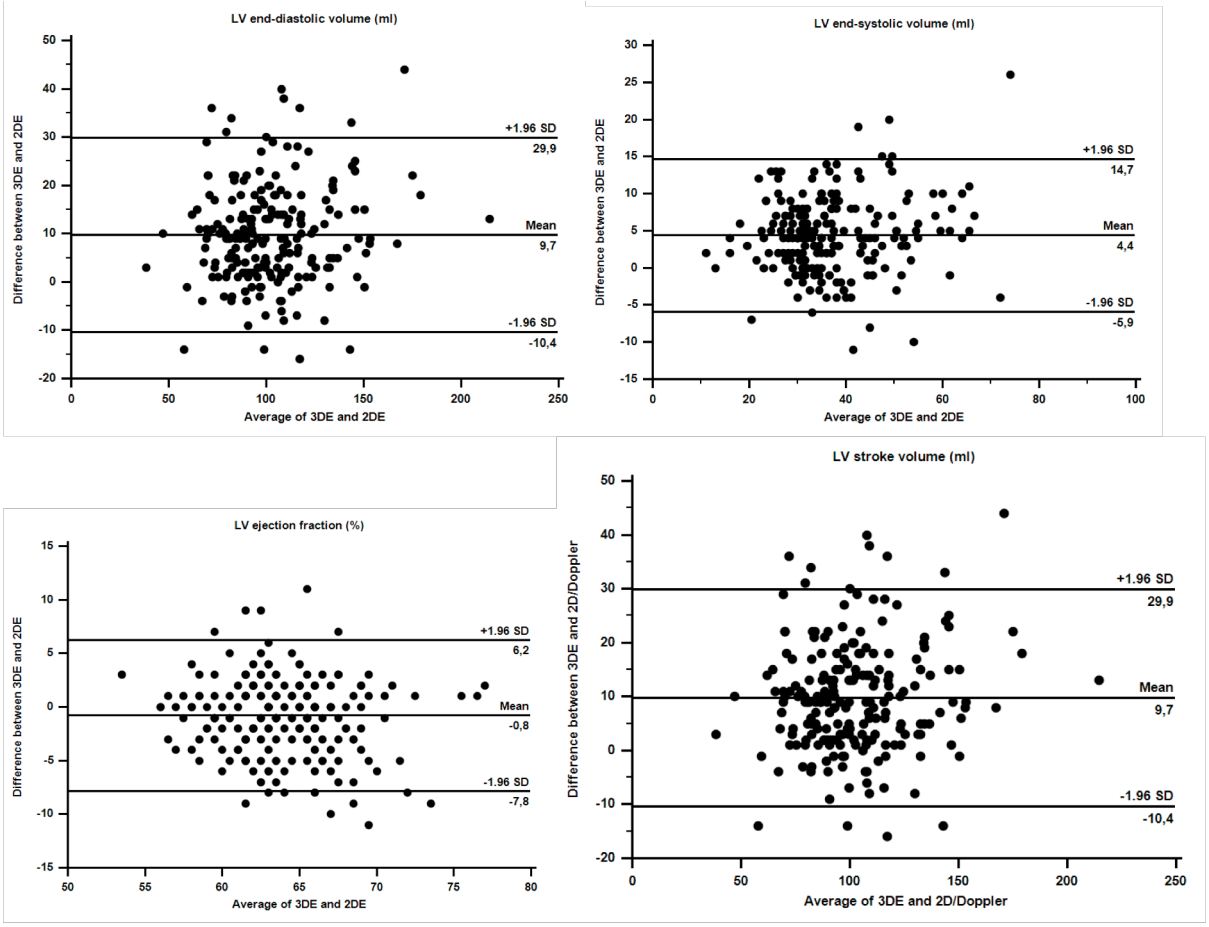

Figure 5.3. Bland-Altman plots comparing left ventricular volumes, ejection fraction and stroke volume obtained by three- and two–dimensional echocardiography.

LV shape assessed in terms of sphericity index measured at end-diastole was similar between genders (Table 5.3). Overall, the end-diastolic LV longitudinal axis was longer by 3DE (8.4±0.7 cm) than its average calculated from 2DE 4- and 2-chamber views (8.2±0.7 cm, $p<0.0001$), reflecting LV foreshortening and accounting, at least in part, for the smaller LV volumes by 2DE. When 3DE LV end-diastolic sphericity index was compared with the corresponding values obtained by 2DE, no significant differences in LV shape were identified (Table 5.4).

LV mass was significantly larger in men than in women and this difference persisted even after indexation by body surface area (Table 5.3). Conversely, the LV mass/volume ratio was significantly higher in women than in men. Upper limits of reference values (mean+2 SD) were 97 g/m^2 and 90 g/m^2 for 3DE LV mass/BSA, and 1.6 and 1.66 for 3D mass/volume ratio

in men and women, respectively. LV mass measured with 3DE was significantly lower than the value calculated using the M-mode formula in both men (150±22 g vs 171±35 g) and women (124±16 g vs 141±30 g) ($p<0.0001$ for both).

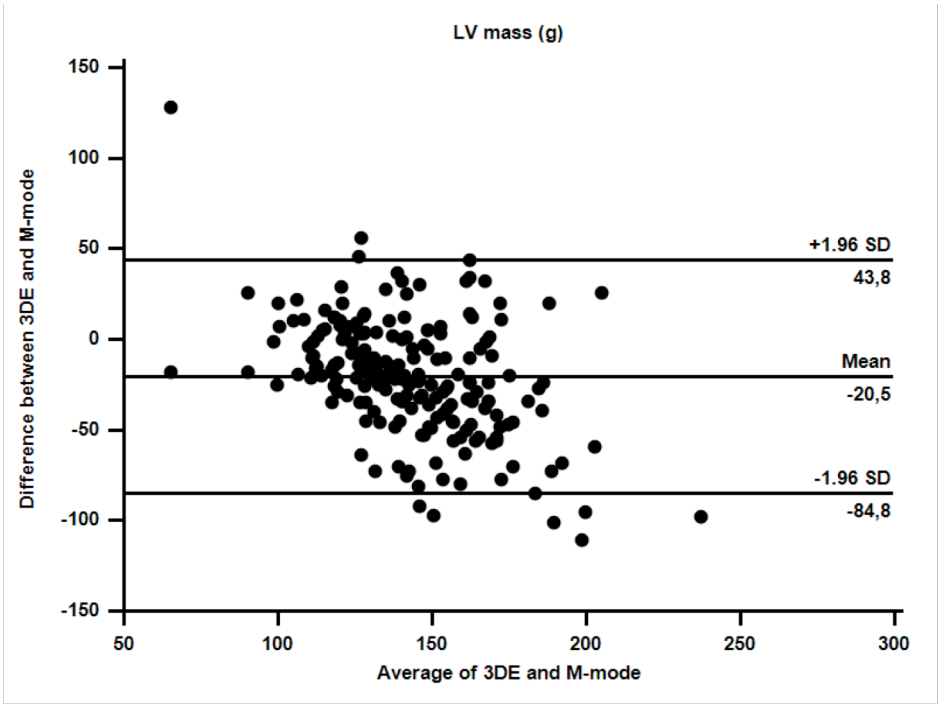

Figure 6.4. Bland-Altman plot comparing measurements of left ventricular mass with three- dimensional and M-mode echocardiography.

Table 5.5 summarizes the relationship of LV parameters with age.

LV volumes decreased with ageing in both genders. These relationships were still evident after indexation for both BSA, and were closer in women than in men. 3DE SV and LV EF did not show any significant relationship with age in men, but SV decreased and LV EF increased significantly with age in women. There was no correlation between age and LV mass or LV mass indexed by BSA in men, while LV mass decreased with age in women. The mass/volume ratio increased with age in both genders.

TABLE 5.5 - Relationship between left ventricular parameters by three-dimensional echocardiography and age for both genders.

	Men (n=101)		**Women** (n=125)	
	r	p value	r	p value
EDV (ml)	-0.25	0.014	-0.36	<0.0001
EDV/BSA (ml/m^2)	-0.25	0.012	-0.42	<0.0001
ESV (ml)	-0.28	0.005	-0.44	<0.0001
ESV/BSA (ml/m^2)	-0.28	0.005	-0.49	<0.0001
SV (ml)	-0.20	0.052	-0.20	0.031
SV/BSA (ml/ m^2)	-0.20	0.053	-0.25	0.005
EF (%)	0.18	0.067	0.28	0.002
Mass (g)	0.01	0.940	-0.18	0.050
Mass/BSA (g/m^2)	0.03	0.749	-0.20	0.024
Sphericity index	0.16	0.107	0.10	0.256
Mass/EDV (g/ml)	0.32	0.001	0.29	0.001

Abbreviations as in Table 5.2.

Finally, Table 5.6 reports the reference values for LV geometry and function grouped in the young (18-39 years), middle age (40 -59 years) and elderly (≥ 60 years) cohorts.

TABLE 5.6 - Left ventricular geometry and function by three-dimensional echocardiography presented by age groups in men and women.

	18-39 years			40-59 years			≥60 years		
	Men (n=40)	Women (n=44)	p Value	Men (n=38)	Women (n=54)	p Value	Men (n=24)	Women (n=26)	p Value
EDV (ml)	128±27 (182)	98±16 (130)	<0.0001	119±21 (161)	94±16 (126)	<0.0001	116±26 (168)	84±12 (108)	<0.0001
EDV/BSA (ml/m^2)	66±11 (88)	60±8 (76)	0.001	61±9 (79)	56±8 (72)	0.021	62±12 (86)	51±7 (65)	0.001
ESV (ml)	50±11 (72)	36±7 (50)	<0.0001	44±9 (62)	33±5 (43)	<0.0001	44±11 (66)	28±6 (40)	<0.0001
ESV/BSA (ml/m^2)	26±5 (36)	22±4 (30)	<0.0001	23±4 (31)	20±3 (26)	<0.0001	23±5 (33)	17±4 (25)	<0.0001
SV (ml)	78±17 (44)*	62±10 (42)*	<0.0001	75±13 (49)*	60±14 (32)*	<0.0001	74±15 (44)*	56±9 (38)*	<0.0001
SV/BSA (ml/m^2)	41±7 (27)*	37±5 (27)*	0.027	38±6 (24)*	36±6 (24)*	0.261	39±7 (25)*	34±5 (24)*	0.016
EF (%)	61±4 (53)*	63±3 (57)*	0.016	63±3 (57)*	65±4 (57)*	0.009	63±3 (57)*	66±5 (56)*	0.008
Mass (g)	149±22 (193)	124±15 (154)	<0.0001	150±22 (194)	126±16 (158)	<0.0001	150±23 (196)	118±19 (156)	<0.0001
Mass/BSA (g/m^2)	78±9 (96)	75±8 (91)	0.250	76±11 (98)	75±8 (91)	0.450	79±10 (99)	72±10 (92)	0.027
Mass/BSA (g/m^2)	112±16 (144)	96±11 (118)	<0.0001	113±13 (139)	98±11 (120)	<0.0001	113±15 (143)	92±14 (120)	<0.0001
Mass/EDV (g/ml)	1.19±0.16 (1.51)	1.29±0.16 (1.61)	0.004	1.28±0.20 (1.68)	1.35±0.20 (1.75)	0.078	1.29±0.18 (1.65)	1.42±0.15 (1.72)	0.013
Sphericity index	0.33±0.06 (0.45)	0.34±0.07 (0.48)	0.827	0.35±0.08 (0.51)	0.34±0.06 (0.46)	0.807	0.37±0.08 (0.53)	0.36±0.07 (0.50)	0.684

Data are reported as mean value±SD (upper or *lower limits of normality).

Abbreviations as in Table 5.2.

5.2.3. Comparison with previous studies

Comparisons of our findings with the 3D LV reference values from previous studies are reported in Table 5.7.

TABLE 5.7 - Data comparison with other two studies reporting left ventricular parameters obtained by three-dimensional echocardiography in healthy subjects.

Author	Present study(9)		Aune et al. (88)		Fukuda et al.(89)	
Echo machine	Vivid E9		iE33		Sonos 7500/iE33	
Gender	Men	Women	Men	Women	Men	Women
Sample size	(n=101)	(n=125)	(n=79)	(n=87)	(n=222)	(n=134)
EDV/BSA (ml/m^2)	63±11	56±8	66±10	58±8	50±12*	46±9*
ESV/BSA (ml/m^2)	24±5	20±4	29±6*	23±5*	19±5*	17±4*
SV/BSA (ml/m^2)	39±7	36±6	-	-	-	-
EF (%)	62±4	65±4	57±4*	61±6*	61±4†	63±4*
Mass (g/m^2)	77±10	74±8	-	-	64±12*	56±11*
Mass/EDV (g/ml)	1.24±0.18	1.30±0.18	-	-	1.3±0.3	1.3±0.2

*<0.0001; †<0.05. Abbreviations as in Table 5.1.

5.2.4 Reproducibility.

Three-dimensional LV parameters showed an excellent intra-observer and inter-observer reproducibility (Table 5.8). In comparison with 3D parameters, 2D LV volumes and particularly 2D LV EF showed more variability at repeated measurements: for 2D LV EDV ICC were 0.970 and 0.945; for 2D LV ESV ICC were 0.963 and 0.957; for 2D LV ejection fraction ICC were 0.741 and 0.742 for intra- and inter-observer analysis, respectively.

TABLE 5.8 - Reproducibility of left ventricular geometry and function parameters by three-dimensional echocardiography in 15 healthy subjects.

	Intra-observer			Inter-observer		
	CR	ICC*	95% CI	CR	ICC*	95% CI
EDV (mL)	8.5	0.998	0.968-0.996	9.3	0.990	0.971-0.997
ESV (mL)	5.5	0.982	0.947-0.994	5.4	0.981	0.944-0.993
EF (%)	2.9	0.906	0.745-0.968	3.7	0.816	0.536-0.934
SV (mL)	6.1	0.980	0.942-0.993	8.9	0.967	0.905-0.989
Sphericity index	0.06	0.878	0.675-0.957	0.06	0.914	0.764-0.970
Mass (g)	10.2	0.863	0.640-0.952	17.0	0.875	0.668-0.956

*p<0.0001. *CI*, confidence interval; *CR*, coefficient of repeatability; *ICC*, intraclass correlation coefficient

5.3 Discussion

The present study provides a comprehensive analysis of LV geometry and function using 3DE in a relatively large cohort of Caucasian healthy volunteers with a wide age range. The main results can be summarized as follows: (i). Reference values for LV volumes and mass by 3DE were found to be significantly different from those obtained with conventional echocardiography, highlighting the importance of applying method-specific reference values for a reliable identification of LV dysfunction; (ii). LV parameters measured by 3DE had excellent reproducibility, and were more robust than 2D indices (particularly regarding LV EF) at repeated measurements; (iii). Most LV indices should be defined according to age and gender, since indexing them only for BSA does not account for all variations in LV geometry and function.

5.3.1 Method-specific reference values for LV geometry and function by 3DE.

LV volumes, EF and spherical shape are powerful predictors of morbidity and mortality in both clinical and population studies. However, LV parameters derived from conventional echocardiography (M-mode, 2DE and Doppler) are based on a limited number of actual measurements. In fact, they mostly derive from calculations involving several assumptions on LV geometry (i.e. LV wall thickness distribution, LV outflow tract circularity etc) and on their anatomically-correct imaging by 2DE, despite a significant error may result from restricted imaging capabilities inherent to a tomographic technique, foreshortening errors or insufficient experience in image acquisition or analysis. Hence, despite these LV indices are of utmost clinical importance, traditional echocardiographic methods are inherently flawed. This has been demonstrated by several studies comparing the accuracy of 2DE with CMR or cardiac computerized tomography. (90) Since CMR and cardiac computerized tomography have also their own limitations such as limited availability, costs, time consumption, use of contrast agents and radiation exposure (for cardiac computerized tomography only), there is a need of a robust non-invasive imaging modality to be routinely used to quantify LV performance and remodelling in patients with known or suspected cardiovascular disease. 3DE measurements are neither affected by cardiac chamber foreshortening nor by any geometric assumptions. Specifically, previous studies have shown that 3DE is not only accurate in measuring LV volumes and mass when compared with CMR, (1) but it is also more reproducible than 2DE, demonstrating a low observer and test/re-test variability. (57,69,87) However, the lack of specific reference values for 3DE might have hindered, at least partially, the use of 3DE in clinical practice and research. Available recommendations on LV quantification (38) rely either on 2DE- or M-mode -derived cut-off values to define normality of LV volumes, EF or mass, and to date there is no clear evidence that these reference values

can be extrapolated for 3DE measurements. Studies comparing 3DE and 2DE with CMR in patients reported that LV volumes by 3DE were significantly larger than those obtained with 2DE (41,91), while 3DE LV mass was larger than the value obtained by 2DE (78) and smaller than the one calculated using cubed formula by M-mode echocardiography. (92,93) Our findings in healthy subjects demonstrate that LV reference values from conventional echocardiography should not be used interchangeably with 3D LV volumes and mass, emphasizing once more that method-specific normality ranges should be applied for clinical decision-making. In addition, an excellent intra- and inter-observer reproducibility for 3DE parameters was confirmed in our study, as well as the superiority of 3DE in comparison with 2DE regarding LV volumes and ejection fraction measurement reproducibility.

5.3.2 Comparison with LV reference values from other 3DE and CMR studies.

To our knowledge, four studies have previously reported reference values for LV geometry and function in healthy subjects using 3DE and all have used BSA to index LV volumes and mass. Aune et al. (88) studied 166 healthy Norvegian subjects (46% males, 29-80 years) and found reference values very similar to ours (differences in upper limits of normality for end-diastolic and end-systolic LV volumes of 2 and 1 ml/m^2, respectively). Kaku et al. (13) studied the effect of aging on LV geometry and function in 280 healthy US and Japanese subjects (49% men, age 1-88 years). LV volumes and mass in their adult subgroup were very similar to the ones obtained in our cohorts. Finally, Fukuda et al. (89) recently reported reference data for the LV and LA obtained in 222 Japanese healthy subjects (61% me, age 20-69 years). Their reference values for LV EDVs were smaller than ours (-13 ml/m^2 in men and -10 ml/m^2 in women), but they studied Japanese subjects with smaller BSA (1.8 m^2 in men and 1.5 m^2 in women). It is possible that race or ethnicity-specific 3DE reference values for the LV need to be identified as well, however only a multicenter study specifically

designed for this purpose or a meta-analysis of existing data(94) could clarify for this aspect.

Recently, Chahal et al. (95) reported average values of 49±9 ml/m^2 and 42±8 ml/m^2 for 3DE LV EDVs in healthy European men and women, respectively. These volumes are significantly smaller than those reported in our study and by the other Authors who performed similar studies: 66±10 ml/m^2 and 58±8 ml/m^2, respectively, found by Aune et al. (88); and 55±7 ml/m^2 and 49±6 ml/m^2, respectively, reported by Kaku et al. (25) for the same age group. Even Fukuda et al. (89) in their Japanese population (significantly smaller body size than Europeans) found larger LV EDVs: 50±12 ml/m^2 and 46±9 ml/m^2 in men and women, respectively. Furthermore, the upper normal values (mean values+2 SDs) for 3DE LV EDVs and ESVs reported by Chahal et al. (95) (e.g. 67 ml/m^2 and 29 ml/m^2 in men) are smaller than the 2DE upper normal limits reported in current guidelines (75 ml/m^2 and 30 ml/m^2, respectively)(38), contradicting all previous studies showing a larger underestimation of LV volumes measured by 2DE than by 3DE. Finally, making a simple calculation from the data in the Table 1 included in the paper by Cahal et al. (95), it seems that the European subjects were in low flow state (average SV index 30 ml/m^2 in men, and 26 ml/m^2 in women). These data raise the issue of the accuracy of the measurements performed in that study, particularly when no reference (or at least comparison) modality such as the simple SV measured with 2DE and Doppler has been provided. One possible explanation of the underestimation of the LV volumes reported by Chahal et al. (95) may be the limited experience of the sonographers who performed measurements as acknowledged by the Authors ("*…all underwent a 4-wk period of training in 3DE volume acquisition and off-line analysis by the vendor representative at the beginning of the study*"). (96) The effect of the reader experience on accuracy of 3D LV volume measurements has already been documented. (42)

Hudsmith et al. (97) have reported the upper normal limits (mean + 2SD) for LV EDV and ESV by CMR in 108 apparently healthy subjects (58% men): 106 ml/m^2 in men and 39 ml/m^2 in women. The upper limits for LV volumes in the study of Hudsmith et al. (97) exceeded our corresponding values for LV EDVs with 19% in men and 34% in women, while ESVs were very similar. An underestimation of LV volumes obtained by 3DE in comparison to CMR has also been documented by the recently performed meta-analysis by Dorosz et al. (90) They reviewed data from 23 studies enrolling 1,638 echocardiograms and found pooled biases ± 2SDs for 3DE of -19±34 ml, -10±30 ml, and 0.6±12% for LV EDV, ESV and EF, respectively. Mor-Avi et al. (42), in a multicenter study comparing 3DE and CMR found that 3DE LV volumes were highly correlated with CMR measurements (EDV: r = 0.91; ESV: r = 0.93), but were 26% and 29% lower, consistently across institutions, with a bias magnitude inversely related to the level of experience of the operators. They found that the main reason for this underestimation was the limited spatial resolution of 3DE, which cannot provide clear definition of endocardial trabeculae which are, therefore, included into the myocardium rather being part of the LV as it is done when tracing endocardium with CMR. Greater underestimation seems to occur for LV EDVs and this is consistent with the fact that our reference values for EDV were significantly lower than those reported by Hudsmith et al. (97) while ESVs were closer. The same issue about the underestimation of the LV EDVs with 3DE has been reported by Aune et al. (88). This limitation may have contributed to the underestimation of the SV by 3DE in comparison with conventional 2D-Doppler method in our study.

In a recent meta-analysis, Dorosz et al. (90) have also identified significantly larger biases and limits of agreement for 2DE (-48±56 ml, -28±46 ml, and 0.1±14% for LV volumes and EF) than 3DE, when both were compared to CMR. These data, together with the superior reproducibility of 3DE warrant its use as the preferred method to assess LV size and function

by echocardiography.

5.3.3 Relationship with gender and age.

Our findings show that reference values for most LV size and function parameters should be gender-specific since the simple normalization of LV volumes by BSA does not eliminate gender differences for these parameters. These findings are consistent with the data reported by other similar studies(13,89,98). LV mass/volume ratio and ejection fraction were also significantly higher in women than in men. Conversely, LV sphericity index was similar in men and women. These gender differences in LV geometry and function are consistent with previous reports in which both 3DE and CMR were used (13,97).

It is widely accepted that age-related changes in cardiovascular structure and function occur in healthy subjects. In our study population, LV size decreased with age, whereas LV mass and shape did not change. As a result the LV mass/volume ratio increased with age. These age-related changes evolving as a concentric LV remodelling, and interpreted as a "physiological" response to increased arterial pressure and afterload with age (99,100), were particularly evident in women. LV volume reductions are compensated by an increase in LV ejection fraction (which was statistically significant in women in our study) to maintain cardiac output. Our findings are consistent with those reported by others who used either echocardiography(13) or CMR (91,99) to assess age-related changes in LV morphology and function.

CHAPTER 6

Reference values for right ventricular geometry and function by three-dimensional echocardiography

6.1 Background

2DE quantification of RV size and function is challenging, due to the anterior position of the RV in the chest, its complex asymmetric geometry, irregularity of the highly trabeculated endocardial border, impossibility to visualize in the same view both inflow and outflow tracts and lack of realistic geometric models to use for volume calculation. (101) 3DE has been demonstrated to have a good accuracy in measuring RV volumes compared to CMR. (102)

A good correlation between CMR and 3DE parameters reflecting RV geometry and function has been demonstrated, although, as for the LV, an underestimation of 3DE RV volumes is often reported (Table 6.1). Shimada et al. (102) reported that the underestimation of RV volumes occurs mainly with large EDVs, whereas an overestimation was more likely for smaller ESVs. Age accounted for a part of the error, RV volumes being overestimated and RV EF underestimated in the elderly. Possible reasons for this systematic bias may be the poorly-defined endocardial border in a dilated RV, the non-inclusion of RV outflow tract in the analysis and the limited temporal resolution. In a recent study, Tamborini et al. (103) proposed reference values for RV volumes and EF obtained from 245 normal subjects. RV volumes were significantly correlated with age, gender and BSA.

TABLE 6.1 - Differences between right ventricular volumes assessed by three-dimensional echocardiography and cardiac magnetic resonance.

		Mean difference (95% CI) from CMR
Author	**Parameter**	**3DE**
Shimada et al. (102)	End-diastolic volume (ml)	-14 (-18, -10)
	End-systolic volume (ml)	-6 (-8, -3)
	Ejection fraction (%)	-1 (-2, -0,1)
Grapsa et al. (104)	End-diastolic volume (ml)	-4 (-11, 4)
	End-systolic volume (ml)	0 (-6, 6)
	Ejection fraction (%)	-1 (-3, 0)
Sugeng et al. (105)	End-diastolic volume (ml)	-14 (-28, 0)
	End-systolic volume (ml)	-9 (-19, 1)
	Ejection fraction (%)	-2 (-4, 0)
Van der Zwaan et al (46)	End-diastolic volume (ml)	-34 (-43, -25)
	End-systolic volume (ml)	-11 (-19, 3)
	Ejection fraction (%)	-4 (-6, -2)
Leibundgut et al. (45)	End-diastolic volume (ml)	-10 (-15, -6)
	End-systolic volume (ml)	-5 (-8, -1)
	Ejection fraction (%)	0 (-2, 1)

CI, confidence interval. Other abbreviations as in Table 5.1

Amaki et al. (106) demonstrated that RV quantification by 3DE can be accurately performed also in patients with pulmonary hypertension. They reported that the abnormal end-diastolic interventricular septal convexity visualized by 3DE was a predictor of mortality.

In congenital heart diseases, RV volumes are important predictors of patient outcome, may help in choosing the timing of interventions and in monitoring the post-surgical result. An added value of 3DE is the ability of quantificating RV function after surgery, when TAPSE and RV myocardial velocities by tissue-Doppler are no longer reliable indicators of global systolic performance. (107,108)

6.2 Development of reference values for RV geometry and function by 3DE

Analysis of 3D RV volumes and EF was feasible in 507 of the 542 healthy subjects enrolled in this multicenter study. The overall feasibility of 3DE was very similar among centers: 94% for Padua, 93% for Naples, and 93% for Milan.

TABLE 6.2 - Clinical, echocardiographic and demographic characteristics of the study population.

	All (n=507)	**Women** (n=260)	**Men** (n=247)	**p-value**
Age (years)	45±16	47±16	43±16	<0.01
Height (m)	170±9	164±6	177±7	<0.01
Weight (kg)	69±12	61±9	77±10	<0.01
BMI (kg/m^2)	23.8±3.3	23.0±3.4	24.7±3.0	<0.01
BSA (m^2)	1.79±0.19	1.66±0.12	1.93±0.14	<0.01
Systolic BP (mmHg)	121±15	117±14	125±14	<0.01
Diastolic BP (mmHg)	73±10	71±10	75±9	<0.01
Heart rate (bpm)	68±11	69±11	67±11	0.02
RV systolic pressure (mmHg)	24.5±5.4	24.7±5.3	24.2±5.6	0.37
TAPSE (mm)	24.7±3.0	24.5±2.8	24.9±3.2	0.22
RV ED Area (cm^2)	18.0±4.2	15.7±2.8	20.8±3.9	<0.01
RV ES Area (cm^2)	9.2±2.6	7.9±1.8	10.8±2.6	<0.01
RV FAC (%)	49±8	50±7	48±8	<0.01
LV EDV (mL)	95±20	83±13	108±18	<0.01
LV ESV (mL)	36±11	30±8	42±11	<0.01
LV EF (%)	63±7	64±7	62±7	<0.01

p-value refers to unpaired Student's t-test, Women vs Men.
Abbreviations: bpm, beats per minute; BMI, body mass index; EDA, end-diastolic area; ESA, end-systolic area; FAC, fractional area change; RV, right ventricular; TAPSE, tricuspid annulus peak systolic excursion. Other abbreviations as in Table 5.3.

The age of the study cohort ranged between 18 and 90 years, with a slight prevalence of women (51%). At least 37 subjects per age decade were included in the study (mean 85±27 subjects per age decade), having a similar gender distribution among age decades (p=0.13). All anthropometric

measurements were greater in men than in women. Male gender was associated with larger LV volumes and RV areas, and lower LV EF and RV FAC, while TAPSE, heart rate and RV systolic pressure were similar in men and women (Table 7.2).

6.2.1 3D RV Volumes and Function.

As expected, gender effect was largely significant in all age groups, with RV volumes larger in men than in women.

TABLE 6.3 - Normal ranges for 3DE right ventricular end-diastolic volume, end-systolic volume and ejection fraction by gender and age decade. Unless otherwise stated, all Women vs Men comparisons are significant ($p<0.01$).

		RV End-diastolic Volume (mL)			**RV End-systolic Volume** (mL)		
Age (years)	**n** (Women, Men)	All	Women	Men	All	Women	Men
<30	114 (46,68)	105 (69,183)	88 (66,136)	122 (80,189)	46 (18,88)	35 (14,71)	51 (30,94)
30-39	98 (50,48)	92 (64,147)	85 (63,117)	114 (72,153)	36 (18,67)	31 (17,52)	45 (25,66)
40-49	98 (53,45)	90 (63,132)	82 (64,106)	101 (75,137)	35 (16,54)	30 (15,44)	40 (23,62)
50-59	91 (49,42)	90 (62,138)	79 (62,117)	101 (72,138)	33 (18,62)	29 (18,46)	37 (22,63)
60-69	69 (39,30)	85 (47,139)	79 (43,100)	98 (76,149)	32 (14,61)	30 (13,40)	37 (20,68)
≥70	37 (23,14)	77 (50, 125)	70 (51,86)	98 (64,129)	23 (11,53)	20 (12,32)	34 (18,54)
All	507 (260,247)	91 (61,150)	81 (58,120)	107 (74,163)	35 (16,72)	30 (15,52)	44 (22,80)
		RV Stroke Volume (mL)			**RV Ejection Fraction** (%)		
Age (years)	**n** (Women, Men)	All	Women	Men	All	Women	Men
<30	114 (46,68)	63 (41,95)	56 (42,77)	69 (41,101)	58 (42,75)	60 (45,80)	56 (42,68)
30-39	98 (50,48)	60 (36, 93)	56 (38,72)	68 (37,97)	61 (48,76)	63 (52,77)	60 (48,72)
40-49	98 (53,45)	56 (37,82)	51 (39,71)	63 (39,86)	63 (51,79)	65 (50,79)	61 (51,75)
50-59	91 (49,42)	56 (35,78)	50 (35,68)	63 (44,84)	62 (46,75)	62 (47,76)	62 (45,73), p=0.51
60-69	69 (39,30)	52 (28,85)	49 (25,61)	64 (48,88)	61 (50,79)	61 (53,75)	63 (50,78), p=0.75
≥70	37 (23,14)	54 (31,77)	49 (31,64)	61 (45,79)	68 (56,81)	71 (60,81)	65 (56,75)
All	507 (260,247)	57 (36,87)	52 (35,72)	66 (40,91)	62 (47,77)	63 (49,79)	60 (45,75)

Data expressed median (5^{th}, 95^{th} percentile). p-value refers to unpaired Student's t-test, Women vs Men. Abbreviations as in Table 6.2.

Overall, RV EF was lower in men than in women, even if this difference was not significant in all age groups.

RV EDV and ESV were significantly larger in men than in women and these differences persist even after adjusting for body size.

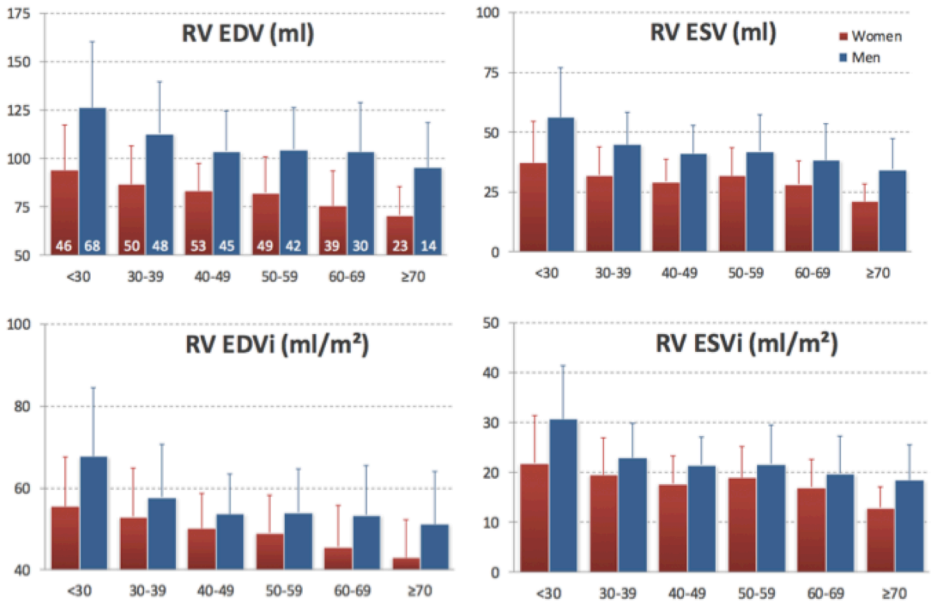

Figure 6.1. Right ventricular end-diastolic (left panels) and end-systolic (right panels) volume in absolute values (upper panels) and indexed to body surface area; values are shown as mean±SD, separately for women and men.
The numbers indicate the number of patients in each age decade (women, men).

6.2.2 Relationship with age, gender and body size.

The relationship of RV measurements with age and anthropometric data was explored using bivariate and multivariate linear regressions.

TABLE 6.4 - Results of the bivariate correlations (pearson correlation) between right ventricular volumes and ejection fraction, age, and body size parameters (i.e. height, weight, BMI and BSA)

	RV EDV	RV ESV	RV SV	RV EF
Age	-0.36*	-0.37*	-0.25*	0.24*
Height	0.54*	0.46*	0.49*	-0.20*
Weight	0.47*	0.38*	0.44*	-0.16*
BMI	0.17*	0.13*	0.17*	-0.05
BSA	0.55*	0.45*	0.50*	-0.19*

*: correlation is significant at the 0.01 level (two-tailed t test)

Abbreviations as in Table 6.2.

RV volumes showed a progressive reduction with age in both genders, and this effect was more pronounced in women. Conversely, RV EF increased with age, and was inversely related to body size. Among body size measurements, BMI showed the weakest correlation with RV volumes, and no correlation with EF. For this reason, BSA has been preferred to BMI in multivariate analysis. Heart rate was found negatively associated with RV volumes (EDV, r=-0.16; ESV, r=-0.17; SV, r=-0.09) and positively with EF (r=0.13).

Multivariate analysis was performed introducing different sets of predictors: model AGr included age and gender; model AGBr, age, gender and BSA; model AGHWr considered age, gender, height and weight. The latter model, considering height and weight separately, avoided the assumptions proper of BSA, while it allowing to account for differences in body size. (7) Age and gender were independently associated with RV volumes and function.

TABLE 6.5 - Results of the multivariate linear regression for right ventricular measurements, adjusted for gender, and age (Model AGr, ratiometric), age and BSA (Model AGBr, ratiometric, or Model AGBa, allometric), age, height and weight (Model AGHWr, ratiometric). Data presented as model coefficient (β), 95% confidence interval (CI), and Pearson's correlation coefficient (r^2).

	RV EDV (ml)		**RV ESV** (ml)		**RV SV** (mL)		**RV EF** (%)	
	β (95% CI)	r^2	β (95% CI)	r^2	β (95% CI)	r^2	β (95% CI)	r^2
Model AGr		0.34		0.29		0.22		0.10
Constant	108.2 (101.6, 114.7)*		46.6 (42.6, 50.6)*		61.6 (57.6, 65.5)*		58.0 (55.6, 60.4)*	
Gender	25.9 (21.9, 30.0)*		13.3 (10.8, 15.7)*		12.7 (10.2, 15.1)*		-3.4 (-4.9, -1.9)*	
Age (years)	-0.53 (-0.66, -0.40)*		-0.34 (-0.41, -0.26)*		-0.19 (-0.27, -0.12)*		0.12 (0.08, 0.17)*	
Model AGBr		0.42		0.34		0.30		0.10
Constant	15.7 (-9.6, 41.0)		7.1 (-8.9, 23.2)		8.6 (-6.8, 23.9)		62.0 (52.0, 71.9)*	
Gender	11.4 (5.9, 17.0)*		7.3 (3.7, 10.8)*		4.2 (0.8, 7.6)*		-2.9 (-5.1, -0.7)*	
Age (years)	-0.55 (-0.67, -0.43)*		-0.35 (-0.43, -0.27)*		-0.20 (-0.27, -0.12)*		0.13 (0.08, 0.18)*	
BSA (m^2)	56.2 (41.5, 70.9)*		24.2 (14.9, 33.5)*		32.0 (23.1, 40.9)*		-2.5 (-8.3, 3.2)	
Model AGHWr		0.42		0.34		0.30		0.10
Constant	-15.5 (-66.8, 35.9)		-0.2 (-32.8, 32.4)		-15.2 (-46.4, 15.9)		55.8 (35.7, 76.0)*	
Gender	11.2 (5.4, 16.9)*		7.4 (3.7, 11.0)*		3.8 (0.3, 7.3)*		-3.2 (-5.4, -0.9)*	
Age (years)	-0.53 (-0.66, -0.40)*		-0.35 (-0.43, -0.27)*		-0.18 (-0.26, -0.10)*		0.13 (0.08, 0.18)*	
Height (cm)	0.55 (0.23, 0.88)*		0.19 (0.01, 0.40)*		0.36 (0.16, 0.55)*		0.03 (-0.10, 0.16)	
Weight (kg)	0.55 (0.32,0.77)*		0.25 (0.11, 0.40)*		0.29 (0.16, 0.43)*		-0.05 (-0.14, 0.04)	
Model AGBa		0.43		0.35		0.28		0.11
Constant	4.79 (4.56, 5.02)*		4.19 (3.80, 4.18)*		4.01 (3.76, 4.26)*		3.83 (3.67, 3.98)*	
Gender	0.11 (0.06, 0.17)*		0.18 (0.09, 0.27)*		0.07 (0.01, 0.13)*		-0.05 (-0.08, -0.01)*	
Age (years)	-0.24 (-0.29, -0.19)*		-0.39 (-0.47, -0.30)*		-0.14 (-0.20, -0.09)*		0.10 (0.06, 0.13)*	
BSA (m^2)	1.02 (0.77, 1.28)*		1.23 (0.80, 1.66)*		0.94 (0.67, 1.22)*		-0.08 (-0.25, 0.09)	
Normative equations (ABGa)								
Women	$120.4 \cdot Age^{-0.24} \cdot BSA^{1.02}$		$66.2 \cdot Age^{-0.39} \cdot BSA^{1.23}$		$55.2 \cdot Age^{-0.14} \cdot BSA^{0.94}$		$45.9 \cdot Age^{0.10}$	
Men	$134.9 \cdot Age^{-0.24} \cdot BSA^{1.02}$		$79.3 \cdot Age^{-0.39} \cdot BSA^{1.23}$		$59.0 \cdot Age^{-0.14} \cdot BSA^{0.94}$		$43.8 \cdot Age^{0.10}$	

*: p<0.01 versus null coefficient. Abbreviations: BSA, body surface area; RV, right ventricular.
Indexed RV measures can be obtained by applying the following formulas:
AGr: RV index = RV parameter/($constant_{F/M} + \beta_{Age} \cdot Age$)
AGBr: RV index = RV parameter/($constant_{F/M} + \beta_{Age} \cdot Age + \beta_{BSA} \cdot BSA$)
AGHWr: RV index = RV parameter/($constant_{F/M} + \beta_{Age} \cdot Age + \beta_{BSA} \cdot Height + \beta_{Weight} \cdot Weight$)
AGBa: RV index = RV parameter/($constant_{F/M} \cdot Age^{\beta Age} \cdot BSA^{\beta BSA}$)

Specifically, there was an average expected age-related decrement of 5 ml/decade for EDV, 3 ml/decade for ESV and 2 ml/decade for SV Moreover, ageing was associated with a small (≈ 1%/decade), but significant increase in RV EF.

The inclusion of BSA (Table 6.5, Model AGBr) resulted in a significant improvement of the overall variation in RV volumes explained by the model (up to 40% for the EDV). BSA was associated with EDV, ESV and SV, with an expected increase of ≈ 5 ml, ≈ 2 ml and ≈ 3 ml respectively per each 0.1 m^2 of BSA increase. The effects of age and gender persisted in Model AGBr, with coefficients similar to those derived in Model AGr. No significant improvement was observed when including BSA in the regression model for RV EF. Considering height and weight separately (Table 6.5, Model AGHWr) instead of their combination as BSA (Table 6.5, Model AGBr) did not lead to significant improvements in terms of R^2, the two models showing similar values in terms of constant and coefficients for age and gender. For this reason, and also to avoid the possible issue of collinearity, multivariate regressions on log-log transformed variables were performed using BSA, and not height and weight separately.

6.2.3 Normative equations for 3DE RV volume and EF.

Normative equations for RV parameters were obtained using linear regression, after log-transforming dependent and independent variables, to allow allometric scaling of RV volumes and function. (109) Gender was included as a dummy variable in the model, resulting in different intercepts for women and men. Derived normative equations for 3DE RV volumes and EF are reported in Table 6.5. To validate the 3DE normative equations, a split and sample approach was used. A comparison between the derived normative equations and those obtained in a similar population using CMR, (7) has been carried out applying the two sets of equations to our population. The difference between the two predicted values was investigated as a function of the mean expected value.

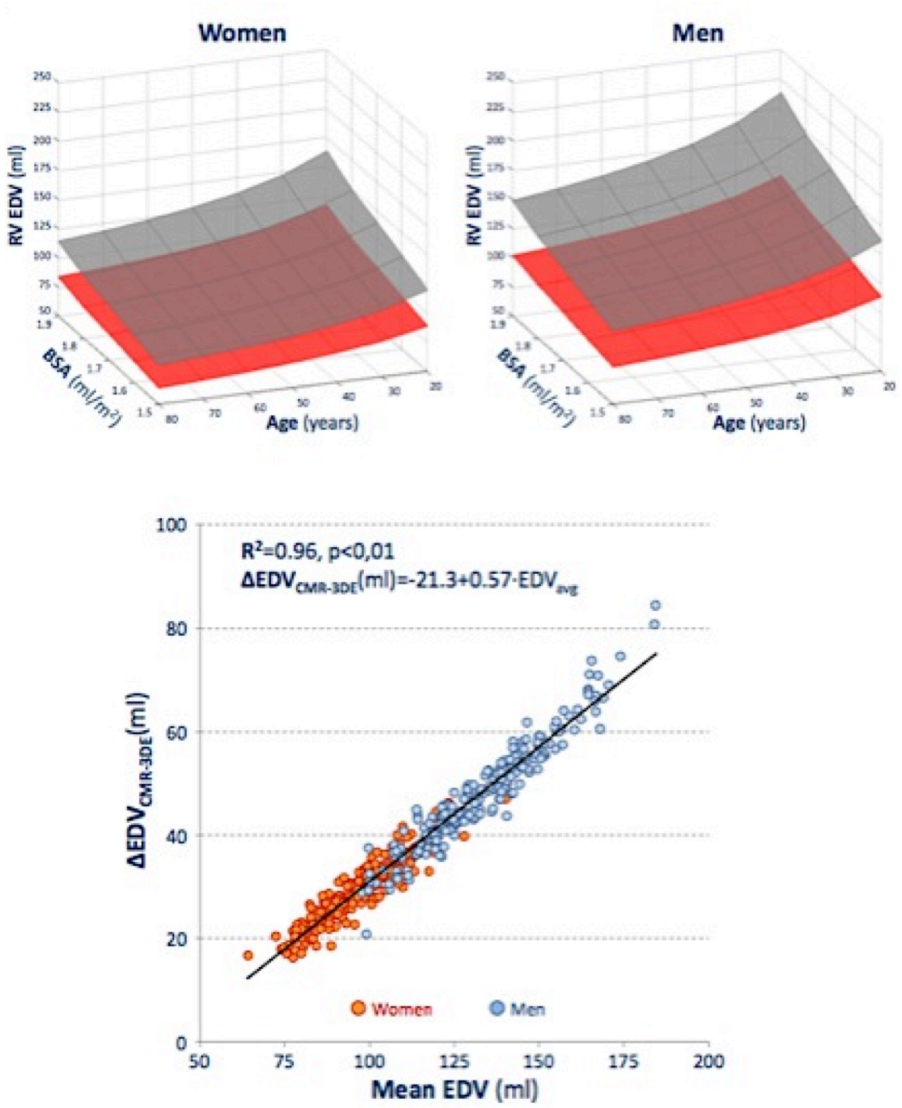

Figure 6.2. Comparison between the values of end-diastolic volume (EDV) obtained applying to the study population the normative equations in Table 6.5 derived using 3D echocardiography (gray surfaces) and EDVs obtained in the same population using normative equations developed for CMR (7) (red surface). Normative surfaces are shown as a function of BSA and age, separately for men (top right) and women (top left). Scatter plot (bottom represents the difference between the expected values ($\Delta EDV_{CMR\text{-}3DE}$) as a function of the mean expected value (EDV_{avg}). The r^2 value refers to the Pearson coefficient between $\Delta EDV_{CMR\text{-}3DE}$ and EDV_{avg}.

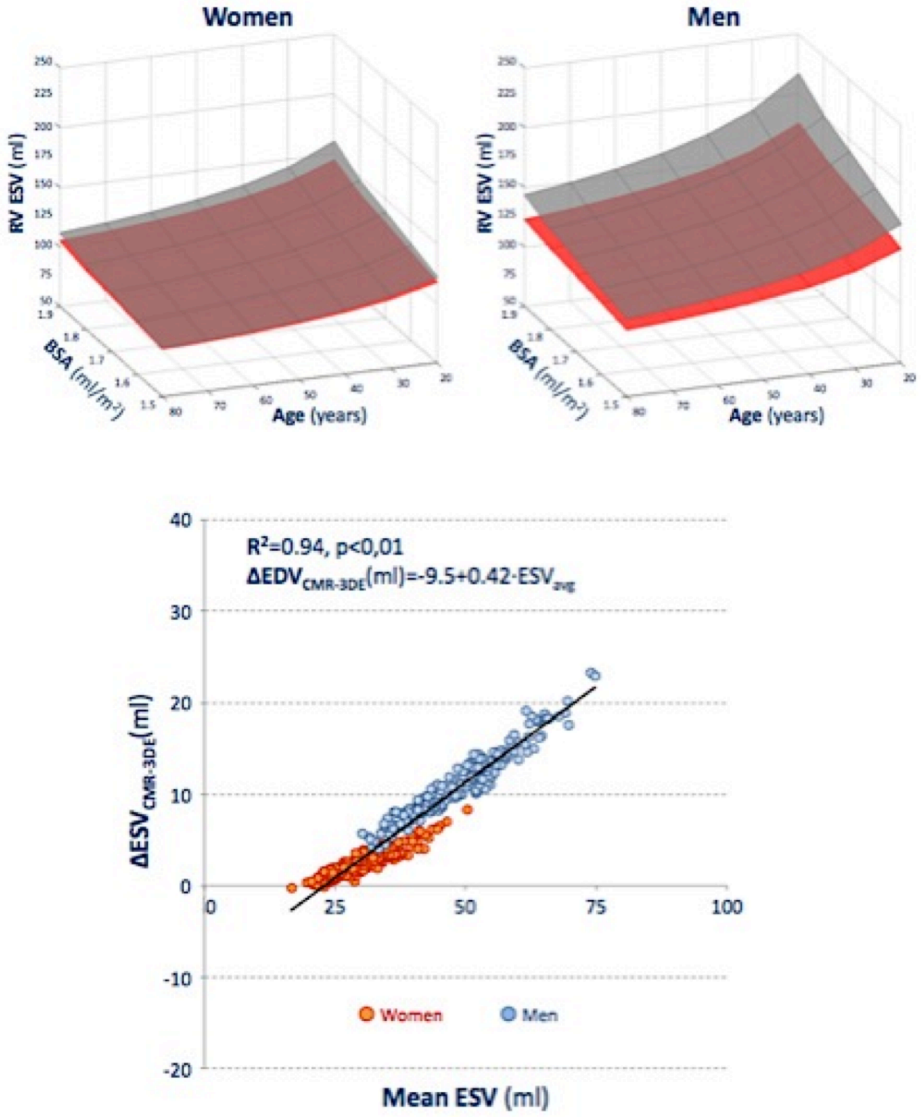

Figure 6.3. Comparison between the values of end-diastolic volume (EDV) obtained applying to the study population the normative equations in Table 6.5 derived using 3D echocardiography (gray surfaces) and EDVs obtained in the same population using normative equations developed for CMR (7) (red surface). See figure 6.2 for detailed description of the graphs.

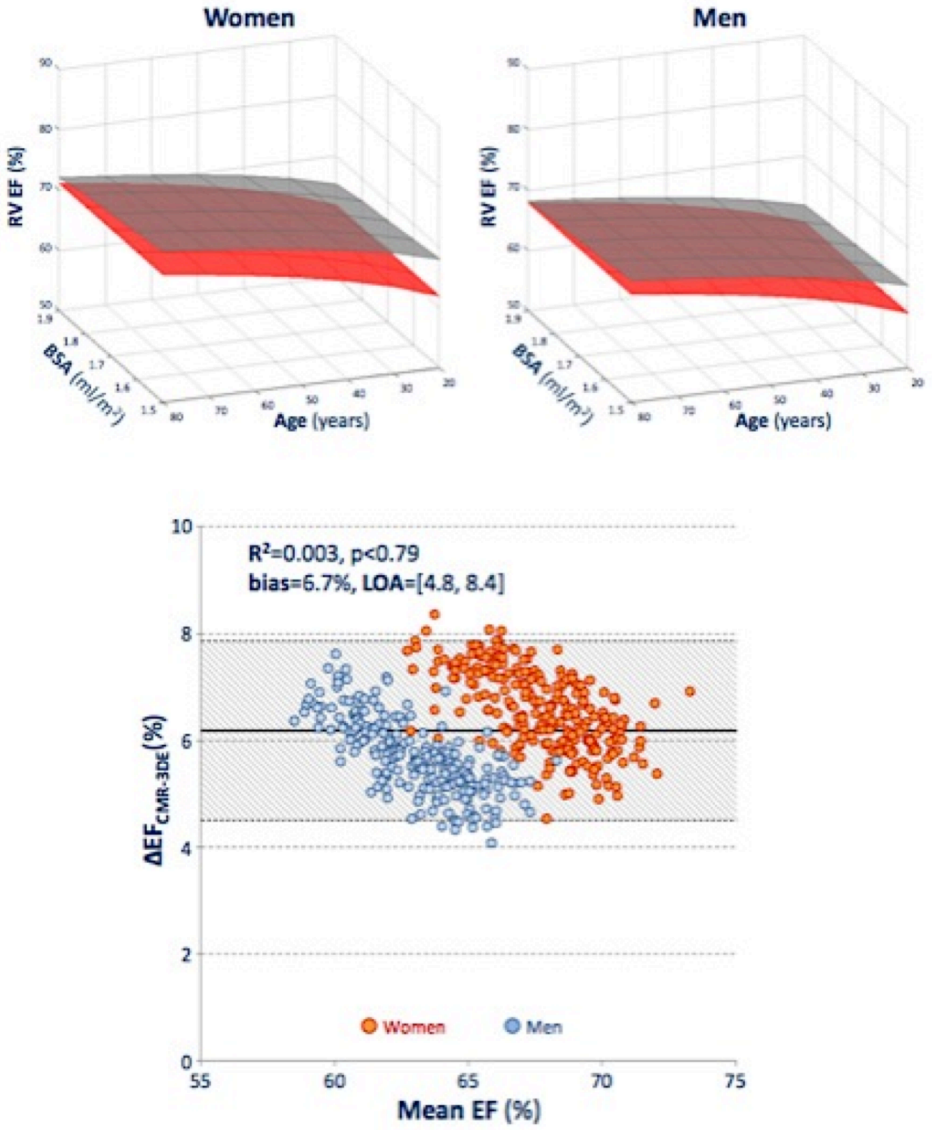

Figure 6.4. Comparison between the values of end-diastolic volume (EDV) obtained applying to the study population the normative equations in Table 6.5 derived using 3D echocardiography (gray surfaces) and EDVs obtained in the same population using normative equations developed for CMR (7) (red surface). See figure 6.2 for detailed description of the graphs.

Contrary to general assumptions about scaling effects, in our study 3D RV volumes and EF maintain significant residual correlations with both height and weight, even after indexing them to BSA or BMI.

TABLE 6.6. Pearson correlation coefficients for indexed right ventricular parameters with height and weight.

Parameter	Model	Height	Weight
RV EDV	RV EDV_{Abs}	0.54*	0.47*
	RV EDV_{BSA}	0.29*	0.16*
	RV EDV_{BMI}	0.52*	0.12*
	RV EDV_{AGBr}	0.00 (p=0.92)	-0.02 (p=0.59)
	RV EDV_{AGHWr}	-0.02 (p=0.63)	-0.01 (p=0.81)
	RV EDV_{AGBa}	0.02 (p=0.62)	0.01 (p=0.88)
RV ESV	RV ESV_{Abs}	0.46*	0.38*
	RV ESV_{BSA}	0.29*	0.18*
	RV ESV_{BMI}	0.45*	0.16*
	RV ESV_{AGBr}	-0.02 (p=0.60)	-0.02 (p=0.68)
	RV ESV_{AGHWr}	-0.04 (p=0.38)	-0.02 (p=0.61)
	RV ESV_{AGBa}	-0.01 (p=0.80)	-0.01 (p=0.89)
RV SV	RV SV_{Abs}	0.49*	0.44*
	RV SV_{BSA}	0.18*	0.07 (p=0.15)
	RV SV_{BMI}	0.45*	0.04 (p=0.37)
	RV SV_{AGBr}	0.01 (p=0.82)	-0.03 (p=0.56)
	RV SV_{AGHWr}	-0.01 (p=0.83)	0.00 (p=0.96)
	RV SV_{AGBa}	0.04 (p=0.41)	0.00 (p=0.95)
RV EF	RV EF_{Abs}	-0.20*	-0.16*
	RV EF_{BSA}	-0.59*	-0.63*
	RV EF_{BMI}	-0.17*	-0.63*
	RV EF_{AGBr}	0.02 (p=0.70)	-0.01 (p=0.83)
	RV EF_{AGHWr}	0.00 (p=0.95)	0.00 (p=0.99)
	RV EF_{AGBa}	0.03 (p=0.52)	-0.01 (p=0.84)

Abbreviations: Abs, absolute value; BMI, body mass index; BSA, body surface area; AGBa, adjusted for age and BSA (allometric); AGBr, adjusted for age, gender and BSA (ratiometric); AGHWr, adjusted for age, gender, height and weight (ratiometric); EDV, end-diastolic volume; EF, ejection fraction; ESV, end-systolic volume; RV, right ventricular, SV, stroke volume.

*: correlation is significant at the 0.01 level (2-tailed t-test).

Ratiometric scaling for RV parameters adjusted for age and BSA (AGBr), or age, height and weight (AGHWr) resulted in RV volumes and EF values independent of body size. Similarly, allometric scaling for normative equation listed in Table 6.5 (Model ABa) resulted in negligible residual correlations with height and weight.

6.2.4 Comparison with CMR-derived normative equations.

Comparison with normative equations derived from CMR (7) applied to our study population, showed a consistent underestimation of RV volumes calculated using 3DE vs. CMR normative equations (Figures 6.2 and 6.3).

The differences between the CMR and 3DE expected normative values showed a strong positive correlation with their average. For every 10 mL increase of average 3DE and CMR RV volumes, there was an increase in the inter-modality difference of approximately 6 ml, 4 ml and 5 ml, for EDV, ESV and SV, respectively (Figures 6.2 and 6.3). Conversely, the inter-modality difference of expected EF showed no correlation with the average expected value, resulting in a bias of 6.7% at Bland-Altman analysis (Figure 4.4).

6.2.5 Reproducibility.

Intra-observer analysis showed good to excellent reproducibility (R^2 ranges between 0.76 to 0.94), with negligible bias and narrow limits of agreement (4.3 ml for ESV at Padua, 11.5 for EDV at Milan). Inter-center measurements using the standardized method showed higher variability (R^2 between 0.43 and 0.87), with no significant biases (absolute values comprised between 2 and 9 ml) between repeated measurements and acceptable limits of agreement, ranging between 13 and 33 ml.

TABLE 6.7 - Results of intra-operator and inter center reproducibility analysis, evaluated using Pearson correlation coefficient (r^2) and Bland-Altman analysis between repeated measurements.

		EDV (ml)	**ESV** (ml)
Intra-operator	Padua, PD	0.6±5.1 (0.94)	0.7±4.3 (0.92)
	Naples, NA	0.4±5.8 (0.96)	1.2±5.2 (0.91)
	Milan, MI	0.3±11.5 (0.91)	1.5±8.5 (0.76)
Inter-center	PD vs. NA	-9±33 (0.58)	-3±13 (0.60)
	PD vs. MI	-3±15 (0.87)	-5±13 (0.63)
	NA vs. MI	6±33 (0.58)	-2±17 (0.43)

Values expressed as bias±1.96 SD (r^2).

6.3 Discussion

This is the first prospective multi-center study providing reference values for 3D RV volumes and EF, separately for age and gender. To foster the clinical application of 3DE in individual patients, a set of normative equations for RV volumes and EF was derived from this large cohort of healthy adults, taking into account demographic and anthropometric parameters.

The main findings of this study can be summarized as follows: (i) the normal ranges of absolute and BSA-indexed values of RV volumes and EF measured using 3DE are now available separately for gender and age decades; (ii) demographic and anthropometric parameters were strong independent predictors of 3DE RV volumes at multivariate analysis; (iii) RV EF showed a weak correlation with age and gender, and no correlation with body size; (iv) normative allometric equations for 3D RV volumes and EF have been developed, effectively indexing RV parameters for body size; (v) a strong agreement between 3DE and CMR predicted normative values was found; (vi) individual reference values for RV size and function parameters calculated using 3DE normative equations were systematically lower than those calculated using CMR normative equations.

Quantification of RV size and function with conventional echocardiography is challenging, due to the anterior position of the RV in the chest, its complex asymmetric geometry and highly trabeculated endocardial border, impossibility to simultaneously visualize both inflow and outflow tracts and lack of realistic geometric models for volume calculation. (101) 3DE has been

demonstrated to have a good accuracy in measuring RV volumes compared to CMR. (102) This, in conjunction with the availability of specifically designed software not requiring a priori modeling or geometric assumptions, (110) made 3DE a feasible, fast and accurate technique for RV assessment in different clinical settings. (45,111-113)

6.3.1 Influence of demographic parameters and body size on RV volumes

Several biological processes and anatomic structures, including cardiovascular structural and functional variables, scale with anthropometric and demographic data. (114) However, while scaling is commonly performed in pediatric medicine, allowing to eliminate the possible confounding effect of the rapid somatic growth process, the practice of indexing is less used in adult clinical cardiology. (109) The goal of scaling cardiac structure is to eliminate, or at least substantially decrease, the overlap between normal and abnormal ranges that could be influenced by body size. In the present study, besides providing normative values of RV volumes and ejection fraction stratified for gender and age, we also derived different models and normative equations to index RV values according to demographic and anthropometric parameters. Independently of the adopted model, aging was associated with a decrease of 5 ml/decade for EDV, 3 ml/decade for ESV, and 2 ml/decade for SV. Conversely, EF increased by 1%/decade. Body size was also significantly related with RV volumes. For every 0.1 m^2 increase in BSA, there was an increase of 6 ml, 2 ml and 3 ml in RV EDV, ESV and SV, respectively. Height and weight were also positively associated with RV volumes. However, their inclusion in the statistical model separately, and not merged into BSA, did not increase the predictive power of the model.

We also demonstrated the importance of gender in all RV parameters: RV volumes were larger and EF lower in men than in women. Albeit these dissimilarities can be partially explained by different biometric characteristics between women and men, gender was a significant determinant of RV size even after scaling for anthropometric variables.

From an empirical point of view, adequate model fitting should result in negligible residual association between the values indexed by body size (e.g. BSA) and the independent variables,

specifically height and weight. (115) Our results showed a residual correlation with height and weight after ratiometric indexing (Table 6.6) suggesting that the assumption of linearity between 3DE RV volumes and BSA is not completely satisfied, even after adjusting for age and gender. Furthermore, indexing RV ESV to Model AGBr overcompensated the association with anthropometric measures. Conversely, applying the allometric scaling led to the calculation of RV volumes which were independent of age and body size. These findings imply that simply indexing by BSA may be suboptimal, and the use of an exponential allometric model could be more appropriate to scale RV volumes and SV. Alternatively, ratiometric scaling for the Model AGHWr, considering height and weight separately and not in fixed proportion as in BSA calculated by Du Bois and Du Bois formula (37), resulted in RV volumes independent of body size. In addition, the appropriateness of normalization achieved via scaling ratiometrically to BSA may be questionable from a theoretical point of view. Indeed, the theory of similarity states that relative geometries determine in part the relationships between body size variables. As RV volume is proportional to a length measure raised to the third power, and BSA is proportional to a length raised to the second power, the scaling relationship is dimensionally not consistent. Thus, indexing to BSA, despite widely used in clinical practice in all cardiac imaging modalities, may be suboptimal in certain circumstances. (109)

The observed association between RV size, demographic and anthropometric parameters has been previously reported in other studies, both using echocardiography and other imaging modalities. In a large series of subjects with normal echocardiographic findings, D'Oronzio et al. (116) concluded that gender and BSA are important determinants of 2D echocardiographic RV dimensions, and proposed to use gender-specific RV measures indexed to BSA for the assessment of RV in the clinical routine. Of note, D'Oronzio et al. (116) reported only a weak inverse association between aging and RV area, which may be due to the lower accuracy of 2D echocardiography in comparison with 3DE in assessing RV size (116).

Our study corroborate and extend the results of Tamborini et al. (103) to a larger population, investigating the demographic and anthropometric determinants of RV morphology and function in a multi-center setting. This is an important step towards the definition of clinically applicable reference ranges. Indeed, systematic biases among laboratories have been reported for left LV assessment by 3DE (115,117,118), and similar biases affecting RV measurements could not be excluded a priori. In this view, a multi-center design is crucial for identifying reliable normative values.

6.3.2 Comparison with CMR

Nowadays, CMR is considered the gold standard for the assessment of RV volumes and function, and different studies have reported RV reference values for this modality (119,120). Our findings confirm previous studies reporting a slight systematic underestimation of RV volumes by 3DE in comparison with CMR (117,121). The potential source of bias has been documented in both *in vivo* and *in vitro* studies(102,105). Despite the bias in absolute values, the role of aging, gender and anthropometric variables as determinants of RV size and function demonstrated by Maceira et al. (119) using steady-state free precession CMR are in complete agreement with our findings. The comparison of normative non-linear equations obtained in our study with those presented by Kawut et al. (7) obtained in a similar number of subjects, represents an even more interesting parallelism between 3DE and CMR in the setting of RV evaluation. Indeed (as depicted in Figure 6.2 and 6.3) normative surfaces of the present study obtained applying the derived normative equations show similar behaviors, with exponential positive influence of both BSA and age on RV EDV, ESV and SV. Also, from the comparison of these two models we demonstrated that the bias between the predicted normal values by 3DE and CMR is not constant, but has a rather strong positive linear correlation with the average expected RV volume. Normative surfaces of RV EF were very similar, with a significant and constant underestimation of 3DE versus CMR (approximately 7%), with narrow limits of agreement.

6.3.3 Reliability of 3DE to quantify RV volumes

From a clinical standpoint, the reliability of a quantitative method is more important that its accuracy in comparison with the reference value obtained using a universally-accepted "gold-standard". Accordingly, for patient follow-up most clinicians would prefer to use a precise method with a reproducible bias, despite less accurate, instead of using a highly accurate method affected by large random error. (122) For the first time, we evaluated the inter-center reproducibility of 3DE RV volumes using different echocardiographic equipment and the same post-processing software. Interinstitutional variability constitutes a serious threat for measurement reproducibility and it is potentially the most serious source of bias in multicenter study. In agreement with previous study (123), we demonstrated that the definition of a standardized method by joint consensus significantly improved the inter-center agreement. We demonstrated that RV 3DE measurements are fairly robust and reproducible. However, the limits of agreements of measurements among different centers were still relatively high and, apart the described standardization of the image acquisition and post-processing steps, further technological advances towards a fully-automated quantitation of cardiac chamber volumes would be desirable to further improve the robustness of 3DE.

CHAPTER 7

Reference values for left atrial geometry and function by three-dimensional echocardiography

7.1 Background

A growing interest has been recently dedicated to atrial cavities due to their prognostic value in various cardiac diseases and the rapid development of cardiac interventional electrophysiology.

Left atrial (LA) size assessment is clinically relevant in a comprehensive patient evaluation. The finding of an enlarged LA could be indicative of significant ventricular, (124-126) atrial (127) or valvular disease, (52) being also a proved marker of adverse cardiovascular outcomes. (128,129)

Even if LA size has been assessed using different parameters, it has been shown that LA volume is a more robust cardiovascular risk marker than LA area or linear dimensions. (129) The current guidelines recommend biplane calculation of LA volume using both Simpson's or area-length methods on 2DE apical four- and two-chamber views. (38,129,130). Both algorithms are heavily dependent on geometric assumptions about LA geometry and have been shown to underestimate LA volumes measured with cardiac computed tomography (131) and CMR. (132)

Recently, 3DE has been incorporated into the clinical practice of many echocardiography laboratories. When 3DE has been used to measure LA volumes, it showed significantly better

agreement than 2DE with other imaging modalities including computerized tomographic imaging (133) and CMR. (48,134) In addition, LA volume assessment by 3DE has shown prognostic value for cardiovascular events, (135,136) which was incremental compared to 2DE LA volumes, (137) and the most favorable test-retest variation with the least intra- and inter-observer variability compared with other echocardiographic techniques. (138) However, implementation of 3DE LA volume measurements in the routine of the echocardiographic laboratories requires the availability of reliable reference values. (130) At present, reference values about 3DE LA volumes and phasic function parameters are very limited. (139)

7.2 Development of reference values for LA geometry and function by 3DE

19 volunteers met all criteria for inclusion but were excluded from enrolment: 6 because their acoustic window was inadequate for 2DE and 3DE analysis and 13 due minimal abnormal echocardiographic findings (e.g. interatrial septal aneurysm). Among the remaining 244 subjects, 23 could not be evaluated by 3DE due to poor image quality.

TABLE 7.1 - Demographic Characteristics

	All (n=244)	**Men** (n=103)	**Women** (n=141)	p*
Age (years)	43 ± 14	42 ± 14	44 ± 14	NS
Age range (years)	18 - 75	18 – 74	18 - 75	NS
Heart rate (bpm)	68 ± 12	67 ± 12	69 ± 11	NS
Height (cm)	170 ± 9	178 ± 6	165 ± 7	< 0.001
Weight (kg)	67 ± 11	76 ± 9	61 ± 8	< 0.001
Body mass index (kg/m^2)	23.1 ± 2.8	24.1 ± 2.4	22.3 ± 2.8	< 0.001
Body surface area (m^2)	1.78 ± 0.18	1.93 ± 0.13	1.67 ± 0.13	< 0.001
Systolic blood pressure (mmHg)	121 ± 13	126 ± 11	117 ± 14	< 0.001
Diastolic blood pressure (mmHg)	74 ± 8	77 ± 8	71 ± 8	< 0.001

* p values refer to gender differences

Thus in our study population, the feasibility of 3DE and 2DE LA volume measurements were 91% and 96% (p=0.59). Temporal resolution of 3DE LA data sets was 44±10 volumes/s.

Fifty-seven percent of study subjects were women. There were no differences in age and heart rate between men and women. Women showed significantly smaller body size and lower blood pressure compared to men.

7.2.1. 3DE LA volumes and function and their relationship with gender

LA size and function parameters obtained with 3DE and 2DE are summarized in Table 7.2. Irrespective on the echo technique used, parameters of LA size were significantly larger in men than in women, but these differences disappeared for 2DE Vmax, Vmin and Vpre A, and 3DE Vmax and Vpre A after indexing for BSA. Upper limits for 3DE LA Vmax, Vmin and VpreA were 39 ml/m^2, 17 ml/m^2 and 24 ml/m^2 in men and 36 ml/m^2, 16 ml/m^2 and 23 ml/m^2 in women. 3DE LA total, passive and active EVs were larger in men, but these differences disappeared after indexing for BSA (Table 7.2). Lower limits of normality for 3DE total, passive and active LA indexed EV in men were 9 ml/m^2, 4 ml/m^2 and 1 ml/m^2, and in women 10 ml/m^2, 6 ml/m^2 and 1 ml/m^2 respectively. 3D LA total EmptFr was similar between genders while women showed higher passive EmptFrs. Lower limits of normality for 3DE total, passive and active LA EmptFrs were 46%, 20% and 16% in men and 50%, 27% and 14% in women.

TABLE 7.2 – Left atrial volumes and function by two- and three-dimensional echocardiography

2DE parameters	**Overall** (n= 235)	**Men** (n= 99)		**Women** (n= 136)		p*
		Average	Normal Limit	Average	Normal Limit	
Vmax (ml)	43 ± 11	47 ± 11	69 [a]	41 ± 10	60 [a]	<0.001
Vmax/BSA (ml/m²)	24 ± 5	24 ± 5	34 [a]	24 ± 6	36 [a]	NS
Vmin (ml)	14 ± 6	15 ± 7	29 [a]	13 ± 6	25 [a]	0.02
Vmin/BSA (ml/m²)	8 ± 3	8 ± 3	14 [a]	8 ± 3	14 [a]	NS
Vpre A (ml)	26 ± 9	29 ± 10	49 [a]	24 ± 8	40 [a]	<0.001
Vpre A/BSA (ml/m²)	14 ± 5	15 ± 5	25 [a]	14 ± 5	24 [a]	NS
Total EV (ml)	29 ± 7	31 ± 6	19 [b]	27 ± 7	13 [b]	<0.001
Total EV/BSA (ml/m²)	16 ± 3	16 ± 3	10 [b]	16 ± 4	8 [b]	NS
Passive EV (ml)	17 ± 6	17 ± 5	7 [b]	17 ± 6	5 [b]	NS
Passive EV/BSA (ml/m²)	10 ± 3	9 ± 3	3 [b]	10 ± 3	4 [b]	0.01
Active EV (ml)	12 ± 4	13 ± 5	3 [b]	11 ± 4	3 [b]	<0.001
Active EV/BSA (ml/m²)	7 ± 2	7 ± 2	3 [b]	6 ± 2	2 [b]	NS
Total EmptFr (%)	68 ± 9	69 ± 9	51 [b]	69 ± 8	53 [b]	NS
Passive EmptFr (%)	41 ± 11	40 ± 11	18 [b]	43 ± 11	21 [b]	0.03
Active EmptFr (%)	47 ± 10	48 ± 11	26 [b]	46 ± 10	26 [b]	NS
Expansion index (%)	237 ± 107	235±105	445[a]	239±109	457[a]	NS
3DE Parameters	**Overall** (n= 221)	**Men** (n= 92)		**Women** (n= 129)		p*
		Average	Limit	Average	Limit	
Vmax (ml)	48 ± 11	53 ± 12	77 [a]	43 ± 9	61 [a]	<0.001
Vmax/BSA (ml/m²)	27 ± 5	27 ± 6	39 [a]	26 ± 5	36 [a]	NS
Vmin (ml)	19 ± 6	21 ± 6	33 [a]	17 ± 4	25 [a]	<0.001
Vmin/BSA (ml/m²)	10 ± 3	11 ± 3	17 [a]	10 ± 3	16 [a]	0.03
Vpre A (ml)	27 ± 8	30 ± 9	48 [a]	24 ± 7	38 [a]	<0.001
Vpre A/BSA (ml/m²)	15 ± 4	16 ± 4	24 [a]	15 ± 4	23 [a]	NS
Total EV (ml)	29 ± 7	32 ± 8	16 [b]	27 ± 6	15 [b]	<0.001
Total EV/BSA (ml/m²)	16 ± 3	17 ± 4	9 [b]	16 ± 3	10 [b]	NS
Passive EV (ml)	21 ± 7	23 ± 8	7 [b]	20 ± 6	8 [b]	<0.001
Passive EV/BSA (ml/m²)	12 ± 4	12 ± 4	4 [b]	12 ± 3	6 [b]	NS
Active EV (ml)	8 ± 4	9 ± 4	1 [b]	7 ± 4	1 [b]	0.002
Active EV/BSA (ml/m²)	5 ± 2	5 ± 3	1 [b]	5 ± 2	1 [b]	NS
Total EmptFr (%)	61 ± 6	60 ± 7	46 [b]	62 ± 6	50 [b]	NS
Passive EmptFr (%)	44 ± 10	42± 11	20 [b]	45 ± 9	27 [b]	0.02
Active EmptFr (%)	30 ± 7	30 ± 7	16 [b]	30 ± 8	14 [b]	NS
Expansion index (%)	163±45	158±48	254[a]	167±43	253[a]	NS

2DE: two-dimensional echocardiography; 3DE: three-dimensional echocardiography; BSA: body surface area; EmptFr: emptying fraction; EV: emptying volume; Vmax: maximum volume; Vmin: minimum volume; VpreA: preA volume; * p values refer to gender differences; [a] upper limit; [b] lower limit.

7.2.2. Relationships of 3DE LA volumes and function with age

Table 7.3 summarizes the relationships between age and 3DE LA volumes and function parameters. Total and passive EV didn't change significantly with age, but active EV increased with age. Total EmptFr decreased with age while passive and active didn't change significantly.

TABLE 7.3. Relationship between age and left atrial volumes and function parameters measured by three-dimensional echocardiography

	Overall (n=221)	
	r	p
Vmax (ml/m²)	.2	0.004
Vmin (ml/m²)	.22	0.001
Vpre A (ml/m²)	.22	.002
Total EV (ml/m²)	.11	NS
Passive EV (ml/m²)	.02	NS
Active EV (ml/m²)	.15	0.02
Total EmptFr (%)	-.14	0.03
Passive EmptFr (%)	-.07	NS
Active EmptFr (%)	-.07	NS

Abbreviations as in Table 8.2

7.2.3. Comparison between 2DE and 3DE LA volumes

All parameters, excluding VpreA volume and total EV, calculated on 2DE images were significantly different than those measured using 3DE (Table 7.4). In general, all 2DE measurements were lower than those obtained by 3DE, while active EV, and total and active EF were higher.

TABLE 7.4 - Comparison between three- and two-dimensional echocardiographic parameters of left atrial size and function

	3DE	2DE*	p Value
Vmax (ml)	48 ± 11	43 ± 11	<0.001
Vmin (ml)	18 ± 5	14 ± 6	<0.001
Vpre A (ml)	26 ± 8	26 ± 9	NS
Total EV (ml)	29 ± 7	29 ± 7	NS
Passive EV (ml)	21 ± 7	17 ± 5	<0.001
Active EV (ml)	8 ± 4	12 ± 4	<0.001
Total EmptFr (%)	61 ± 6	68 ± 9	<0.001
Passive EmptFr (%)	44 ± 10	41 ± 11	0.002
Active EmptFr (%)	30 ± 7	47 ± 10	<0.001
Expansion index (%)	163±45	237 ± 107	<0.001

Abbreviations as in Table 7.2.

7.2.4. Reproducibility

Interobserver reproducibility of 3DE LA volumes was significantly better than that of 2DE LA volumes.

TABLE 7.5 - Intra- and interobserver variability of two- and three-dimensional left atrium volumes

	Intraobserver variability		Interobserver variability	
	bias	95%CI	bias	95%CI
2DE Vmax (ml)	1.37	-0.76 – 3.51	0.89	-1.3 – 3.09
2DE Vmin (ml)	-0.64	-1.79 – 0.51	-0.2	-1.88 – 1.5
2DE VpreA (ml)	-0.55	-2.07 – 0.97	2.58	0.37 – 4.79
3DE Vmax (ml)	0.96	-0.81 – 2.75	-0.66	-1.7 – 0.37
3DE Vmin (ml)	0.38	-0.93 – 1.7	-0.07	-0.82 – 0.68
3DE VpreA (ml)	-0.35	-2 – 1.3	0.9	-0.06 – 1.86

Abbreviations as in Table 7.2.

7.3 Discussion

The present study provides normative values of 3DE-derived LA volumes and a comprehensive analysis of LA phasic function obtained from a large sample of healthy volunteers. Our main results can be summarize as: (i). Assessment of LA volumes and phasic function parameters with 3DE is feasible and reproducible; (ii). LA volume values obtained with 3DE cannot be used interchangeably with 2DE-derived volumes; and (iii). reference values of LA volumes indexed by BSA are similar between genders but they increase slightly with ageing.

7.3.1 Prognostic value of LA volumes and functional parameter

The degree of the enlargement of the LA caused by pressure and/or volume overload reflects severity and chronicity of underlying pathologic conditions rather than instantaneous left ventricular filling pressure. (140) Accordingly, several previous studies demonstrated that LA Vmax measured by 2DE is a robust predictor of future cardiovascular events in various clinical scenarios. (128,129) Recently, many researchers have focused on the importance of assessing LA phasic function and not only Vmax, because of the close interdependence between LA and left ventricular function. (128) It is physiologically explained, as LA modulates left ventricular filling through its reservoir, conduit, and booster pump function, whereas left ventricular function influences LA function throughout the cardiac cycle. However, normal values of LA volumes available in current guidelines are only maximal LA Vmax and LA Vmax indexed to BSA. (38) Biplane 2DE calculation of LA volume is the recommended method, which sometimes is inaccurate due to the complexity of LA shape and the inability to obtain optimal cutting planes.(38,141) Transthoracic 3DE has been reported to be more accurate than 2DE in assessing LA volumes because it does not rely on geometric assumptions about LA shape(48,133). Although, there are limited data about normal values of LA volumes (139) and no data about LA phasic function parameters obtained

with 3DE.

7.3.2 Accuracy of 2DE and 3DE to assess LA volumes

Our results showed that LA volumes obtained by 3DE are significantly larger than those calculated by 2DE, and relative cut-off values to define LA enlargement cannot be used interchangeably. Other authors did not find significant difference between 3DE and 2DE LA volumes, which was probably due to the use of a software developed for LV volume measurements and never validated for the LA. (137,142) However, investigations showed that 3DE LA volumes correlated much better with CMR-derived LA volumes than 2DE LA volumes. (143,144) Additionally, recent investigations revealed that 3DE LA volumes correlated closely with 64-slice multidetector computed tomography with only 8% underestimation. (133,145) Nevertheless, studies reported underestimation of LA volumes assessed by 3DE in comparison with cardiac CMR. (144,146) In recently published meta-analysis Shimada et al. revealed that underestimation of LA volume by 3DE in comparison with cardiac CMR is -9.4 ml (95% confidence interval, -13.2 to -5.6 ml; $p < 0.001$). (147) Authors claimed that underestimation is likely to increase in pathological conditions. (147)

The LA phasic function is very important because it modulates LV function. Namely, early impairment of LV diastolic function increases LV filling pressure, which induces a reduction of LA passive emptying and a compensatory increase of the booster function to preserve cardiac output. (148) Recent study revealed that 3DE LA Vmin was a better correlate of left ventricular diastolic function than 3DE LA Vmax (126,137) since LA Vmin size is determined by the direct exposure of LV diastolic pressure and seem to reflect more reliably the underlying pathology by the influence of LV longitudinal systolic function on LA reservoir function. (126) Furthermore, Wu et al. demonstrated that 3DE derived LA Vmin volume was a better predictor of cardiac death, whereas 3DE LA Vmin and Vmax were independent predictors of major cardiovascular events. (137)

By comparing 2DE and 3DE assessment of LA phasic function we found that LA reservoir and pump functions were significantly lower by 3DE than 2DE, whereas the estimation of the conduit function was independent of the echocardiographic technique.

In agreement with other Authors (149), we found that 3DE-derived LA volumes increased with aging.

CHAPTER 8

Reference values for right atrial geometry and function by three-dimensional echocardiography

8.1 Background

The right atrium (RA) plays an integral role in cardiac performance by modulating RV function with its reservoir, conduit and contractile functions. (51) Recent reports have documented that RA size enlarges in patients with atrial arrhythmias, chronic heart failure, pulmonary hypertension and congenital heart diseases. (150-152) Although data on clinical significance of RA enlargement are sparse, 2DE RA area has been demonstrated to be a predictor of outcome in primary pulmonary hypertension and chronic heart failure. (151,153,154)

Conventional assessment of RA size includes measurement of RA diameters and area on 2DE 4-chamber apical view. (38,50) RA volumetric assessment is not currently recommended. (38,50) In addition, 2DE calculation of atrial volume is limited by view dependency and geometric assumptions about atrial shape. However, atrial remodeling as a consequence of disease processes is often asymmetrical, rendering these assumptions inadequate. 3DE overcomes these limitations enabling accurate RA volume measurement. (48,134) Moreover, 3DE enables assessment of atrial phasic volume changes, permitting to describe atrial function over its size. (155)

Knowledge of reference echocardiographic values of RA volumes and function is a prerequisite for the introduction of RA quantitation in the clinical routine. At present, only one study reported normal values of 3DE RA maximal and minimal volumes, but it did not report phasic RA function parameters. (139)

Accordingly, we have designed this prospective, observational study to: (i). determine the normative values for RA geometry and function in a large cohort of healthy subjects using 3DE; (ii). analyze the effects of age and gender on these parameters; and (iii). compare the parameters measured by 3DE with the same values calculated using 2DE.

8.2 Development of reference values for RA geometry and function by 3DE

Six volunteers met all criteria for inclusion but were excluded from enrolment because their acoustic window was inadequate for 2DE and 3DE analysis. Among the remaining 204 subjects, 4 could not be evaluated by 3DE due to poor image quality. Thus in our study population, feasibility of RA 3DE volume measurements was 95.2%. Temporal resolution of 2DE images was 73 frames/s, and that of 3DE data sets was 34±9 volumes/s.

TABLE 8.1 - Demographic characteristics of the study population

	All (n=200)	**Men** (n=87)	**Women** (n=113)	p Value*
Age (years)	43±15	41±14	45±14	0.078
Height (cm)	170±10	177±7	164±8	<0.0001
Weight (kg)	67±11	76±9	61±9	<0.0001
Body mass index (kg/m^2)	23±3	24±2	23±3	0.001
Body surface area (m^2)	1.78±0.19	1.93±0.13	1.67±0.15	<0.0001
Heart rate (bpm)	68±11	67±12	69±11	0.15
Systolic blood pressure (mmHg)	122±14	127±11	118±14	<0.0001
Diastolic blood pressure (mmHg)	74±8	76±7	71±8	<0.0001

Fifty-six percent of study subjects were women. There were no differences in age and heart rate between men and women (Table 8.1). Women showed significantly smaller body size and lower blood pressure compared to men (Table 8.1).

8.2.1. 3DE RA volume and function and their relationships with gender

RA size and function parameters obtained with 2DE and 3DE are summarized in Table 8.2. Irrespective on the echo technique used, parameters of RA size were significantly larger in men than in women, even after normalization for BSA. Upper limits for 3DE RA Vmax, Vmin and VpreA were 49 ml/m^2, 20 ml/m^2 and 27 ml/m^2 in men and 38 ml/m^2, 16 ml/m^2 and 22 ml/m^2 in women. 3DE RA total, passive and active EV were higher in men, but these differences disappeared after indexing for BSA (Table 8.2).

Lower limits of normality for 3DE total, passive and active RA indexed EV were 11 ml/m^2, 6 ml/m^2 and 2 ml/m^2. 3D RA total, passive and active EmptFrs were higher in women (Table 8.2). Lower limits of reference values for 3DE total, passive and active RA EmptFrs were 44%, 27% and 18% in men and 50%, 22% and 19% in women (Table 8.2).

TABLE 8.2 - Right atrial size and function by two- and three-dimensional echocardiography and right atrial myocardial wall function by 2D-speckle tracking echocardiography in healthy subjects

	All (n=200)	**Men** (n=87)	**Women** (n=113)	p Value*
RA max diameter (mm)	46±5	49±5	44±4	<0.0001
RA min diameter (mm)	38±6	41±6	36±5	<0.0001
RA area (cm^2)	15±3	17±3	13±2	<0.0001
RA area/BSA (cm^2/m^2)	8.4±1.5	8.9±1.6	8.1±1.3	<0.0001
2D RA VMax (ml)	41±14	50±15	35±10	<0.0001
2D RA Vmax/BSA (ml/m^2)	23±7	26±7	21±6	<0.0001
2D RA VMin (ml)	17±7	21±7	14±5	<0.0001
2D RA Vmin/BSA (ml/m^2)	10±4	11±4	8±3	<0.0001
2D RA VpreA (ml)	27±11	33±11	22±8	<0.0001
2D RA VpreA/BSA (ml/m^2)	15±5	17±5	13±4	<0.0001
3D RA Vmax (ml)	52±15	60±16	45±11	<0.0001
3D RA Vmax/BSA (ml/m^2)	29±7	31±8	27±6	<0.0001
3D RA Vmin (ml)	19±8	24±8	16±5	<0.0001
3D RA Vmin/BSA (ml/m^2)	11±4	12±4	9±3	<0.0001
3D RA VpreA (ml)	28±10	34±10	24±7	<0.0001
3D RA VpreA/BSA (ml/m^2)	16±5	18±5	14±4	<0.0001
3D RA total EV (ml)	33±10	37±11	30±8	<0.0001
3D RA total EV/BSA (ml/m^2)	18±5	19±5	18±5	0.22
3D passive EV (ml)	24±9	27±10	22±8	<0.0001
3D passive EV/BSA (ml/m^2)	13±5	14±5	13±4	0.34
3D RA active EV (ml)	9±4	10±4	8±4	0.001
3D RA active EV/BSA (ml/m^2)	5±2	5±2	5±2	0.37
3D RA total EmptFr (%)	63±9	61±8	65±8	<0.0001
3D RA passive EmptFr (%)	46±11	44±10	48±12	0.013
3D RA active EmptFr (%)	31±8	29±7	33±9	0.002

Abbreviations: EmptFr= emptying fraction; EV = emptying volume; LS= longitudinal strain; LS, longitudinal strain; RA= right atrium; Vmax= maximum volume; Vmin= minimum volume; VpreA= preA volume

8.2.2 Relationship of 3DE RA volumes anf function parameters with age

Total EV didn't change significantly with age, but passive EV decreased and active EV increased with age in both genders. Similarly, passive EmptFr decreased with age and active EmptFr increased with a mild decrease of total EmptFr in both genders (Table 8.3).

TABLE 8.3 - Relationship between age and right atrial volumes and function parameters assessed by 3DE

	All (n=200)		**Men** (n=87)		**Women** (n=113)	
	r	p Value	r	p Value	r	p Value
3D RA Vmax (ml)	-0.05	0.52	0.016	0.88	0.031	0.75
3D RA Vmin (ml)	0.10	0.14	0.17	0.12	0.26	0.005
3D RA VpreA (ml)	0.16	0.026	0.21	0.05	0.32	<0.0001
3D RA Total EV (ml)	-0.14	0.05	-0.10	0.34	-0.10	0.26
3D RA Passive EV (ml)	-0.26	<0.0001	-0.23	0.04	-0.25	0.008
3D RA Active EV (ml)	0.25	<0.0001	0.31	0.003	0.27	0.004
3D RA Total EF (%)	-0.24	0.001	-0.26	0.015	-0.31	0.001
3D RA Passive EF (%)	-0.38	<0.0001	-0.43	<0.0001	-0.40	<0.0001
3D RA Active EF (%)	0.15	0.035	0.04	0.71	0.17	0.06

Abbreviations as in Table 8.2

8.2.3. Comparison between 2DE nad 3DE RA volumes and function

RA volumes calculated on 2DE images were significantly smaller than those measured using 3DE (Table 8.4). Total and passive EV and EF obtained with 2DE were lower than those obtained by 3DE (Table 8.4).

TABLE 8.4 - Comparison between 3DE and 2DE parameters of RA size and function

	3DE	2DE	p	Limit 3D	Limit 2D
Vmax (ml)	52±15	41±14	<0.0001	78§	69§
Vmin (ml)	19±8	17±7	<0.0001	36§	33§
VpreA (ml)	28±10	27±11	<0.0001	49§	49§
Total SV (ml)	33±10	24±9	<0.0001	17*	11*
Passive SV (ml)	24±9	14±7	<0.0001	10*	4*
True SV (ml)	9±4	10±5	0.017	4*	3*
Total EmptFr (%)	63±9	58±9	<0.0001	49*	42*
Passive EmptFr (%)	46±11	34±12	<0.0001	24*	14*
True EmptFr (%)	31±8	35±11	<0.0001	18*	17*

§upper limit. *lower limit.

Abbreviations as in Table 8.2

8.2.4. Reproducibility

All three techniques showed very good intra- and inter-observer reproducibility (Table 8.5). However, interobserver reproducibility of 3DE RA volumes was significantly better than that of 2DE RA volumes.

TABLE 9.5 - Intra- and interobsever variability of two- and three-dimensional right atrial volumes and longitudinal strain

	Intraobserver variability			Interobserver variability		
	bias	**95%CI**	**ICC**	**bias**	**95%CI**	**ICC**
2DE Vmax (ml)	-1.2	-14.3 ; 11.9	0.91	-1.3	-19.2 ; 16.6	0.85
2DE Vmin (ml)	-0.2	-4.9 ; 4.5	0.95	-5.3	-15 ; 4.3	0.56
2DE VpreA (ml)	-1.7	-8.3 ; 4.9	0.94	-5.3	-21.3 ; 10.8	0.69
3DE Vmax (ml)	0	-9.6 ; 9.7	0.94	3.7	-9.1 ; 16.5	0.86
3DE Vmin (ml)	1	-3.4 ; 5.5	0.95	-1.5	-7.3 ; 4.4	0.91
3DE VpreA (ml)	-0.2	-10.6 ; 10.2	0.9	-1	-9.3 ; 7.2	0.92

Abbreviations as in Table 8.2

8.3 Discussion

The present study provides the reference values for RA size and function measured by 3DE in a relatively large cohort of healthy volunteers with a wide age range. We found that: (i). RA assessment with 3DE is feasible and reproducible; (ii). 3DE allows to assess not only RA volumes, but also its phasic function parameters; (iii). RA volume values obtained with 3DE cannot be used interchangeably with 2DE derived volumes; (iv). Reference values of RA volumes should be gender specific while reference values for RA function should be age specific.

8.3.1. Echocardiographic assessment o RA size and additional value of 3DE

There is increasing evidence that RA enlargement is an outcome predictor in pathologic conditions, such as primary pulmonary hypertension and chronic heart failure. (151-153,156) However, before introducing RA size and function assessment in the routine of the echo

laboratories, the reference values for these parameters should be identified. At present, diameters and area measured in a 2DE apical 4-chamber view are the only recommended methods to assess RA size while RA volume computation is not included in routine echocardiography because of the lack of reference data. (38,50) In the present study, we used 3DE to obtain reference values of RA volume and function because of recognized superiority of 3DE over 2DE in heart chamber measurement. (1) In particular, a previous study by Keller et al. (134) demonstrated that 3DE measurement of RA volume is comparable to CMR and it is superior to current 2DE techniques. In addition, the software we have used to quantitate 3DE RA datasets has been recently validated against CMR in a multicentre validation study of 3DE left atrial volumes. (48) Finally, our results about RA Vmax (upper limit 49 ml/m^2 vs 50 ml/m^2, and 38 ml/m^2 vs 41 ml/m^2, for men and women, respectively) and total EF (lower limit 49% vs 46%) are very similar to those previously reported by Aune et al. (139) Therefore, we are confident that our study has provided robust data about the reference values of RA size and function.

8.3.2 Importance of assessing RA phasic function

In addition to data reported by Aune and coworkers, the measurement of the RA Vprea allowed us to assess also the conduit and booster functions of the RA, providing a comprehensive assessment of RA phasic functions.

Assessment of RA phasic function parameters is clinically important because the RA is a dynamic structure whose role is to assist filling the RV. The three components of RA function are: i. reservoir function, storing blood when the tricuspid valve is closed; ii. conduit function, passive blood transfer directly from the coronary and systemic veins to the right ventricle when the tricuspid valve is open; and iii. booster pump function, atrial contraction in late diastole to complete ventricular filling. (51) RA is able to modulate the relationship between reservoir and conduit function in a dynamic manner. The RA conduit-to-reservoir ratio is

directly related to the right ventricular pressure-RA pressure gradient at the time of maximum RA volume, with increased ventricular pressures favoring conduit function, but it is inversely related to cardiac output, with an increase in the reservoir contribution favoring improved cardiac output. (51) Since pathological conditions could affect and modify RA phasic functions, there is a need to know reference values of each phase to be able to understand the pathophysiology of RA function in various cardiac diseases.

8.3.3. Relationship of 3DE RA volumes and function parameters with age and gender

Our results showed significantly different RA volumes between men and women even after indexing for BSA, suggesting the need for gender-specific reference values. These findings are consistent with data reported by Aune et al(139). RA EmptFr was also higher in women than in men.

In our study there was no relation between age and Vmax and Vmin, confirming previous findings. (139) Conversely, VpreA increased significantly with age. This finding parallels the age-related changes in RA function with a significant decrease in passive RA function parameters (passEV, passEmptFr,) associated with an increase in active RA function (ActEV, ActEmptFr) in order to maintain constant TotEV. These results are in agreement with the documented age-related decrease of the tricuspid valve E/A ratio(50) and with previous reports showing an age related increase in active LA contraction in response to increased left ventricular stiffness. (157)

CHAPTER 9

Research project limitations and clinical relevance

9.1 Study limitations

3DE data set acquisitions have been performed using a single vendor platform which may have implications for the applicability of these reference values to volumetric data sets that are acquired with other vendor-specific platforms. However, conversely from myocardial deformation measurements, (158) no significant intervendor inconsistency of cardiac chamber volume has ever been reported. In addition, quantification of 3DE data sets of the RV, LA and RA have been performed using a vendor-independent software using DICOM file which should ensure generalizability of our results.

The generalizability of our research project results may be limited by the homogeneity of our study cohort with respect to race and ethnicity, too.

The identification of 'abnormal' relies on the definition of 'normal' and needs to acknowledge normal physiological variation that may arise from factors such as age, body size, gender, and ethnicity. (11) So far, the studies that have been designed to obtain the normative values for echocardiographic measurements have related the measured parameters to subjects' age, height, weight, BSA and gender. Only a few have taken into account the role of ethnicity. As a result current guidelines for chamber quantification by echocardiography (38) contains reference values that have been obtained from European (Western Europe) and American (United States) Caucasian subjects. However, ethnicity is an

important factor and studies which have compared measurements performed in Caucasians, Indians, Malaysian and Chinese (95,159), Japanese (89) or African American (160) subjects have shown significant differences in measurements between the different ethnical groups. Therefore, the use of the reference values reported in current guidelines to define normality or abnormality of cardiac chamber size and function in population others than European and White Americans may be misleading and bring to erroneous conclusions.

This is not only a medical problem of the areas of the world non-represented in current guidelines like Middle- East, Asia, Africa or South America but, since more and more people move from their area of origin to different areas of the world for working, tourism either to escape from war or persecution this lack of proper reference values is becoming a worldwide medical problem. Accordingly, several initiatives have been undertaken to collect normative data from larger cohorts of normal subjects who may include different ethnicities. (94,161) The NORRE study is a large prospective, observational multicenter study in which transthoracic echocardiographic studies will be collected in 22 European EACVI accredited echo laboratories and in one US echocardiographic laboratory to obtain reference values for cardiac chamber geometry and function in normal subjects between 25 and 75 years of age. African American subjects will be enrolled by the US laboratory. The EchoNoRMAL study is an individual person data meta-analysis of echocardiographic measurements obtained from healthy subjects aimed to re-define normal echocardiographic reference ranges (for the left heart including dimensions, areas, volumes, and associated calculated variables) for populations across the world, and to do that, the organizing Institution (the University of Auckland, New Zealand) asked data from those populations to the different reasearchers around the world. (94)

Another important limitation of this reaserach project is that the samples of men and women were not equal, particularly for the middle and advanced decades of life, raising the

possibility that some gender differences may have been amplified or not adequately detected. In addition, the number of subjects older than 60 years of age was limited. Therefore, reference values in our elderly cohort (≥ 70 years) should be considered cautiously, given the small size of this age group. Despite elderly patients are the majority of patients examined in our echocardiographic laboratories, specific reference values for the oldest decades (i.e. >70 years) are lacking. However, the enrolment of truly healthy subjects at this age is rather difficult.

The absence of a comparison with a reference standard, such as CMR, could be regarded as a limitation of this research project. However, several studies comparing 3DE and CMR to assess LV, RV and LA volumes have documented the accuracy of 3DE and consistently reported smaller volumes by 3DE than by CMR in normal subjects, as well as in a variety of cardiac diseases. (1) There is now enough evidence that the two techniques are different and that specific references values are needed for each of them. Furthermore, the analysis algorithms used in this study has been extensively validated against CMR. (41,44,48) Moreover, limited availability and costs of CMR, as well as ethical reasons prevented its use for studying healthy subjects having no clinical indication for CMR examination. The inclusion of weight as a predictor may be questionable as it may change rapidly in adults. However, the exclusion of overweight subjects could have prevented this confounding factor.

Finally, despite subjects fulfilled all the inclusion criteria as healthy adults, we cannot exclude the possibility of subclinical coronary artery disease, particularly in older subjects.

10.2 Clinical implications

3DE is a novel imaging technique based on acquisition and display of volumetric data sets in the beating heart. This permits a comprehensive evaluation of cardiac anatomy and function from a single acquisition and expands the diagnostic possibilities of non-invasive

cardiology. It provides the possibility to quantitate geometry and function of cardiac chambers without pre-established assumptions regarding cardiac chamber shape and allows an echocardiographic assessment of the heart that is less operator-dependent and therefore more reproducible.

Further developments and improvements for widespread routine applications include higher spatial and temporal resolution to improve image quality, faster acquisition, processing and reconstruction, and easier approaches to quantitative analysis. At present, 3DE complements routine 2DE in clinical practice, overcoming some of its limitations and offering additional valuable quantitative and morphological information that has led to recommend its use for routine examination in selected fields. 3DE is currently gaining popularity, as a more accurate and reproducible technique for cardiac chamber evaluation in various conditions and it is likely that, in the future, 3DE may become the standard echocardiographic examination procedure. The availability of reference values obtained in a large population of healthy subjects is an important step towards the inclusion of 3DE in everyday clinical practice.

The present research project provides a comprehensive quantitative analysis of the four cardiac chamber geometry and function using 3DE in a relatively large cohort of Caucasian healthy volunteers with a wide age range. The main results can be summarized as follows: (i). Cardiac chamber quantification with 3DE is feasible and reproducible; (ii) Reference values for cardiac chamber size and function 3DE were found to be significantly different from those obtained with conventional echocardiography, highlighting the importance of applying method-specific reference values for a reliable identification of remodeling and/or dysfunction of cardiac chambers; (iii). Cardiac chamber parameters measured by 3DE showed excellent reproducibility, and were more robust than 2DE indices at repeated measurements; (iii). Most parameters describing cardiac chamber size should be defined according to age and

gender, since indexing them only for BSA does not account for all the physiologic variations in geometry and function

Availability of reference values and age- and gender-specific cut-off values should facilitate the implementation of 3DE to identify cardiac chamber remodelling and dysfunction in both clinical routine and research. (162)

REFERENCES

1. Badano LP, Boccalini F, Muraru D et al. Current clinical applications of transthoracic three-dimensional echocardiography. J Cardiovasc Ultrasound 2012;20:1-22.
2. Lang RM, Badano LP, Tsang W et al. EAE/ASE recommendations for image acquisition and display using three-dimensional echocardiography. J Am Soc Echocardiogr 2012;25:3-46.
3. Muraru D, Boccalini F, Cattarina M et al. Quantitation of cardiac chamber geometry and function using transthoracic three-dimensional echocardiography. J Cardiovasc Echocardiogr 2012;22:146-58.
4. Muraru D, Badano LP, Peluso D et al. Comprehensive analysis of left ventricular geometry and function by three-dimensional echocardiography in healthy adults. J Am Soc Echocardiogr 2013;26:618-28.
5. Peluso D, Badano LP, Muraru D et al. Right atrial size and function assessed with three-dimensional and speckle-tracking echocardiography in 200 healthy volunteers. Eur Heart J Cardiovasc Imaging 2013.
6. Heyde B, Jasaityte R, Barbosa D et al. Elastic image registration versus speckle tracking for 2-D myocardial motion estimation: a direct comparison in vivo. IEEE Trans Med Imaging 2013;32:449-59.
7. Kawut SM, Lima JA, Barr RG et al. Sex and race differences in right ventricular structure and function: the multi-ethnic study of atherosclerosis-right ventricle study. Circulation 2011;123:2542-51.
8. Liang T, Yung L, Yu W. On feature motion decorrelation in ultrasound speckle tracking. IEEE Trans Med Imaging 2013;32:435-48.
9. Muraru D, Badano LP, Peluso D et al. Comprehensive analysis of left ventricular geometry and function by three-dimensional echocardiography in healthy adults. JAmSocEchocardiogr 2013;26:618-28.
10. Maffessanti F, Muraru D, Esposito R et al. Age-, Body Size- and Gender-specific Reference Values for Right Ventricular Volumes and Ejection Fraction by Three-dimensional Echocardiography: A Multicenter Echocardiographic Study in 507 Healthy Volunteers. Circ Cardiovasc Imaging 2013.
11. Badano L, Solinas L, Cassin M, Zanuttini D. [Inescapable relativity of normal values in echocardiography]. Cardiologia 1999;44:147-53.

12. Elveback LR, Guillier CL, JKeating jr FR. Health, normality and the ghost of Gauss. JAMA : the journal of the American Medical Association 1970;211:69-75.
13. Kaku K, Takeuchi M, Otani K et al. Age- and gender-dependency of left ventricular geometry assessed with real-time three-dimensional transthoracic echocardiography. J Am Soc Echocardiogr 2011;24:541-7.
14. Cramer H. Mathematical Methods of Statistics. Princeton, N.J.: Princeton University press, 1946.
15. Smith HW. Plato and Clememntine. Bull NY Acad Med 1947;23:352.
16. Grasbeck R, Saris NE. Establishment and use of normal values. Scandinavian journal of clinical and laboratory investigation 1969;26 (suppl 110):62-63.
17. Motoji Y, Tanaka H, Fukuda Y et al. Efficacy of right ventricular free-wall longitudinal speckle-tracking strain for predicting long-term outcome in patients with pulmonary hypertension. Circ J 2013;77:756-63.
18. Badano LP, Dall'Armellina E, Monaghan MJ et al. Real-time three-dimensional echocardiography: technological gadget or clinical tool? J Cardiovasc Med (Hagerstown) 2007;8:144-62.
19. Dekker DL, Piziali RL, Dong E, Jr. A system for ultrasonically imaging the human heart in three dimensions. Computers and biomedical research, an international journal 1974;7:544-53.
20. Moritz WE, Shreve PL. A microprocessor based spatial locating system for use with diagnostic ultrasound. IEEE Trans Biomed Eng 1976;64:966-74.
21. Raab FH, Blood EB, Steiner TO, al. e. Magnetic position and orientation tracking system. IEEE Trans Aerospace Elec Sys 1979;15:709-18.
22. Geiser EA, Lupkiewicz SM, Christie LG, Ariet M, Conetta DA, Conti CR. A framework for three-dimensional time-varying reconstruction of the human left ventricle: sources of error and estimation of their magnitude. Computers and biomedical research, an international journal 1980;13:225-41.
23. Ghosh A, Nanda NC, Maurer G. Three-dimensional reconstruction of echo-cardiographic images using the rotation method. Ultrasound Med Biol 1982;8:655-61.
24. Matsumoto M, Matsuo H, Kitabatake A et al. Three-dimensional echocardiograms and two-dimensional echocardiographic images at desired planes by a computerized system. Ultrasound Med Biol 1977;3:163-78.

25. Matsumoto M, Inoue M, Tamura S, Tanaka K, Abe H. Three-dimensional echocardiography for spatial visualization and volume calculation of cardiac structures. J Clin Ultrasound 1981;9:157-65.
26. Nanda N, Pinheiro L, Sanyal R, al. e. Multiplane transesophagal echocardiographic imaging and three-dimensional reconstruction. Echocardiography 1992;9.
27. Pandian NG, Nanda NC, Schwartz SL et al. Three-dimensional and four-dimensional transesophageal echocardiographic imaging of the heart and aorta in humans using a computed tomographic imaging probe. Echocardiography 1992;9:677-87.
28. Flachskampf FA, Franke A, Job FP et al. Three-dimensional reconstruction of cardiac structures from transesophageal echocardiography. Am J Card Imaging 1995;9:141-7.
29. Vogel M, Losch S. Dynamic three-dimensional echocardiography with a computed tomography imaging probe: initial clinical experience with transthoracic application in infants and children with congenital heart defects. Br Heart J 1994;71:462-7.
30. Ludomirsky A, Vermilion R, Nesser J et al. Transthoracic real-time three-dimensional echocardiography using the rotational scanning approach for data acquisition. Echocardiography 1994;11:599-606.
31. Kupferwasser I, Mohr-Kahaly S, Stahr P et al. Transthoracic three-dimensional echocardiographic volumetry of distorted left ventricles using rotational scanning. J Am Soc Echocardiogr 1997;10:840-52.
32. Sheikh K, Smith SW, von Ramm O, Kisslo J. Real-time, three-dimensional echocardiography: feasibility and initial use. Echocardiography 1991;8:119-25.
33. von Ramm OT, Smith SW. Real time volumetric ultrasound imaging system. Journal of digital imaging : the official journal of the Society for Computer Applications in Radiology 1990;3:261-6.
34. Rabben SI. Technical principles of transthoracic three-dimensional echocardiography. In: Badano LP, Lang RM, Zamorano JL, editors. Textbook of real-time three dimensional echocardiography. London: Springer, 2011:9.24.
35. Grothues F, Smith GC, Moon JC et al. Comparison of interstudy reproducibility of cardiovascular magnetic resonance with two-dimensional echocardiography in normal subjects and in patients with heart failure or left ventricular hypertrophy. Am J Cardiol 2002;90:29-34.
36. DG. A. Practical statistics for medical research. London, United KIngdom: Chapman & Hall eds, 1991.

37. Dubois D, Dubois EF. Clinical calorimetry. A formula to extimate the approximate surface area if height and weight are known. Arch Int Med 1916;17:863-71.
38. Lang RM, Bierig M, Devereux RB et al. Recommendations for chamber quantification. European journal of echocardiography : the journal of the Working Group on Echocardiography of the European Society of Cardiology 2006;7:79-108.
39. Ilercil A, O'Grady MJ, Roman MJ et al. Reference values for echocardiographic measurements in urban and rural populations of differing ethnicity: the Strong Heart Study. J Am Soc Echocardiogr 2001;14:601-11.
40. Sahn DJ, DeMaria A, Kisslo J, Weyman A. Recommendations regarding quantitation in M-mode echocardiography: results of a survey of echocardiographic measurements. Circulation 1978;58:1072-83.
41. Muraru D, Badano LP, Piccoli G et al. Validation of a novel automated border-detection algorithm for rapid and accurate quantitation of left ventricular volumes based on three-dimensional echocardiography. Eur J Echocardiogr 2010;11:359-68.
42. Mor-Avi V, Jenkins C, Kuhl HP et al. Real-time 3-dimensional echocardiographic quantification of left ventricular volumes: multicenter study for validation with magnetic resonance imaging and investigation of sources of error. JACC Cardiovasc Imaging 2008;1:413-23.
43. Mannaerts HF, van der Heide JA, Kamp O, Stoel MG, Twisk J, Visser CA. Early identification of left ventricular remodelling after myocardial infarction, assessed by transthoracic echocardiography. Eur Heart J 2004;25:680-7.
44. Niemann PS, Pinho L, Balbach T et al. Anatomically oriented right ventricular volume measurements with dynamic three-dimensional echocardiography validated by 3-Tesla magnetic resonance imaging. J Am Coll Cardiol 2007;50:1668-76.
45. Leibundgut G, Rohner A, Grize L et al. Dynamic assessment of right ventricular volumes and function by real-time three-dimensional echocardiography: a comparison study with magnetic resonance imaging in 100 adult patients. J Am Soc Echocardiogr 2010;23:116-26.
46. van der Zwaan HB, Helbing WA, McGhie JS et al. Clinical value of real-time three-dimensional echocardiography for right ventricular quantification in congenital heart disease: validation with cardiac magnetic resonance imaging. J Am Soc Echocardiogr 2010;23:134-40.
47. Muraru D, Sarais C. Lo studio 3D della struttura e della funzione del ventricolo destro: la riscoperta della camera dimensticata. In: Badano LP, Galderisi M, Muraru D,

Mondillo S, editors. Ecocardiografia multiplanare e tridimensionale real-time. Livorno: MB&Care, 2011:41-50.

48. Mor-Avi V, Yodwut C, Jenkins C et al. Real-time 3D echocardiographic quantification of left atrial volume: multicenter study for validation with CMR. JACC Cardiovascular imaging 2012;5:769-77.
49. Klitsie LM, Roest AA, Blom NA, Ten Harkel AD. Ventricular Performance After Surgery for a Congenital Heart Defect as Assessed Using Advanced Echocardiography: From Doppler Flow to 3D Echocardiography and Speckle-Tracking Strain Imaging. Pediatr Cardiol 2013.
50. Rudski LG, Lai WW, Afilalo J et al. Guidelines for the echocardiographic assessment of the rigth heart in adults: a report from the American Society of Echocardiography. J Am Soc Echocardiogr 2010;23:685-713.
51. Gaynor SL, Maniar HS, Prasad SM, Steendijk P, Moon MR. Reservoir and conduit function of right atrium: impact on right ventricular filling and cardiac output. Am J Physiol Heart Circ Physiol 2005;288:H2140-5.
52. Vahanian A, Alfieri O, Andreotti F et al. Guidelines on the management of valvular heart disease (version 2012): The Joint Task Force on the Management of Valvular Heart Disease of the European Society of Cardiology (ESC) and the European Association for Cardio-Thoracic Surgery (EACTS). Eur Heart J 2012;33:2451-96.
53. Dickstein K, Vardas PE, Auricchio A et al. 2010 Focused Update of ESC Guidelines on device therapy in heart failure: an update of the 2008 ESC Guidelines for the diagnosis and treatment of acute and chronic heart failure and the 2007 ESC guidelines for cardiac and resynchronization therapy. Developed with the special contribution of the Heart Failure Association and the European Heart Rhythm Association. Eur Heart J 2010;31:2677-87.
54. Jenkins C, Bricknell K, Chan J, Hanekom L, Marwick TH. Comparison of two- and three-dimensional echocardiography with sequential magnetic resonance imaging for evaluating left ventricular volume and ejection fraction over time in patients with healed myocardial infarction. Am J Cardiol 2007;99:300-6.
55. Badano LP. The clinical benefit of adding a third dimension to assess the left ventricle with echocardiography. Scientifica (Cairo) 2014:in press.
56. Shimada YJ, Shiota T. A meta-analysis and investigation for the source of bias of left ventricular volumes and function by three-dimensional echocardiography in comparison with magnetic resonance imaging. Am J Cardiol 2011;107:126-38.

57. Jenkins C, Bricknell K, Hanekom L, Marwick TH. Reproducibility and accuracy of echocardiographic measurements of left ventricular parameters using real-time three-dimensional echocardiography. J Am Coll Cardiol 2004;44:878-86.
58. Kuhl HP, Schreckenberg M, Rulands D et al. High-resolution transthoracic real-time three-dimensional echocardiography: quantitation of cardiac volumes and function using semi-automatic border detection and comparison with cardiac magnetic resonance imaging. J Am Coll Cardiol 2004;43:2083-90.
59. Caiani EG, Corsi C, Zamorano J et al. Improved semiautomated quantification of left ventricular volumes and ejection fraction using 3-dimensional echocardiography with a full matrix-array transducer: comparison with magnetic resonance imaging. J Am Soc Echocardiogr 2005;18:779-88.
60. Shiota T, McCarthy PM, White RD et al. Initial clinical experience of real-time three-dimensional echocardiography in patients with ischemic and idiopathic dilated cardiomyopathy. Am J Cardiol 1999;84:1068-73.
61. Zeidan Z, Erbel R, Barkhausen J, Hunold P, Bartel T, Buck T. Analysis of global systolic and diastolic left ventricular performance using volume-time curves by real-time three-dimensional echocardiography. J Am Soc Echocardiogr 2003;16:29-37.
62. Chan J, Jenkins C, Khafagi F, Du L, Marwick TH. What is the optimal clinical technique for measurement of left ventricular volume after myocardial infarction? A comparative study of 3-dimensional echocardiography, single photon emission computed tomography, and cardiac magnetic resonance imaging. J Am Soc Echocardiogr 2006;19:192-201.
63. Corsi C, Lamberti C, Catalano O et al. Improved quantification of left ventricular volumes and mass based on endocardial and epicardial surface detection from cardiac MR images using level set models. Journal of cardiovascular magnetic resonance : official journal of the Society for Cardiovascular Magnetic Resonance 2005;7:595-602.
64. Sugeng L, Mor-Avi V, Weinert L et al. Quantitative assessment of left ventricular size and function: side-by-side comparison of real-time three-dimensional echocardiography and computed tomography with magnetic resonance reference. Circulation 2006;114:654-61.
65. Nikitin NP, Constantin C, Loh PH et al. New generation 3-dimensional echocardiography for left ventricular volumetric and functional measurements: comparison with cardiac magnetic resonance. Eur J Echocardiogr 2006;7:365-72.

66. Jacobs LD, Salgo IS, Goonewardena S et al. Rapid online quantification of left ventricular volume from real-time three-dimensional echocardiographic data. Eur Heart J 2006;27:460-8.
67. Gutierrez-Chico JL, Zamorano JL, Perez de Isla L et al. Comparison of left ventricular volumes and ejection fractions measured by three-dimensional echocardiography versus by two-dimensional echocardiography and cardiac magnetic resonance in patients with various cardiomyopathies. Am J Cardiol 2005;95:809-13.
68. van den Bosch AE, Robbers-Visser D, Krenning BJ et al. Real-time transthoracic three-dimensional echocardiographic assessment of left ventricular volume and ejection fraction in congenital heart disease. J Am Soc Echocardiogr 2006;19:1-6.
69. Pouleur AC, le Polain de Waroux JB, Pasquet A et al. Assessment of left ventricular mass and volumes by three-dimensional echocardiography in patients with or without wall motion abnormalities: comparison against cine magnetic resonance imaging. Heart 2008;94:1050-7.
70. Qi X, Cogar B, Hsiung MC et al. Live/real time three-dimensional transthoracic echocardiographic assessment of left ventricular volumes, ejection fraction, and mass compared with magnetic resonance imaging. Echocardiography 2007;24:166-73.
71. Bicudo LS, Tsutsui JM, Shiozaki A et al. Value of real time three-dimensional echocardiography in patients with hypertrophic cardiomyopathy: comparison with two-dimensional echocardiography and magnetic resonance imaging. Echocardiography 2008;25:717-26.
72. Muraru D, Badano LP, Ermacora D, Piccoli G, Iliceto S. Sources of variation and bias in assessing left ventricular volumes and dyssynchrony using three-dimensional echocardiography. Int J Cardiovasc Imaging 2012;28:1357-68.
73. Tighe DA, Rosetti M, Vinch CS et al. Influence of image quality on the accuracy of real time three-dimensional echocardiography to measure left ventricular volumes in unselected patients: a comparison with gated-SPECT imaging. Echocardiography 2007;24:1073-80.
74. Krenning BJ, Kirschbaum SW, Soliman OI et al. Comparison of contrast agent-enhanced versus non-contrast agent-enhanced real-time three-dimensional echocardiography for analysis of left ventricular systolic function. Am J Cardiol 2007;100:1485-9.
75. Jenkins C, Moir S, Chan J, Rakhit D, Haluska B, Marwick TH. Left ventricular volume measurement with echocardiography: a comparison of left ventricular opacification,

three-dimensional echocardiography, or both with magnetic resonance imaging. Eur Heart J 2009;30:98-106.

76. Mannaerts HF, van der Heide JA, Kamp O, Stoel MG, Twisk J, Visser CA. Early identification of left ventricular remodelling after myocardial infarction, assessed by transthoracic 3D echocardiography. Eur Heart J 2004;25:680-7.
77. Galderisi M, Henein MY, D'Hooge J et al. Recommendations of the European Association of Echocardiography: how to use echo-Doppler in clinical trials: different modalities for different purposes. Eur J Echocardiogr 2011;12:339-53.
78. Mor-Avi V, Sugeng L, Weinert L et al. Fast measurement of left ventricular mass with real-time three-dimensional echocardiography: comparison with magnetic resonance imaging. Circulation 2004;110:1814-8.
79. Caiani EG, Corsi C, Sugeng L et al. Improved quantification of left ventricular mass based on endocardial and epicardial surface detection with real time three dimensional echocardiography. Heart 2006;92:213-9.
80. Qin JX, Shiota T, Thomas JD. Determination of left ventricular volume, ejection fraction, and myocardial mass by real-time three-dimensional echocardiography. Echocardiography 2000;17:781-6.
81. Oe H, Hozumi T, Arai K et al. Comparison of accurate measurement of left ventricular mass in patients with hypertrophied hearts by real-time three-dimensional echocardiography versus magnetic resonance imaging. Am J Cardiol 2005;95:1263-7.
82. van den Bosch AE, Robbers-Visser D, Krenning BJ et al. Comparison of real-time three-dimensional echocardiography to magnetic resonance imaging for assessment of left ventricular mass. Am J Cardiol 2006;97:113-7.
83. Takeuchi M, Nishikage T, Mor-Avi V et al. Measurement of left ventricular mass by real-time three-dimensional echocardiography: validation against magnetic resonance and comparison with two-dimensional and m-mode measurements. J Am Soc Echocardiogr 2008;21:1001-5.
84. Corsi C, Lang RM, Veronesi F et al. Volumetric quantification of global and regional left ventricular function from real-time three-dimensional echocardiographic images. Circulation 2005;112:1161-70.
85. Jaochim Nesser H, Sugeng L, Corsi C et al. Volumetric analysis of regional left ventricular function with real-time three-dimensional echocardiography: validation by magnetic resonance and clinical utility testing. Heart 2007;93:572-8.

86. Seo Y, Ishizu T, Enomoto Y et al. Validation of 3-dimensional speckle tracking imaging to quantify regional myocardial deformation. Circ Cardiovasc Imaging 2009;2:451-9.
87. Lang RM, Badano LP, Tsang W et al. EAE/ASE recommendations for image acquisition and display using three-dimensional echocardiography. Eur Heart J Cardiovasc Imaging 2012;13:1-46.
88. Aune E, Baekkevar M, Rodevand O, Otterstad JE. Reference values for left ventricular volumes with real-time 3-dimensional echocardiography. Scand Cardiovasc J 2010;44:24-30.
89. Fukuda S, Watanabe H, Daimon M et al. Normal values of real-time 3-dimensional echocardiographic parameters in a healthy Japanese population: the JAMP-3D Study. Circ J 2012;76:1177-81.
90. Dorosz JL, Lezotte DC, Weitzenkamp DA, Allen LA, Salcedo EE. Performance of 3-dimensional echocardiography in measuring left ventricular volumes and ejection fraction: a systematic review and meta-analysis. J Am Coll Cardiol 2012;59:1799-808.
91. Nikitin NP, Loh PH, de Silva R et al. Left ventricular morphology, global and longitudinal function in normal older individuals: a cardiac magnetic resonance study. Int J Cardiol 2006;108:76-83.
92. Missouris CG, Forbat SM, Singer DR, Markandu ND, Underwood R, MacGregor GA. Echocardiography overestimates left ventricular mass: a comparative study with magnetic resonance imaging in patients with hypertension. Journal of hypertension 1996;14:1005-10.
93. Kuhl HP, Hanrath P, Franke A. M-mode echocardiography overestimates left ventricular mass in patients with normal left ventricular shape: a comparative study using three-dimensional echocardiography. Eur J Echocardiogr 2003;4:312-9.
94. Poppe KK, Doughty RN, Whalley GA. Redefining normal reference ranges for echocardiography: a major new individual person data meta-analysis. Eur Heart J Cardiovasc Imaging 2013;14:347-8.
95. Chahal NS, Lim TK, Jain P, Chambers JC, Kooner JS, Senior R. Population-based reference values for 3D echocardiographic LV volumes and ejection fraction. JACC Cardiovasc Imaging 2012;5:1191-7.
96. Badano LP. Defining normative values for 3D LV volumes: the devil is in the details. JACC Cardiovasc Imaging 2013;6:530.
97. Hudsmith LE, Petersen SE, Francis JM, Robson MD, Neubauer S. Normal human left and right ventricular and left atrial dimensions using steady state free precession magnetic

resonance imaging. Journal of cardiovascular magnetic resonance : official journal of the Society for Cardiovascular Magnetic Resonance 2005;7:775-82.

98. Abo K, Hozumi T, Fukuda S et al. [Usefulness of transthoracic freehand three-dimensional echocardiography for the evaluation of mitral valve prolapse]. J Cardiol 2004;43:17-22.
99. Cheng S, Fernandes VR, Bluemke DA, McClelland RL, Kronmal RA, Lima JA. Age-related left ventricular remodelling and associated risk for cardiovascular outcomes: the Multi-Ethnic study of atherosclerosis. Circ Cardiovasc Imaging 2009;2:191-8.
100. Lakatta EG. Cardiovascular regulatory mechanisms in advanced age. Physiological reviews 1993;73:413-67.
101. Badano LP, Ginghina C, Easaw J et al. Right ventricle in pulmonary arterial hypertension: haemodynamics, structural changes, imaging, and proposal of a study protocol aimed to assess remodelling and treatment effects. Eur J Echocardiogr 2010;11:27-37.
102. Shimada YJ, Shiota M, Siegel RJ, Shiota T. Accuracy of right ventricular volumes and function determined by three-dimensional echocardiography in comparison with magnetic resonance imaging: a meta-analysis study. J Am Soc Echocardiogr 2010;23:943-53.
103. Tamborini G, Marsan NA, Gripari P et al. Reference values for right ventricular volumes and ejection fraction with real-time three-dimensional echocardiography: evaluation in a large series of normal subjects. J Am Soc Echocardiogr 2010;23:109-15.
104. Grapsa J, Gibbs JS, Dawson D et al. Morphologic and functional remodeling of the right ventricle in pulmonary hypertension by real time three dimensional echocardiography. Am J Cardiol 2012;109:906-13.
105. Sugeng L, Mor-Avi V, Weinert L et al. Multimodality comparison of quantitative volumetric analysis of the right ventricle. JACC Cardiovasc Imaging 2010;3:10-8.
106. Amaki M, Nakatani S, Kanzaki H et al. Usefulness of three-dimensional echocardiography in assessing right ventricular function in patients with primary pulmonary hypertension. Hypertens Res 2009;32:419-22.
107. Tamborini G, Muratori M, Brusoni D et al. Is right ventricular systolic function reduced after cardiac surgery? A two- and three-dimensional echocardiographic study. Eur J Echocardiogr 2009;10:630-4.

108. Giusca S, Dambrauskaite V, Scheurwegs C et al. Deformation imaging describes right ventricular function better than longitudinal displacement of the tricuspid ring. Heart 2010;96:281-8.
109. Dewey FE, Rosenthal D, Murphy DJ, Jr., Froelicher VF, Ashley EA. Does size matter? Clinical applications of scaling cardiac size and function for body size. Circulation 2008;117:2279-87.
110. Mor-Avi V, Sugeng L, Lindner JR. Imaging the forgotten chamber: is the devil in the boundary? J Am Soc Echocardiogr 2010;23:141-3.
111. De Castro S, Cavarretta E, Milan A et al. Usefulness of tricuspid annular velocity in identifying global RV dysfunction in patients with primary pulmonary hypertension: a comparison with 3D echo-derived right ventricular ejection fraction. Echocardiography 2008;25:289-93.
112. Fusini L, Tamborini G, Gripari P et al. Feasibility of intraoperative three-dimensional transesophageal echocardiography in the evaluation of right ventricular volumes and function in patients undergoing cardiac surgery. J Am Soc Echocardiogr 2011;24:868-77.
113. Grewal J, Majdalany D, Syed I, Pellikka P, Warnes CA. Three-dimensional echocardiographic assessment of right ventricular volume and function in adult patients with congenital heart disease: comparison with magnetic resonance imaging. J Am Soc Echocardiogr 2010;23:127-33.
114. Sluysmans T, Colan SD. Theoretical and empirical derivation of cardiovascular allometric relationships in children. J Appl Physiol 2005;99:445-57.
115. Mawad W, Drolet C, Dahdah N, Dallaire F. A review and critique of the statistical methods used to generate reference values in pediatric echocardiography. J Am Soc Echocardiogr 2013;26:29-37.
116. D'Oronzio U, Senn O, Biaggi P et al. Right heart assessment by echocardiography: gender and body size matters. J Am Soc Echocardiogr 2012;25:1251-8.
117. Gopal AS, Chukwu EO, Iwuchukwu CJ et al. Normal values of right ventricular size and function by real-time 3-dimensional echocardiography: comparison with cardiac magnetic resonance imaging. J Am Soc Echocardiogr 2007;20:445-55.
118. Lipshultz SE, Easley KA, Orav EJ et al. Reliability of multicenter pediatric echocardiographic measurements of left ventricular structure and function: the prospective P(2)C(2) HIV study. Circulation 2001;104:310-6.

119. Maceira AM, Prasad SK, Khan M, Pennell DJ. Reference right ventricular systolic and diastolic function normalized to age, gender and body surface area from steady-state free precession cardiovascular magnetic resonance. Eur Heart J 2006;27:2879-88.
120. Tandri H, Daya SK, Nasir K et al. Normal reference values for the adult right ventricle by magnetic resonance imaging. Am J Cardiol 2006;98:1660-4.
121. Kjaergaard J, Petersen CL, Kjaer A, Schaadt BK, Oh JK, Hassager C. Evaluation of right ventricular volume and function by 2D and 3D echocardiography compared to MRI. Eur J Echocardiogr 2006;7:430-8.
122. Marwick TH. Consistency of myocardial deformation imaging between vendors. Eur J Echocardiogr 2010;11:414-6.
123. Beerbaum P, Barth P, Kropf S et al. Cardiac function by MRI in congenital heart disease: impact of consensus training on interinstitutional variance. Journal of magnetic resonance imaging : JMRI 2009;30:956-66.
124. Dedobbeleer C, Hadefi A, Naeije R, Unger P. Left ventricular adaptation to acute hypoxia: a speckle-tracking echocardiography study. J Am Soc Echocardiogr 2013;26:736-45.
125. Tsang TS, Barnes ME, Gersh BJ, Bailey KR, Seward JB. Left atrial volume as a morphophysiologic expression of left ventricular diastolic dysfunction and relation to cardiovascular risk burden. The American journal of cardiology 2002;90:1284-9.
126. Tschope C, Kasner M. Can speckle-tracking imaging improve the reliability of echocardiographic parameters for outcome evaluation in clinical trials? Eur Heart J 2013.
127. Khoo NS, Smallhorn JF, Kaneko S, Kutty S, Altamirano L, Tham EB. The assessment of atrial function in single ventricle hearts from birth to Fontan: a speckle-tracking study by using strain and strain rate. J Am Soc Echocardiogr 2013;26:756-64.
128. Liu HY, Deng YB, Liu K et al. Left ventricular systolic strain of the cardiac allograft evaluated with three-dimensional speckle tracking echocardiography. J Huazhong Univ Sci Technolog Med Sci 2013;33:765-9.
129. Tsang TS, Abhayaratna WP, Barnes ME et al. Prediction of cardiovascular outcomes with left atrial size: is volume superior to area or diameter? Journal of the American College of Cardiology 2006;47:1018-23.
130. Lang RM, Badano LP, Tsang W et al. EAE/ASE recommendations for image acquisition and display using three-dimensional echocardiography. European heart journal cardiovascular Imaging 2012;13:1-46.

131. Avelar E, Durst R, Rosito GA et al. Comparison of the accuracy of multidetector computed tomography versus two-dimensional echocardiography to measure left atrial volume. The American journal of cardiology 2010;106:104-9.
132. Kuhl JT, Lonborg J, Fuchs A et al. Assessment of left atrial volume and function: a comparative study between echocardiography, magnetic resonance imaging and multi slice computed tomography. The international journal of cardiovascular imaging 2012;28:1061-71.
133. Lee Y, Mori N, Nakamura D et al. New Approach for Rotational Dyssynchrony Using Three-Dimensional Speckle Tracking Echocardiography. Echocardiography 2013.
134. Syeda B, Hofer P, Pichler P et al. Two-dimensional speckle-tracking strain echocardiography in long-term heart transplant patients: a study comparing deformation parameters and ejection fraction derived from echocardiography and multislice computed tomography. Eur J Echocardiogr 2011;12:490-6.
135. Sehgal A, Doctor T, Menahem S. Cardiac function and arterial indices in infants born small for gestational age: Analysis by Speckle tracking. Acta Paediatr 2013.
136. Wang A, Cabreriza SE, Cheng B, Shanewise JS, Spotnitz HM. Feasibility of Speckle-Tracking Echocardiography for Assessment of Left Ventricular Dysfunction after Cardiopulmonary Bypass. J Cardiothorac Vasc Anesth 2013.
137. Li YJ, Li C, Li CM et al. [Value of three-dimensional speckle-tracking echocardiography and the novel area strain in detecting wall motion abnormalities of coronary artery diseases]. Sichuan da xue xue bao Yi xue ban = Journal of Sichuan University Medical science edition 2013;44:651-6.
138. Jenkins C, Bricknell K, Marwick TH. Use of real-time three-dimensional echocardiography to measure left atrial volume: comparison with other echocardiographic techniques. Journal of the American Society of Echocardiography : official publication of the American Society of Echocardiography 2005;18:991-7.
139. Moen CA, Samlminen PR, Dahle GO, Hjertaas JJ, Matre K. Is strain by speckle tracking echocardiography dependent on user controlled spatial and temporal smoothing? Cardiovasc Ultrasound 2013;11:32.
140. Kocabay G, Karabay CY, Colak Y et al. Left atrial deformation parameters in patients with non-alcoholic fatty liver disease: a 2D speckle tracking imaging study. Clin Sci (Lond) 2014;126:297-304.
141. Altiok E, Neizel M, Tiemann S et al. Quantitative analysis of endocardial and epicardial left ventricular myocardial deformation-comparison of strain-encoded cardiac

magnetic resonance imaging with two-dimensional speckle-tracking echocardiography. J Am Soc Echocardiogr 2012;25:1179-88.

142. Yodwut C, Weinert L, Klas B, Lang RM, Mor-Avi V. Effects of frame rate on three-dimensional speckle-tracking-based measurements of myocardial deformation. J Am Soc Echocardiogr 2012;25:978-85.
143. Saito K, Okura H, Watanabe N et al. Comprehensive evaluation of left ventricular strain using speckle tracking echocardiography in normal adults: comparison of three-dimensional and two-dimensional approaches. J Am Soc Echocardiogr 2009;22:1025-30.
144. Nelson MR, Hurst RT, Raslan SF, Cha S, Wilansky S, Lester SJ. Echocardiographic measures of myocardial deformation by speckle-tracking technologies: the need for standardization? J Am Soc Echocardiogr 2012;25:1189-94.
145. Zoroufian A, Razmi T, Taghavi-Shavazi M, Lotfi-Tokaldany M, Jalali A. Evaluation of Subclinical Left Ventricular Dysfunction in Diabetic Patients: Longitudinal Strain Velocities and Left Ventricular Dyssynchrony by Two-Dimensional Speckle Tracking Echocardiography Study. Echocardiography 2013.
146. Onishi T, Saha SK, Ludwig DR et al. Feature tracking measurement of dyssynchrony from cardiovascular magnetic resonance cine acquisitions: comparison with echocardiographic speckle tracking. Journal of cardiovascular magnetic resonance : official journal of the Society for Cardiovascular Magnetic Resonance 2013;15:95.
147. Shimada YJ, Shiota T. Underestimation of left atrial volume by three-dimensional echocardiography validated by magnetic resonance imaging: a meta-analysis and investigation of the source of bias. Echocardiography 2012;29:385-90.
148. Ternacle J, Gallet R, Champagne S et al. Changes in Three-Dimensional Speckle-Tracking-Derived Myocardial Strain during Percutaneous Coronary Intervention. J Am Soc Echocardiogr 2013.
149. Park CM, March K, Williams S et al. Feasibility and reproducibility of left ventricular rotation by speckle tracking echocardiography in elderly individuals and the impact of different software. PloS one 2013;8:e75098.
150. Do DH, Therrien J, Marelli A, Martucci G, Afilalo J, Sebag IA. Right atrial size relates to right ventricular end-diastolic pressure in an adult population with congenital heart disease. Echocardiography 2011;28:109-16.
151. Sallach JA, Tang WH, Borowski AG et al. Right atrial volume index in chronic systolic heart failure and prognosis. JACC Cardiovasc Imaging 2009;2:527-34.

152. Cioffi G, de Simone G, Mureddu G, Tarantini L, Stefenelli C. Right atrial size and function in patients with pulmonary hypertension associated with disorders of respiratory system or hypoxemia. Eur J Echocardiogr 2007;8:322-31.
153. Raymond RJ, Hinderliter AL, Willis PW et al. Echocardiographic predictors of adverse outcomes in primary pulmonary hypertension. J Am Coll Cardiol 2002;2002:1214-9.
154. Bustamante-Labarta M, Perrone S, De La Fuente RL et al. Right atrial size and tricuspid regurgitation severity predict mortality or transplantation in primary pulmonary hypertension. J Am Soc Echocardiogr 2002;15:1160-4.
155. Murata M, Iwanaga S, Tamura Y et al. Real-time three-dimensional echocardiographic quantitative analysis of left ventricular diastolic dysfunction Am J Card 2008;8:1097-102.
156. Azran MS, Kwong R, Chen FY, Shernan SK. A potential use for intraoperative three-dimensional transesophageal echocardiography in predicting left ventricular chamber dimensions and ejection fraction after aneurysm resection. Anesth Analg 2010;111:1362-5.
157. Spencer KT, Mor-Avi V, Gorcsan J, 3rd et al. Effect of aging on left atrial reservoir, conduit and booster pump function: a multi-institution acoustic quantification study. Heart 2001;85:272-7.
158. Badano LP, Cucchini U, Muraru D, Al Nono O, Sarais C, Iliceto S. Use of three-dimensional speckle tracking to assess left ventricular myocardial mechanics: inter-vendor consistency and reproducibility of strain measurements. Eur Heart J Cardiovasc Imaging 2013;14:285-93.
159. Xia J, Gao Y, Wang Q, Ma W. Left atrial function examination of healthy individuals with 2D speckle-tracking imaging. Experimental and therapeutic medicine 2013;5:243-246.
160. Khan UA, de Simone G, Hill J, Tighe DA, Aurigemma GP. Depressed atrial function in diastolic dysfunction: a speckle tracking imaging study. Echocardiography 2013;30:309-16.
161. Lancellotti P, Badano LP, Lang RM et al. Normal Reference Ranges for Echocardiography: rationale, study design, and methodology (NORRE Study). Eur Heart J Cardiovasc Imaging 2013;14:303-8.
162. Kauer F, van Dalen BM, Michels M et al. Diastolic abnormalities in normal phenotype hypertrophic cardiomyopathy gene carriers: a study using speckle tracking echocardiography. Echocardiography 2013;30:558-63.

PUBLICATIONS DURING PHD PERIOD (2011-2013)

Books (n= 6)

1. **Badano LP**, Zamorano JL, Lang RM. **Textbook of real-time three-dimensional echocardiography**", Springler, London, 2011
2. Galiuto L, **Badano LP**, Fox K, Sicari R, Zamorano JL "**EAE Textbook of echocardiography**", Oxford University Press, London 2011
3. **Badano LP**, Galderisi M, Muraru D, Mondillo S. "**Ecocardiografia multi planare e tridimensionale real-time**", MB&Care, Livorno; 2011
4. **Badano LP**, Galderisi M, Muraru D, Mondillo S. "**Speckle Tracking Echocardiography**", MB&Care, Livorno; 2011
5. Plonska-Gosciniak E, Lancellotti P, **Badano LP**. **Echocardiography for internal medicine**. Medical tribune Polska, Warsaw, 2011
6. Zamorano JL, Bax JJ, Knuuti J, Sechtem P, Lancellotti P, **Badano LP**: **ESC textbook of cardiovascular imaging 2nd Edition**. Oxford University Press, Oxford. 2014, in stampa

Book chapters (n= 20)

1. Badano LP, Muraru D. "Three-dimensional echocardiography in clinical practice". In Badano LP, Lang RM, Zamorano JL "**Textbook Of Real-Time Three-Dimensional Echocardiography**" Springer-Verlag London Ltd, London, 2011:33-44.
2. Muraru D, Badano LP. "Assessment of tricuspid valve morphology and function". In Badano P, Lang RM, Zamorano JL "**Textbook Of Real-Time Three-Dimensional Echocardiography**" Springer-Verlag London Ltd, London, 2011:173-182.
3. Rigo F, Galderisi M, Muraru D, Badano LP. „Role of three-dimensional echocardiography in drug trials". In Badano LP, Lang RM, Zamorano JL "**Textbook Of Real-Time Three-Dimensional Echocardiography**" Springer-Verlag London Ltd, London, 2011:183-192
4. Badano LP, Losi C. "La storia degli aspetti tecnici e metodologici". In: Badano LP, Galderisi M, Muraru D, Mondillo S. "**Ecocardiografia multi planare e tridimensionale real-time**", MB&Care, Livorno; 2011: 5-10

5. Badano LP, Soldà E. "Il full-volume: tutto in un battito". In: Badano LP, Galderisi M, Muraru D, Mondillo S. "**Ecocardiografia multi planare e tridimensionale real-time**", MB&Care, Livorno; 2011: 17-24
6. Badano LP, Cucchini U. "Lo studio 3D della struttura e della funzione del ventricolo sinistro: l'accuratezza diagnostica della "vera" frazione d'eiezione". In: Badano LP, Galderisi M, Muraru D, Mondillo S. "**Ecocardiografia multi planare e tridimensionale real-time**", MB&Care, Livorno; 2011: 25-40
7. Badano LP, Soldà E. "Valvole tricuspide e polmonare: le nuove prospettive di valutazione non invasiva". In: Badano LP, Galderisi M, Muraru D, Mondillo S. "**Ecocardiografia multi planare e tridimensionale real-time**", MB&Care, Livorno; 2011: 85-95
8. Badano L, Muraru D, Iliceto S. Echocardiography of cardiac masses: from two- to three-dimensional imaging in Basso C, Valente M, Thiene G eds. **Cardiac tumor pathology**. Humana press, New York, 2013: 101-114
9. Muraru D, Enache R, Popescu BA, Ginghina C, Badano LP. The role of three-dimensional echocardiography in the assessment of valvular heart diseases. On behalf of Romanian Working Group of Echocardiography, in Progrese in Cardiologie 2012 (Romanian)
10. Badano L, Muraru D, Da Lin C, Iliceto S. Instrumentation and Data Acquisition in Shernan S, Lang R, Mor-Avi V and Shirali G. **Atlas of Three-Dimensional Echocardiography**. Lippincott Williams & Wilkins 2012: 13-28
11. Basso C, Muraru D, Badano L, Thiene G. Anatomy and pathology of right –sided atrio-ventricular and semilunar valves. in Rajamannan N. **Cardiac Valvular Medicine**. Springer-Verlag, London 2013: 211-222
12. Badano L, Muraru D. Natural history of tricuspid regurgitation and timing of intervention. in Rajamannan N. **Cardiac Valvular Medicine**. Springer-Verlag, London 2013: 223-248
13. Badano LP, Muraru D. Evaluation of tricuspid valve morphology and function by transthoracic three-dimensional echocardiography. In Shiota T: "**3D echocardiography, 2nd edition**"CRC Press, Los Angeles, 2014: in stampa
14. Badano LP, Cucchini U, Muraru D, Iliceto S. Il laboratorio digitale di ecocardiografia. In Nicolosi GL, Antonini Canterin F, Pavan D, Piazza R "**Manuale di ecocardiografia clinica**" 2° edizione, Piccin Editore, Padova, 2014, in stampa
15. Piazza R, Badano LP, NIcolosi GL. Approccio sistematico e studio della cinetica regionale del ventricolo sinistro. In Nicolosi GL, Antonini Canterin F, Pavan D, Piazza R

"**Manuale di ecocardiografia clinica**" 2° edizione, Piccin Editore, Padova, 2014, in stampa

16. Badano LP, Muraru D. Valvular prosteses. In Zamorano JL, Bax JJ, Knuuti J, Sechtem P, Lancellotti P, Badano LP: **ESC textbook of cardiovascular imaging 2nd Edition**. Oxford University Press, Oxford. 2014, in stampa
17. Badano LP, Mihaila S, Muraru D, Vinereanu D, Iliceto S. Functional classication of secondary mitral valve regurgitation. In: Lancellotti P, Fattouch K "**Secondary mitral regurgitation at a glance**", Springer Science + Business media, New York 2014, in stampa
18. Badano LP, Addetia K, Muraru D. Introduction, Etiology and Natural History of Tricuspid Regurgitation. In: Lang RM, Khandheria BK, Kronzon I, Mor-Avi, V, Goldstein SA. **Dynamic echocardiography, 2nd edition**. Saunders Elsevier, St Louis, 2014 in stampa
19. Badano LP, Addetia K, Muraru D. Quantification of Tricuspid Regurgitation. In: Lang RM, Khandheria BK, Kronzon I, Mor-Avi, V, Goldstein SA. **Dynamic echocardiography, 2nd edition**. Saunders Elsevier, St Louis, 2014 in stampa
20. Badano LP, Muraru D. Three-dimensional echocardiography. In: Lang RM, Khandheria BK, Kronzon I, Mor-Avi, V, Goldstein SA. **Dynamic echocardiography, 2nd edition**. Saunders Elsevier, St Louis, 2014 in stampa

Full papers indexed by Pubmed-Medline (n= 72)

1. Thomas JD, **Badano LP**. Eacvi-ase-industry initiative to standardize deformation imaging: A brief update from the co-chairs. Eur Heart J Cardiovasc Imaging. 2013;14:1039-1040
2. Steg G, James SK, Atar D, **Badano LP**, Blomstrom Lundqvist C, M AB, di Mario C, Dickstein K, Ducrocq G, Fernandez-Aviles F, A HG, Giannuzzi P, Halvorsen S, Huber K, Juni P, Kastrati A, Knuuti J, M JL, K WM, Valgimigli M, Van't Hof A, Widimsky P, Zahger D, J JB, Baumgartner H, Ceconi C, Dean V, Deaton C, Fagard R, Funck-Brentano C, Hasdai D, Hoes A, Kirchhof P, Knuuti J, Kolh P, McDonagh T, Moulin C, Popescu BA, Reiner Z, Sechtem U, Sirnes PA, Tendera M, Torbicki A, Vahanian A, Windecker S, Astin F, Astrom-Olsson K, Budaj A, Clemmensen P, Collet JP, Fox KA, Fuat A, Gustiene O, Hamm CW, Kala P, Lancellotti P, Pietro Maggioni A, Merkely B, Neumann FJ, Piepoli MF, Werf F, Verheugt F, Wallentin L. Grupo de trabajo para el manejo del infarto agudo de

miocardio con elevacion del segmento st de la sociedad europea de cardiologia (esc). Rev Esp Cardiol. 2013;66:53 e51-53 e46

3. Sicari R, Edvardsen T, **Badano L**, Lancellotti P, Habib G, Maurer G. 2013 european association cardiovascular imaging research grants. Eur Heart J Cardiovasc Imaging. 2013;14:294
4. Peluso D, **Badano LP**, Muraru D, Dal Bianco L, Cucchini U, Kocabay G, Kovacs A, Casablanca S, Iliceto S. Right atrial size and function assessed with three-dimensional and speckle-tracking echocardiography in 200 healthy volunteers. Eur Heart J Cardiovasc Imaging. 2013;14:1106-1114
5. Neskovic AN, Hagendorff A, Lancellotti P, Guarracino F, Varga A, Cosyns B, Flachskampf FA, Popescu BA, Gargani L, Zamorano JL, **Badano LP**. Emergency echocardiography: The european association of cardiovascular imaging recommendations. Eur Heart J Cardiovasc Imaging. 2013;14:1-11
6. Muraru D, Maffessanti F, Kocabay G, Peluso D, Bianco LD, Piasentini E, Jose SP, Iliceto S, **Badano LP**. Ascending aorta diameters measured by echocardiography using both leading edge-to-leading edge and inner edge-to-inner edge conventions in healthy volunteers. Eur Heart J Cardiovasc Imaging. 2013
7. Muraru D, Cattarina M, Boccalini F, Dal Lin C, Peluso D, Zoppellaro G, Bellu R, Sarais C, Xhyheri B, Iliceto S, **Badano LP**. Mitral valve anatomy and function: New insights from three-dimensional echocardiography. J Cardiovasc Med (Hagerstown). 2013;14:91-99
8. Muraru D, **Badano LP**, Peluso D, Dal Bianco L, Casablanca S, Kocabay G, Zoppellaro G, Iliceto S. Comprehensive analysis of left ventricular geometry and function by three-dimensional echocardiography in healthy adults. J Am Soc Echocardiogr. 2013;26:618-628
9. Maffessanti F, Muraru D, Esposito R, Gripari P, Ermacora D, Santoro C, Tamborini G, Galderisi M, Pepi M, **Badano LP**. Age-, body size-, and sex-specific reference values for right ventricular volumes and ejection fraction by three-dimensional echocardiography: A multicenter echocardiographic study in 507 healthy volunteers. Circ Cardiovasc Imaging. 2013;6:700-710
10. Lancellotti P, Tribouilloy C, Hagendorff A, Popescu BA, Edvardsen T, Pierard LA, **Badano L**, Zamorano JL. Recommendations for the echocardiographic assessment of native valvular regurgitation: An executive summary from the european association of cardiovascular imaging. Eur Heart J Cardiovasc Imaging. 2013;14:611-644

11. Lancellotti P, Nkomo VT, **Badano LP**, Bergler-Klein J, Bogaert J, Davin L, Cosyns B, Coucke P, Dulgheru R, Edvardsen T, Gaemperli O, Galderisi M, Griffin B, Heidenreich PA, Nieman K, Plana JC, Port SC, Scherrer-Crosbie M, Schwartz RG, Sebag IA, Voigt JU, Wann S, Yang PC. Expert consensus for multi-modality imaging evaluation of cardiovascular complications of radiotherapy in adults: A report from the european association of cardiovascular imaging and the american society of echocardiography. Eur Heart J Cardiovasc Imaging. 2013;14:721-740
12. Lancellotti P, Nkomo VT, **Badano LP**, Bergler J, Bogaert J, Davin L, Cosyns B, Coucke P, Dulgheru R, Edvardsen T, Gaemperli O, Galderisi M, Griffin B, Heidenreich PA, Nieman K, Plana JC, Port SC, Scherrer-Crosbie M, Schwartz RG, Sebag IA, Voigt JU, Wann S, Yang PC. Expert consensus for multi-modality imaging evaluation of cardiovascular complications of radiotherapy in adults: A report from the european association of cardiovascular imaging and the american society of echocardiography. J Am Soc Echocardiogr. 2013;26:1013-1032
13. Lancellotti P, Magne J, Sicari R, Kitsiou A, Frank H, Miller O, **Badano LP**. Euroecho and other imaging modalities: Highlights. Eur Heart J Cardiovasc Imaging. 2013;14:195-200
14. Lancellotti P, **Badano LP**, Lang RM, Akhaladze N, Athanassopoulos GD, Barone D, Baroni M, Cardim N, Gomez de Diego JJ, Derumeaux G, Dulgheru R, Edvardsen T, Galderisi M, Goncalves A, Habib G, Hagendorff A, Hristova K, Kou S, Lopez T, Magne J, de la Morena G, Popescu BA, Penicka M, Rasit T, Rodrigo Carbonero JD, Salustri A, Van de Veire N, von Bardeleben RS, Vinereanu D, Voigt JU, Voilliot D, Zamorano JL, Donal E, Maurer G. Normal reference ranges for echocardiography: Rationale, study design, and methodology (norre study). Eur Heart J Cardiovasc Imaging. 2013;14:303-308
15. Kocabay G, Peluso D, Muraru D, Iliceto S, **Badano LP**. Diastolic mitral regurgitation in 2:1 atrioventricular block: Insight of the diastolic pressure. Echocardiography. 2013;30:E51-52
16. Gargani L, Pignone A, Agoston G, Moreo A, Capati E, **Badano LP**, Doveri M, Bazzichi L, Costantino MF, Pavellini A, Pieri F, Musca F, Muraru D, Epis O, Bruschi E, De Chiara B, Perfetto F, Mori F, Parodi O, Sicari R, Bombardieri S, Varga A, Cerinic MM, Bossone E, Picano E. Clinical and echocardiographic correlations of exercise-induced pulmonary hypertension in systemic sclerosis: A multicenter study. Am Heart J. 2013;165:200-207
17. Gargani L, Agoston G, Pignone AM, Moreo A, **Badano LP**, Bazzichi L, Costantino MF, Pieri F, Epis O, Bruschi E, De Chiara B, Mori F, Bombardieri S, Cerinic MM, Bossone E,

Picano E. Response to letter to the editor by rui baptista, m.D., rogerio teixeira, m.D. Am Heart J. 2013;166:e15-16

18. Donal E, **Badano L**, Habib G, Maurer G, Lancellotti P. Research and innovations committee a new outlook for the european association of cardiovascular imaging (eacvi). Eur Heart J Cardiovasc Imaging. 2013;14:400
19. Dini FL, Galderisi M, Nistri S, Buralli S, Ballo P, Mele D, **Badano LP**, Faggiano P, de Gregorio C, Rosa GM, Ciavarella M, De Marco E, Borruso E, Marti G, Mondillo S, Marino PN. Abnormal left ventricular longitudinal function assessed by echocardiographic and tissue doppler imaging is a powerful predictor of diastolic dysfunction in hypertensive patients: The sphere study. Int J Cardiol. 2013;168:3351-3358
20. D'Andrea A, Mele D, Nistri S, Riegler L, Galderisi M, Agricola E, Losi MA, Ballo P, Mondillo S, **Badano LP**. The prognostic impact of dynamic ventricular dyssynchrony in patients with idiopathic dilated cardiomyopathy and narrow qrs. Eur Heart J Cardiovasc Imaging. 2013;14:183-189
21. Brignole M, Auricchio A, Baron-Esquivias G, Bordachar P, Boriani G, Breithardt OA, Cleland J, Deharo JC, Delgado V, Elliott PM, Gorenek B, Israel CW, Leclercq C, Linde C, Mont L, Padeletti L, Sutton R, Vardas PE, Zamorano JL, Achenbach S, Baumgartner H, Bax JJ, Bueno H, Dean V, Deaton C, Erol C, Fagard R, Ferrari R, Hasdai D, Hoes AW, Kirchhof P, Knuuti J, Kolh P, Lancellotti P, Linhart A, Nihoyannopoulos P, Piepoli MF, Ponikowski P, Sirnes PA, Tamargo JL, Tendera M, Torbicki A, Wijns W, Windecker S, Kirchhof P, Blomstrom-Lundqvist C, **Badano L**P, Aliyev F, Bansch D, Baumgartner H, Bsata W, Buser P, Charron P, Daubert JC, Dobreanu D, Faerestrand S, Hasdai D, Hoes AW, Le Heuzey JY, Mavrakis H, McDonagh T, Merino JL, Nawar MM, Nielsen JC, Pieske B, Poposka L, Ruschitzka F, Tendera M, Van Gelder IC, Wilson CM. 2013 esc guidelines on cardiac pacing and cardiac resynchronization therapy: The task force on cardiac pacing and resynchronization therapy of the european society of cardiology (esc). Developed in collaboration with the european heart rhythm association (ehra). Eur Heart J. 2013;34:2281-2329
22. Bello VD, Carrubba SL, Antonini-Canterin F, Salvo GD, Caso P, Canna GL, Erlicher A, **Badano L**, Romano MF, Zito C, Vriz O, Conte L, Carerj S. Role of electrocardiography and echocardiography in prevention and predicting outcome of subjects at increased risk of heart failure. European journal of preventive cardiology. 2013

23. **Badano LP**, Nour A, Muraru D. Left atrium as a dynamic three-dimensional entity: Implications for echocardiographic assessment. Rev Esp Cardiol (Engl Ed). 2013;66:1-4
24. **Badano LP**, Nour A, Muraru D. Left atrium as a dynamic three-dimensional entity: Implications for echocardiographic assessment. Rev Esp Cardiol. 2013;66:1-4
25. **Badano LP**, Muraru D, Enriquez-Sarano M. Assessment of functional tricuspid regurgitation. Eur Heart J. 2013;34:1875-1885
26. **Badano LP**, Muraru D. The unbearable futility of deriving the left atrial size from a single-linear dimension. Eur Heart J Cardiovasc Imaging. 2013;14:711-713
27. **Badano LP**, Cucchini U, Muraru D, Al Nono O, Sarais C, Iliceto S. Use of three-dimensional speckle tracking to assess left ventricular myocardial mechanics: Inter-vendor consistency and reproducibility of strain measurements. Eur Heart J Cardiovasc Imaging. 2013;14:285-293
28. **Badano LP**. Defining normative values for 3d lv volumes: The devil is in the details. JACC Cardiovasc Imaging. 2013;6:530
29. Vahanian A, Alfieri O, Andreotti F, Antunes MJ, Baron-Esquivias G, Baumgartner H, Borger MA, Carrel TP, De Bonis M, Evangelista A, Falk V, Iung B, Lancellotti P, Pierard L, Price S, Schafers HJ, Schuler G, Stepinska J, Swedberg K, Takkenberg J, Von Oppell UO, Windecker S, Zamorano JL, Zembala M, Bax JJ, Baumgartner H, Ceconi C, Dean V, Deaton C, Fagard R, Funck-Brentano C, Hasdai D, Hoes A, Kirchhof P, Knuuti J, Kolh P, McDonagh T, Moulin C, Popescu BA, Reiner Z, Sechtem U, Sirnes PA, Tendera M, Torbicki A, Vahanian A, Windecker S, Popescu BA, Von Segesser L, **Badano LP**, Bunc M, Claeys MJ, Drinkovic N, Filippatos G, Habib G, Kappetein AP, Kassab R, Lip GY, Moat N, Nickenig G, Otto CM, Pepper J, Piazza N, Pieper PG, Rosenhek R, Shuka N, Schwammenthal E, Schwitter J, Mas PT, Trindade PT, Walther T. Guidelines on the management of valvular heart disease (version 2012): The joint task force on the management of valvular heart disease of the european society of cardiology (esc) and the european association for cardio-thoracic surgery (eacts). Eur Heart J. 2012;33:2451-2496
30. Vahanian A, Alfieri O, Andreotti F, Antunes MJ, Baron-Esquivias G, Baumgartner H, Borger MA, Carrel TP, De Bonis M, Evangelista A, Falk V, Iung B, Lancellotti P, Pierard L, Price S, Schafers HJ, Schuler G, Stepinska J, Swedberg K, Takkenberg J, Von Oppell UO, Windecker S, Zamorano JL, Zembala M, Bax JJ, Baumgartner H, Ceconi C, Dean V, Deaton C, Fagard R, Funck-Brentano C, Hasdai D, Hoes A, Kirchhof P, Knuuti J, Kolh P,

McDonagh T, Moulin C, Popescu BA, Reiner Z, Sechtem U, Sirnes PA, Tendera M, Torbicki A, Vahanian A, Windecker S, Popescu BA, Von Segesser L, **Badano LP**, Bunc M, Claeys MJ, Drinkovic N, Filippatos G, Habib G, Kappetein AP, Kassab R, Lip GY, Moat N, Nickenig G, Otto CM, Pepper J, Piazza N, Pieper PG, Rosenhek R, Shuka N, Schwammenthal E, Schwitter J, Mas PT, Trindade PT, Walther T. Guidelines on the management of valvular heart disease (version 2012): The joint task force on the management of valvular heart disease of the european society of cardiology (esc) and the european association for cardio-thoracic surgery (eacts). Eur J Cardiothorac Surg. 2012;42:S1-S44

31. Steg PG, James SK, Atar D, **Badano LP**, Lundqvist CB, Borger MA, Di Mario C, Dickstein K, Ducrocq G, Fernandez-Aviles F, Gershlick AH, Giannuzzi P, Halvorsen S, Huber K, Juni P, Kastrati A, Knuuti J, Lenzen MJ, Mahaffey KW, Valgimigli M, Van't Hof A, Widimsky P, Zahger D, Bax JJ, Baumgartner H, Ceconi C, Dean V, Deaton C, Fagard R, Funck-Brentano C, Hasdai D, Hoes A, Kirchhof P, Knuuti J, Kolh P, McDonagh T, Moulin C, Popescu BA, Reiner Z, Sechtem U, Sirnes PA, Tendera M, Torbicki A, Vahanian A, Windecker S, Hasdai D, Astin F, Astrom-Olsson K, Budaj A, Clemmensen P, Collet JP, Fox KA, Fuat A, Gustiene O, Hamm CW, Kala P, Lancellotti P, Maggioni AP, Merkely B, Neumann FJ, Piepoli MF, Van de Werf F, Verheugt F, Wallentin L. Esc guidelines for the management of acute myocardial infarction in patients presenting with st-segment elevation: The task force on the management of st-segment elevation acute myocardial infarction of the european society of cardiology (esc). Eur Heart J. 2012;33:2569-2619
32. Popescu BA, Andrade MJ, **Badano LP**, Fox KF, Flachskampf PL, Varga A, Sicari R, Evangelista A, Nihoyannopoulos10 P. Recomandările asociaţiei europene de ecocardiografie pentru pregătirea, competenţa şi îmbunătăţirea calităţii în domeniul ecocardiografiei. Romanian Journal of Cardiology| Vol. 2012;22
33. Muraru D, Tuveri MF, Marra MP, **Badano LP**, Iliceto S. Carcinoid tricuspid valve disease: Incremental value of three-dimensional echocardiography. Eur Heart J Cardiovasc Imaging. 2012;13:329
34. Muraru D, **Badano LP,** Vannan M, Iliceto S. Assessment of aortic valve complex by three-dimensional echocardiography: A framework for its effective application in clinical practice. Eur Heart J Cardiovasc Imaging. 2012;13:541-555
35. Muraru D, **Badano LP**, Ermacora D, Piccoli G, Iliceto S. Sources of variation and bias in assessing left ventricular volumes and dyssynchrony using three-dimensional echocardiography. Int J Cardiovasc Imaging. 2012;28:1357-1368

36. Miani D, Nucifora G, Piccoli G, Proclemer A, **Badano LP**. Incremental value of three-dimensional strain imaging in danon disease. Eur Heart J Cardiovasc Imaging. 2012;13:804
37. Lang RM, **Badano LP**, Tsang W, Adams DH, Agricola E, Buck T, Faletra FF, Franke A, Hung J, de Isla LP, Kamp O, Kasprzak JD, Lancellotti P, Marwick TH, McCulloch ML, Monaghan MJ, Nihoyannopoulos P, Pandian NG, Pellikka PA, Pepi M, Roberson DA, Shernan SK, Shirali GS, Sugeng L, Ten Cate FJ, Vannan MA, Zamorano JL, Zoghbi WA. Eae/ase recommendations for image acquisition and display using three-dimensional echocardiography. J Am Soc Echocardiogr. 2012;25:3-46
38. Lang RM, **Badano LP**, Tsang W, Adams DH, Agricola E, Buck T, Faletra FF, Franke A, Hung J, de Isla LP, Kamp O, Kasprzak JD, Lancellotti P, Marwick TH, McCulloch ML, Monaghan MJ, Nihoyannopoulos P, Pandian NG, Pellikka PA, Pepi M, Roberson DA, Shernan SK, Shirali GS, Sugeng L, Ten Cate FJ, Vannan MA, Zamorano JL, Zoghbi WA. Eae/ase recommendations for image acquisition and display using three-dimensional echocardiography. Eur Heart J Cardiovasc Imaging. 2012;13:1-46
39. Lancellotti P, Pierard LA, Voigt JU, Miller O, Nieman K, Rademakers FE, **Badano LP**. Euroecho and other imaging modalities: Highlights. Eur Heart J Cardiovasc Imaging. 2012;13:127-131
40. Kocabay G, Muraru D, Peluso D, Iliceto S, **Badano LP**. Three-dimensional transesophageal echocardiography of aortic atherosclerosis. Echocardiography. 2012
41. Gargani L, Muraru D, **Badano LP**, Lancellotti P, Sicari R. European association of echocardiography: Research grant programme. Eur Heart J Cardiovasc Imaging. 2012;13:47-50
42. D'Andrea A, Mele D, Nistri S, Riegler L, Galderisi M, Agricola E, Losi MA, Ballo P, Mondillo S, **Badano LP**. The prognostic impact of dynamic ventricular dyssynchrony in patients with idiopathic dilated cardiomyopathy and narrow QRS. Eur Heart J Cardiovasc Imaging. 2012.
44. **Badano LP**, Nour A, Muraru D. Left atrium as a dynamic three-dimensional entity: Implications for echocardiographic assessment. Rev Esp Cardiol. 2012;66:1-4
48. **Badano LP**, Muraru D. Towards an integrated echocardiographic assessment of valvular mechanics by three-dimensional volumetric imaging. J Am Soc Echocardiogr. 2012;25:532-534

50. **Badano LP**, Boccalini F, Muraru D, Bianco LD, Peluso D, Bellu R, Zoppellaro G, Iliceto S. Current clinical applications of transthoracic three-dimensional echocardiography. J Cardiovasc Ultrasound. 2012;20:1-22
51. Agewall S, DeGroot E, Marcos-Alberca P, Zamorano JL, Barrero AA, **Badano LP**, Perrone-Filardi P. Ultrasound and radiology surrogate endpoints in pharmacological studies. Atherosclerosis. 2012;224:12-24
52. Zamorano JL, **Badano LP**, Bruce C, Chan KL, Goncalves A, Hahn RT, Keane MG, La Canna G, Monaghan MJ, Nihoyannopoulos P, Silvestry FE, Vanoverschelde JL, Gillam LD, Vahanian A, Di Bello V, Buck T. Eae/ase recommendations for the use of echocardiography in new transcatheter interventions for valvular heart disease. Eur J Echocardiogr. 2011;12:557-584
53. Zamorano JL, **Badano LP**, Bruce C, Chan KL, Goncalves A, Hahn RT, Keane MG, La Canna G, Monaghan MJ, Nihoyannopoulos P, Silvestry FE, Vanoverschelde JL, Gillam LD. Eae/ase recommendations for the use of echocardiography in new transcatheter interventions for valvular heart disease. J Am Soc Echocardiogr. 2011;24:937-965
54. Zamorano JL, **Badano LP**, Bruce C, Chan KL, Goncalves A, Hahn RT, Keane MG, La Canna G, Monaghan MJ, Nihoyannopoulos P, Silvestry FE, Vanoverschelde JL, Gillam LD. Eae/ase recommendations for the use of echocardiography in new transcatheter interventions for valvular heart disease. Eur Heart J. 2011;32:2189-2214
55. Sicari R, Galderisi M, Voigt JU, Habib G, Zamorano JL, Lancellotti P, **Badano LP**. The use of pocket-size imaging devices: A position statement of the european association of echocardiography. Eur J Echocardiogr. 2011;12:85-87
58. Onut R, **Badano LP**, Muraru D, Toso F. A large penetrating atherosclerotic ulcer of the ascending aorta. Eur J Echocardiogr. 2011;12:479
59. Muraru D, **Badano LP**, Sarais C, Solda E, Iliceto S. Evaluation of tricuspid valve morphology and function by transthoracic three-dimensional echocardiography. Curr Cardiol Rep. 2011;13:242-249
61. Mor-Avi V, Lang RM, **Badano LP**, Belohlavek M, Cardim NM, Derumeaux G, Galderisi M, Marwick T, Nagueh SF, Sengupta PP, Sicari R, Smiseth OA, Smulevitz B, Takeuchi M, Thomas JD, Vannan M, Voigt JU, Zamorano JL. Current and evolving echocardiographic techniques for the quantitative evaluation of cardiac mechanics: Ase/eae consensus statement on methodology and indications endorsed by the japanese society of echocardiography. J Am Soc Echocardiogr. 2011;24:277-313

62. Mor-Avi V, Lang RM, **Badano LP**, Belohlavek M, Cardim NM, Derumeaux G, Galderisi M, Marwick T, Nagueh SF, Sengupta PP, Sicari R, Smiseth OA, Smulevitz B, Takeuchi M, Thomas JD, Vannan M, Voigt JU, Zamorano JL. Current and evolving echocardiographic techniques for the quantitative evaluation of cardiac mechanics: Ase/eae consensus statement on methodology and indications endorsed by the japanese society of echocardiography. Eur J Echocardiogr. 2011;12:167-205
63. Mondillo S, Galderisi M, Mele D, Cameli M, Lomoriello VS, Zaca V, Ballo P, D'Andrea A, Muraru D, Losi M, Agricola E, D'Errico A, Buralli S, Sciomer S, Nistri S, **Badano L.** Speckle-tracking echocardiography: A new technique for assessing myocardial function. J Ultrasound Med. 2011;30:71-83
64. Miani D, **Badano LP**, De Biaggio P, Albanese MC, Ghidina M, Proclemer A, Fioretti P. Heart failure with preserved ejection fraction: A precursor of heart failure with reduced ejection fraction or a distinct syndrome? Int J Cardiol. 2011;149:139-140
65. Hackam DG, Shojania KG, Spence JD, Alter DA, Beanlands RS, Dresser GK, Goela A, Davies AH, **Badano LP**, Poldermans D, Boersma E, Njike VY. Influence of noninvasive cardiovascular imaging in primary prevention: Systematic review and meta-analysis of randomized trials. Archives of internal medicine. 2011;171:977-982
67. Galderisi M, Nistri S, Mondillo S, Losi MA, Innelli P, Mele D, Muraru D, D'Andrea A, Ballo P, Sgalambro A, Esposito R, Marti G, Santoro A, Agricola E, **Badano LP**, Marchioli R, Filardi PP, Mercuro G, Marino PN. Methodological approach for the assessment of ultrasound reproducibility of cardiac structure and function: A proposal of the study group of echocardiography of the italian society of cardiology (ultra cardia sic) part i. Cardiovasc Ultrasound. 2011;9:26
68. Galderisi M, Henein MY, D'Hooge J, Sicari R, **Badano LP**, Zamorano JL, Roelandt JR. Recommendations of the european association of echocardiography: How to use echo-doppler in clinical trials: Different modalities for different purposes. Eur J Echocardiogr. 2011;12:339-353
69. Gaibazzi N, Reverberi C, **Badano L**. Usefulness of contrast stress-echocardiography or exercise-electrocardiography to predict long-term acute coronary syndromes in patients presenting with chest pain without electrocardiographic abnormalities or 12-hour troponin elevation. Am J Cardiol. 2011;107:161-167
70. Di Salvo G, Di Bello V, Salustri A, Antonini-Canterin F, La Carrubba S, Materazzo C, **Badano L**, Caso P, Pezzano A, Calabro R, Carerj S. Early left ventricular longitudinal systolic dysfunction and cardiovascular risk factors in 1,371 asymptomatic subjects

with normal ejection fraction: A tissue doppler study. Echocardiography. 2011;28:268-275

71. Di Salvo G, Di Bello V, Salustri A, Antonini-Canterin F, La Carrubba S, Materazzo C, **Badano L**, Caso P, Pezzano A, Calabro R, Carerj S. The prognostic value of early left ventricular longitudinal systolic dysfunction in asymptomatic subjects with cardiovascular risk factors. Clin Cardiol. 2011;34:500-506
72. D'Onofrio A, Mazzucco A, Valfre C, Zussa C, Martinelli L, Casabona R, Mazzola A, Gherli T, **Badano LP**, Fabbri A. Left ventricular remodeling, hemodynamics and early clinical outcomes after aortic valve replacement with the pericarbon freedom stentless bioprosthesis: Results from the italian prospective multicenter trial. J Heart Valve Dis. 2011;20:531-539

Publications in press (n= 9)

1. Lang RM, **Badano LP**, Afilalo J, Kouznetsova T, Ernande L,, Flachskampf FA, Foster E, Goldstein SA, Lancellotti P, Mor-Avi V, Muraru D, Picard, MH, Rietzschel E, Rudski L, Spencer KT, Tsang, W, Voigt JU. Recommendations for Cardiac Chamber Quantification by Echocardiography. An Update from the American Society of Echocardiography and the European Association of Cardiovascular Imaging. J Am Soc Echocardiogr 2014: 27
2. Lang RM, **Badano LP**, Afilalo J, Kouznetsova T, Ernande L,, Flachskampf FA, Foster E, Goldstein SA, Lancellotti P, Mor-Avi V, Muraru D, Picard, MH, Rietzschel E, Rudski L, Spencer KT, Tsang, W, Voigt JU. Recommendations for Cardiac Chamber Quantification by Echocardiography: An Update from the American Society of Echocardiography and the European Association of Cardiovascular Imaging. Eur Heart J Cardiovasc Imag 2014:
3. Plana JC, Galderisi M, Anderson M, **Badano LP**, Bonnie K, Cardinale D, Carver J, Edvardsen T, Decara J, Lancellotti P, Marwick T, Rastogi P, Scherrer- Crosbie M, Sicari R. Expert consensus abiut the echocardiographic evaluation and management of patients during and after cancer therapy. Eur Heart J Cardiovasc Imag 2014: 27
4. Plana JC, Galderisi M, Anderson M, **Badano LP**, Bonnie K, Cardinale D, Carver J, Edvardsen T, Decara J, Lancellotti P, Marwick T, Rastogi P, Scherrer- Crosbie M, Sicari R. Expert consensus abiut the echocardiographic evaluation and management of patients during and after cancer therapy. J Am Soc Echocardiogr 2014:

5. **Badano LP**. The clinical benefits of adding a third dimension to assess the left ventricle with echocardiography. Scientifica 2014:
6. Ristić AS, Imazio M, Adler Y, Anastasakis A, **Badano LP**, BrucatoA , Caforio ALP, Dubourg O, Elliott P, Gimeno J, Helio T, Klingel K, Linhart A, Maisch B, Mayosi B, Mogensen J, Pinto Y, Seggewiss H, Seferović P, Tavazzi L, Tomkowski W, Charron P Triage strategy for urgent management of cardiac tamponade: a position statement of the European Society of Cardiology Working Group on Myocardial and Pericardial Diseases. Eur Heart J 2014; 35:
7. Kou S, Caballero L, Voilliot D, Dulgheru R, de Sousas C, Akhaladze N, Athanassopoulos GD, Barone D, Baroni M, Cardim N, Gomez De Diego JJ, Hagendorff A, Christine H, Hristova K, Lopez T, Magne J, de la Morena G, Popescu BA, Penicka M, Rasit T, Rodrigo Carbonero JD, Salustri A, Van DE Veire N; Von Bardelen RS, Vinereanu D, Voigt JU, Zamorano JL, Donal E, Lang RM, **Badano LP**, Lancellotti P. Echocardiographic Reference Ranges for Normal Cardiac Chamber Size: Results from the NORRE Study. Eur Heart J Cardiovasc Imaging 2014;
8. Ermacora D, Muraru D, Pontarollo S, Casablanca S, Livi U, Iliceto S, **Badano LP**. Role of three-dimensional echocardiography in structural complications after acute myocardial infarction. Echocardiography 2014
9. Kocabay G, Muraru D, Peluso D, Cucchini U, Mihaila S, Padayattil-Jose S, Gentian D, Iliceto S, Vinereanu D, **Badano LP**. Normal Left Ventricular Mechanics by Two-Dimensional Speckle-Tracking echocardiography. Reference Values in Healthy Adults. Rev Esp Cardiol 2014;

Abstracts at international congresses (n= 51)

1. Muraru D, Calore C, Melacini P, Cucchini U, Mihaila S, Peluso D, Ucci L, Miglioranza MH, Iliceto S, **Badano LP**. Mitral Valve Abnormalities Correlate With Left Ventricular Remodelling and Obstruction in Hypertrophic Cardiomyopathy: a Quantitative 3D Transthoracic Echocardiographic Study. *ACC 2014* (submitted)
2. Muraru D, Cucchini U, Padayattil-Jose S, Mihaila S, Miglioranza MH, Cecchetto A, Casablanca S, Iliceto S, **Badano LP**. Left Ventricular Myocardial Strain by Three-Dimensional Speckle-Tracking Echocardiography in Healthy Volunteers: a Normative Study. *ACC 2014* (submitted)

3. Miglioranza MH, Muraru D, Mihaila S, Peluso D, Cucchini U, Casablanca S, Iliceto S, **Badano LP**. Reference Values of Tricuspid Annulus Size and Dynamics by Two-Dimensional Transthoracic Echocardiography in 220 Healthy Volunteers. *ACC 2014* (submitted)
4. Muraru D, Addetia K, Veronesi F, Corsi C, Mor-Avi V, Yamat M, Weinert L, Lang RM, **Badano LP**. Dynamic Analysis of the Normal Tricuspid Annulus Using 3D Echocardiography. *Eur Heart J Cardiovasc Imaging* 2013 (in press)
5. Muraru D, Addetia K, Veronesi F, Corsi C, Mor-Avi V, Yamat M, Weinert L, Lang RM, **Badano LP**. Physiological determinants of tricuspid annulus size during the cardiac cycle: implications for tricuspid annulus sizing by three-dimensional echocardiography. *Eur Heart J Cardiovasc Imaging* 2013 (in press)
6. Muraru D, Calore C, **Badano LP**, Melacini P, Mihaila S, Naso P, Casablanca S, Ortile A, Padayattil Jose' S, Iliceto S. Mitral valve abnormalities correlate with left ventricular remodelling and obstruction in hypertrophic cardiomyopathy: a quantitative 3D transthoracic echocardiographic study. *Eur Heart J Cardiovasc Imaging* 2013 (in press)
7. Muraru D, Piasentini E, Mihaila S, Padayattil-Jose' S, Peluso D, Ucci L, Naso P, Puma L, Casablanca S, Iliceto S, **Badano LP**. Reference ranges for left ventricular geometry and function by 3D echocardiography using a vendor-independent software for quantitative analysis. *Eur Heart J Cardiovasc Imaging* 2013 (in press)
8. Muraru D, Calore C, **Badano LP**, Melacini P, Mihaila S, Peluso D, Puma L, Kocabay G, Rizzon G, Iliceto S. Left ventricular outflow tract planimetry by 3D echocardiography predicts obstruction and heart failure symptoms in hypertrophic cardiomyopathy. *Eur Heart J Cardiovasc Imaging* 2013 (in press)
9. Calore C, Muraru D, **Badano LP**, Melacini P, Mihaila S, Denas G, Naso P, Casablanca S, Santi F, Iliceto S. Relationship of 3D left ventricular mass with systolic and diastolic function indices in hypertrophic cardiomyopathy. *Eur Heart J Cardiovasc Imaging* 2013 (in press)
10. Muraru D, Mihaila S, Piasentini E, Casablanca S, Naso P, Puma L, Ermacora D, Zoppellaro G, Iliceto S, **Badano LP**. Do a vendor-specific and a vendor-independent software for 3D echocardiographic analysis provide similar values for left ventricular volumes and ejection fraction? *Eur Heart J Cardiovasc Imaging* 2013 (in press)
11. Muraru D, Piasentini E, Mihaila S, Naso P, Casablanca S, Peluso D, Denas G, Ucci L, Iliceto S, **Badano LP**. Reference values for 3D echo parameters describing left

ventricular mechanics obtained by vendor-independent software. *Eur Heart J Cardiovasc Imaging* 2013 (in press)

12. Calore C, Muraru D, Melacini P, **Badano LP**, Mihaila S, Puma L, Peluso D, Casablanca S, Ortile A, Iliceto S. Left atrial longitudinal strain correlates better than its emptying fraction with left ventricular impairment in hypertrophic cardiomyopathy. *Eur Heart J Cardiovasc Imaging* 2013 (in press)
13. Veronesi F, Muraru D, Addetia K, Corsi C, Lamberti C, Lang RM, Mor-Avi V, **Badano LP.** A novel software tool to semiautomatically characterize tricuspid valve function and shape using transthoracic echocardiography. *Eur Heart J Cardiovasc Imaging* 2013 (in press)
14. Miglioranza MH, Muraru D, Peluso D, Cucchini U, Mihaila S, Naso P, Puma L, Kocabay G, **Badano LP**. Two-dimensional assessment of tricuspid annulus dynamics and diameters: study for new reference values. *Eur Heart J Cardiovasc Imaging* 2013 (in press)
15. Peluso D, Muraru D, Cucchini U, Mihaila S, Casablanca S, Pigatto E, Cozzi F, Punzi L, **Badano LP**, Iliceto S. Right heart function by 3D-echocardiography and 2D-speckle tracking in scleroderma patients in absence of pulmonary hypertension. *Eur Heart J Cardiovasc Imaging* 2013 (in press)
16. Mihaila S, Muraru D, Piasentini E, Peluso D, Casablanca S, Naso P, Puma L, Iliceto S, Vinereanu D, **Badano LP**. Validation of a new, semiautomated software for quantitative assessment of the mitral annulus by three-dimensional echocardiography. *Eur Heart J Cardiovasc Imaging* 2013 (in press)
17. Mihaila S, Muraru D, Piasentini E, Peluso D, Casablanca S, Naso P, Puma L, Iliceto S, Vinereanu D, **Badano LP**. Static and dynamic analysis of the mitral valve annulus in normal subjects: a three-dimensional transthoracic echocardiography study. *Eur Heart J Cardiovasc Imaging* 2013 (in press)
18. Mihaila S, Piasentini E, Muraru D, Peluso D, Casablanca S, Naso P, Puma L, Iliceto S, Vinereanu D, **Badano LP**. Dynamic changes of mitral annular geometry during the cardiac cycle - a three-dimensional echo study in healthy volunteers. *Eur Heart J Cardiovasc Imaging* 2013 (in press)
19. Addetia K, Muraru D, Veronesi F, Corsi C, Mor-Avi V, Yamat M, Weinert L, **Badano LP**, RM. Lang. Dynamic Analysis of the Normal Tricuspid Annulus Using 3D Echocardiography. *Circulation* 2013; abstr suppl (P5214)

20. Thomas L, Poppe KK, Simova I, McMurray JJV, Nagueh S, Hobbs R, **Badano LP**, Doughty RN, Schirmer H, Kim HK, Whalley GA, on behalf of the Echo NoRMAL collaboration. Left atrial volume and function indices: trends with age and gender. Circulation 2013; … (abstract Suppl)
21. Mantovani F, Clavel MA, Suri RM, Mankad S, Maalouf JF, Michelena HI, **Badano LP**, Enriquez-Sarano M. Cleft-like indentation in mixomatous valve disease: 3D quantitative analysis of leaflet tissue and annular dimensions, Circulation 2013; … (abstract Suppl)
22. **Badano L**, Maffessanti F, Muraru D, Gripari P, Esposito R, Galderisi M, Tamborini G, Santoro C, Ermacora D, Pepi M. Reference values for right ventricular geometry and function by 3D echocardiography: a multicenter study of 533 healthy subjects. *J Am Coll Cardiol* 2013; 61 (10-S) doi:10.1016/S0735-1097(13)60893-1
23. **Badano L**, Peluso D, Muraru D, Dal Bianco L, Kovacs A, Iliceto S. Right atrial volumes and phasic functions by 3D echocardiography in healthy subjects. *J Am Coll Cardiol* 2013; 61 (10-S) doi:10.1016/S0735-1097(13)61101-8.
24. **Badano L**, Muraru D, Zoppellaro G, Cucchini U, Ermacora D, De Lazzari M, Peluso D, Marra MP, Iliceto S. Predictive value of 2D and 3D deformation parameters and wall motion score to identify transmural myocardial necrosis in STEMI patients: a comparative study against CMR. *J Am Coll Cardiol.*2013;61(10_S):. doi:10.1016/S0735-1097(13)61013-X.
25. Muraru D, Calore C, **Badano LP**, Melacini P, Mihaila S, Casablanca S, Cucchini U, Miglioranza MH, Polo A, Iliceto S. Radial function correlates with heart failure symptoms in hypertrophic cardiomyopathy with normal ejection fraction. *Eur Heart J* 2013; 34 (suppl 1):doi:10.1093/eurheartj/eht307.P622
26. Maffessanti F, Muraru D, Esposito R, Tamborini G, Gripari P, Ermacora D, Santoro C, Galderisi M, **Badano LP**, Pepi M. Allometric normative equations for 3D right ventricular size and function: development and validation with equations derived using cardiac magnetic resonance. *Eur Heart J* 2013; 34 (Abstract Supplement), 685-686
27. **Badano LP**, Muraru D, Mihaila S, Miglioranza MH, Padayattil-Jose S, Ucci L, Dal Bianco L, Peluso D, Cucchini U, Iliceto S. Quantitative analysis of mitral valve geometry by transthoracic three-dimensional echocardiography: accuracy, feasibility, reproducibility and reference values. Eur Heart J (2013) 34 (suppl 1):doi:10.1093/eurheartj/eht311.5863

28. Ermacora D, **Badano LP**, Muraru D, Gentian D, Dal Bianco L, Casablanca S, Peluso D, Zoppellaro G, Cucchini U, Iliceto S. Reference values of right ventricular longitudinal strain by speckle tracking echocardiography in 219 healthy volunteers. *Eur Heart J* 2013; 34 (suppl 1):doi:10.1093/eurheartj/eht309.P3848
29. Kovacs A, Peluso D, Muraru D, **Badano L**, Casablanca S, Dal Bianco L, Zoppellaro G, Iliceto S. Shift in relative contribution of radial and longitudinal mechanics to right ventricular ejection fraction between normal subjects and patients with pulmonary hypertension. *Eur Heart J* 2013; 34 (suppl 1): doi:10.1093/eurheartj/eht307.P231
30. Peluso D, Muraru D, Cucchini U, Dal Bianco L, Pigatto E, Zanatta E, Punzi L, Cozzi F, **Badano LP**, Iliceto S. Right ventricular function by 3D-echocardiography and 2D-speckle tracking in scleroderma patients in absence of pulmonary hypertension. *Eur Heart J* 2013; 34 (suppl 1):doi:10.1093/eurheartj/eht308.P1181
31. Mihaila S, Muraru D, Casablanca S, Peluso D, Cucchini U, Dal Bianco L, Vinereanu D, Iliceto S, **Badano LP**. Three-dimensional changes in mitral valve annulus geometry in organic and functional mitral regurgitation: insights for mitral valve repair. *Eur Heart J* 2013; 34 (suppl 1): doi:10.1093/eurheartj/eht310.P4751
32. Kovács A, Peluso D, Muraru D, Marra MP, **Badano LP**, Dal Bianco L, Zoppellaro G, Iliceto S. Right ventricular transverse displacement by speckle-tracking echocardiography: reference values in healthy subjects and clinical relevance in pulmonary hypertension. 5th World Symposium on Pulmonary Hypertension 2013 (in press)
33. Kovács A, Peluso D, Muraru D, Marra MP, **Badano LP**, Dal Bianco L, Zoppellaro G, Iliceto S. Characterization of a novel parameter of right ventricular function by speckle tracking echocardiography in healthy subjects. 5th World Symposium on Pulmonary Hypertension 2013
34. Kovács A, Peluso D, Muraru D, Marra MP, **Badano LP**, Dal Bianco L, Zoppellaro G, Iliceto S. Paradoxical septal motion index strongly correlates with invasive hemodynamic parameters. 5th World Symposium on Pulmonary Hypertension 2013
35. Peluso D, Kovács A, Muraru D, Marra MP, **Badano LP**, Dal Bianco L, Zoppellaro G, Iliceto S. Impairment of right atrial function in pulmonary hypertension patients. 5th World Symposium on Pulmonary Hypertension 2013
36. Muraru D, Napodano M, **Badano L**, Tarantini G, Sarais C, Kocabay G, Isabella G, D'Onofrio A, Gerosa G, Iliceto S. Novel three-dimensional transoesophageal echocardiography platform allows a fast and accurate assessment of aortic annulus

size and shape before transcatheter aortic valve implantation. *Eur Heart J Cardiovasc Imaging* 2012; 13(suppl 1):i38-i39

37. Muraru D, Cattarina M, Dal Bianco L, Peluso D, Zoppellaro G, Segafredo B, Calore C, Cucchini U, Iliceto S, **Badano LP**. Quantitative analysis of mitral valve geometry by transthoracic three-dimensional echocardiography: reference values, feasibility and reproducibility. *Eur Heart J Cardiovasc Imaging* 2012; 13(suppl 1)
38. Muraru D, Gripari P, Esposito R, Tamborini G, Galderisi M, Ermacora D, Maffessanti F, Santoro C, Pepi M, **Badano L**. Reference values for right ventricular geometry and function by three-dimensional echocardiography. A multicenter study of a large cohort of healthy subjects. *Eur Heart J Cardiovasc Imaging* 2012; 13(suppl 1)
39. Ippolito R, Gripari P, Muraru D, Esposito R, Kocabay G, Tamborini G, Galderisi M, Maffessanti F, **Badano L**, Pepi M. Age is an independent predictor of right ventricular geometry and function in males only. *Eur Heart J Cardiovasc Imaging* 2012; 13(suppl 1)
40. Kocabay GK, Dal Bianco L, Muraru D, Peluso D, Segafredo B, Iliceto S, **Badano L**. Reference values for aortic diameters obtained using both inner-edge-to-inner-edge and leading-edge-to-leading-edge methods in 190 healthy subjects. *Eur Heart J Cardiovasc Imaging* 2012; 13(suppl 1)
41. Muraru D, **Badano LP**, Ermacora D, Bellu R, De Lazzari M, Marra MP, Dal Bianco L, Peluso D, Boccalini F, Iliceto S. Two-dimensional longitudinal strain is more accurate than three-dimensional longitudinal strain to identify infarcted LV segments in STEMI patients. *Eur Heart J* 2012; 33 (Abstract Supplement), 672-673
42. Muraru D, **Badano LP**, Bellu R, Ermacora D, De Lazzari M, Marra MP, Dal Bianco L, Peluso D, Cucchini U, Iliceto S. Predictive value of 2D/3D deformation parameters and 3D wall motion score to identify transmural myocardial necrosis in STEMI patients: a comparative study against cardiac magnetic resonance. *Eur Heart J* 2012; 33 (Abstract Supplement), 159
43. Muraru D, **Badano LP**, Ermacora D, Bellu R, De Lazzari M, Marra MP, Dal Bianco L, Peluso D, Cucchini U, Iliceto S. Two-dimensional vs three-dimensional deformation parameters to estimate infarct size and global left ventricular function after STEMI: which parameter is better? *Eur Heart J* 2012; 33 (Abstract Supplement), 167-168
44. Muraru D, **Badano LP**, Ermacora D, Bellu R, De Lazzari M, Marra MP, Dal Bianco L, Peluso D, Boccalini F, Iliceto S. Two-dimensional longitudinal strain is more accurate than three-dimensional longitudinal strain to identify infarcted LV segments in STEMI patients. *Eur Heart J* 2012; 33 (Abstract Supplement), 672-673

45. Muraru D, **Badano LP**, Bellu R, Ermacora D, De Lazzari M, Marra MP, Dal Bianco L, Peluso D, Cucchini U, Iliceto S. Predictive value of 2D/3D deformation parameters and 3D wall motion score to identify transmural myocardial necrosis in STEMI patients: a comparative study against cardiac magnetic resonance. *Eur Heart J* 2012; 33 (Abstract Supplement), 159
46. Muraru D, **Badano LP**, Ermacora D, Bellu R, De Lazzari M, Marra MP, Dal Bianco L, Peluso D, Cucchini U, Iliceto S. Two-dimensional vs three-dimensional deformation parameters to estimate infarct size and global left ventricular function after STEMI: which parameter is better? *Eur Heart J* 2012; 33 (Abstract Supplement), 167-168
47. Muraru D, Napodano M, **Badano L**, Tarantini G, Sarais C, Kocabay G, Isabella G, D'Onofrio A, Gerosa G, Iliceto S. Novel three-dimensional transoesophageal echocardiography platform allows a fast and accurate assessment of aortic annulus size and shape before transcatheter aortic valve implantation. *Eur Heart J Cardiovasc Imaging* 2012
48. Muraru D, Cattarina M, Dal Bianco L, Peluso D, Zoppellaro G, Segafredo B, Calore C, Cucchini U, Iliceto S, **Badano LP**. Quantitative analysis of mitral valve geometry by transthoracic three-dimensional echocardiography: reference values, feasibility and reproducibility. *Eur Heart J Cardiovasc Imaging* 2012
49. Muraru D, Gripari P, Esposito R, Tamborini G, Galderisi M, Ermacora D, Maffessanti F, Santoro C, Pepi M, **Badano L**. Reference values for right ventricular geometry and function by three-dimensional echocardiography. A multicenter study of a large cohort of healthy subjects. *Eur Heart J Cardiovasc Imaging* 2012
50. Ippolito R, Gripari P, Muraru D, Esposito R, Kocabay G, Tamborini G, Galderisi M, Maffessanti F, **Badano L**, Pepi M. Age is an independent predictor of right ventricular geometry and function in males only. *Eur Heart J Cardiovasc Imaging* 2012
51. Kocabay GK, Dal Bianco L, Muraru D, Peluso D, Segafredo B, Iliceto S, **Badano L**. Reference values for aortic diameters obtained using both inner-edge-to-inner-edge and leading-edge-to-leading-edge methods in 190 healthy subjects. *Eur Heart J Cardiovasc Imaging 2012*

Abstracts at national congresses (n= 9)

1. Cattarina M, Muraru D, Dal Bianco L, Peluso D, Kocabay G, Boccalini F, Sarais C, Iliceto S, **Badano LP**. Accuratezza e riproducibilità dell'ecocardiografia transtoracica tridimensionale per l'analisi quantitativa della valvola mitrale: confronto con

l'approccio ecocardiografico transesofageo 3D. 73° CONGRESSO NAZIONALE della Società Italiana di Cardiologia Roma, 15 – 17 dicembre 2012

2. Cattarina M, Muraru D, Dal Bianco L, Peluso D, Zoppellaro G, Segafredo B, Calore C, Cucchini U, Iliceto S, **Badano LP**. Analisi quantitativa della geometria della valvola mitrale tramite ecocardiografia transtoracica tridimensionale: valori di riferimento, fattibilità e riproducibilità. 73° CONGRESSO NAZIONALE della Società Italiana di Cardiologia Roma, 15 – 17 dicembre 2012
3. Dal Bianco L, Muraru D, **Badano LP**, Ermacora D, Bellu R, De Lazzari M, Marra MP, Peluso D, Cucchini U, Kocabay G, Nour A, Iliceto S. Confronto tra i parametri di deformazione 2D e 3D nel stimare l'estensione dell'infarto miocardico e la funzione globale del ventricolo sinistro dopo STEMI: quale parametro è migliore? 73° CONGRESSO NAZIONALE della Società Italiana di Cardiologia Roma, 15 – 17 dicembre 2012
4. Dal Bianco L, Muraru D, **Badano LP**, Bellu R, Ermacora D, De Lazzari M, Marra MP, Peluso D, Cucchini U, Kocabay G, Nour A, Iliceto S. Valore predittivo dei parametri 2D/3D di deformazione miocardica e dell'indice di motilità 3D nell'identificare l'estensione della necrosi transmurale in pazienti con STEMI: confronto con la RMC. 73° CONGRESSO NAZIONALE della Società Italiana di Cardiologia Roma, 15 – 17 dicembre 2012
5. Dal Bianco L, Muraru D, Kocabay G, Zoppellaro G, Peluso D, Nour A, Segafredo B, **Badano LP**, Iliceto S. Valori di riferimento per i diametri aortici ottenuti sia con metodo inner-edge-to-inner-edge (interno-interno) che con metodo leading edge-to-leading edge (esterno-interno) in 190 soggetti sani. 73° CONGRESSO NAZIONALE della Società Italiana di Cardiologia Roma, 15 – 17 dicembre 2012
6. Ermacora D, Gripari P, Esposito R, Tamborini G, Galderisi M, Muraru D, Maffesanti F, Santoro C, Pepi M, **Badano LP**. Valori di riferimento della geometria e funzione del ventricolo destro ottenuti con ecocardiografia tridimensionale. Uno studio multicentrico su un'ampia coorte di soggetti sani. 73° CONGRESSO NAZIONALE della Società Italiana di Cardiologia Roma, 15 – 17 dicembre 2012
7. Peluso D, Muraru D, **Badano LP**, Ermacora D, Bellu R, De Lazzari M, Marra MP, Dal Bianco L, Nour A, Sarais C, Cucchini U, Kocabay G, Iliceto S. Superiore accuratezza dello strain longitudinale 2D rispetto a quello 3D nell'identificare i segmenti coinvolti dalla necrosi nei pazienti con STEMI. 73° CONGRESSO NAZIONALE della Società Italiana di Cardiologia Roma, 15 – 17 dicembre 2012

8. Peluso D, Muraru D, **Badano LP**, Bellu R, Ermacora D, De Lazzari M, Marra MP, Dal Bianco L, Zoppellaro G, Kocabay G, Sarais C, Cucchini U, Nour A, Iliceto S. Lo strain longitudinale 2D e lo strain circonferenziale 3D risultano predittori accurati di necrosi transmurale alla risonanza magnetica dopo uno STEMI. 73° CONGRESSO NAZIONALE della Società Italiana di Cardiologia Roma, 15 – 17 dicembre 2012
9. Zoppellaro G, Ippolito R, Gripari P, Muraru D, Esposito R, Nour A, Tamborini G, Galderisi M, Maffesanti F, **Badano LP**, Pepi M. L'età è un predittore indipendente della funzione e geometria del ventricolo destro solo nel genere maschile. 73° CONGRESSO NAZIONALE della Società Italiana di Cardiologia Roma, 15 – 17 dicembre 2012

ACKNOWLEDGEMENTS

A mio padre e a mia madre,
e per Valentina.

Se un figlio di contadini arriva a ottenere il titolo di dottore di ricerca in un'Università di prestigio, come quella di Padova, alla mia età, è anche perché, durante tutta la carriera, ha incontrato molte persone che gli hanno insegnato, l'hanno incoraggiato, aiutato e soprattutto gli hanno offerto delle opportunità.

Il mio primo ringraziamento va ai miei genitori, per tutti i sacrifici fatti per darmi l'opportunità di una vita diversa dalla loro e da quella dei loro padri, e per avermi insegnato che puoi sognare e che, se ci credi e lavori sodo, spesso i sogni si avverano. Se fosse ancora vivo, mio padre sarebbe molto fiero di questo momento. A mia sorella Margherita che segue ogni passo della mia carriera con entusiasmo e incredibile ammirazione, trasformando ogni piccolo successo professionale in un evento nella cerchia familiare.

Tra i colleghi, il mio primo pensiero va al prof Emilio Gatto che accolse nella cardiologia del San Martino di Genova un giovane studente al III anno di Medicina, rifiutato dalla Cattedra di Cardiologia dell'Università, e gli insegnò i fondamenti della cardiologia clinica "iniziando con i prelievi di sangue alle 6 del mattino" fino al cateterismo cardiaco. Il dott Aldo Petillo, aiuto della stessa cardiologia, che mi ha insegnato l'amore per lo studio e il valore aggiunto di stabilire rapporti umani con i propri pazienti. I dott.ri Sandro Mazzantini e Paolo Rubartelli che mi hanno insegnato i rudimenti del cateterismo cardiaco e dell'angiografia e la curiosità per la ricerca scientifica.

Un grazie particolare al dott. Paolo Spirito, ospedale Galliera di Genova, che mi ha insegnato che la scrittura scientifica e la presentazione dei propri dati ai congressi scientifici non si improvvisano, ma richiedono un approccio professionale.

La mia gratitudine e il mio affetto vanno anche alla sig.ra Wendy Marshall che, insegnandomi con grande pazienza l'uso scritto e parlato della lingua Inglese, mi ha aperto le porte del mondo e posto le basi per la mia futura carriera nelle società scientifiche internazionali.

Probabilmente, non mi sarei mai mosso da Genova e avrei mai scritto questa tesi se il dott. Domenico Zanuttini di Pordenone non mi avesse prima accettato come ricercatore del GISSI Eco e poi chiamato come assistente nel suo reparto. Lui è stato una guida e un padre durante un periodo molto difficile della mia carriera. Il dott. Zanuttini mi ha insegnato il valore dell'onestà intellettuale, della capacità di ammettere i propri errori, come unica premessa per poter migliorare, e il rispetto dei colleghi e dei pazienti come codice etico quotidiano.

Una significativa svolta nella mia carriera è stata l'incontro con il dott. Paolo Fioretti. Un amico e un maestro. Da lui ho imparato che la comunità scientifica si estende ben oltre i confini del nostro Paese e che la vera competizione scientifica è quella che ha come platea il mondo. Paolo Fioretti ed Ugolino Livi hanno creduto in me al di là del ragionevole, mi hanno spinto e sostenuto con entusiasmo in tutti i progetti. Grazie a loro abbiamo creato il laboratorio di ecocardiografia di Udine: primo laboratorio interamente digitale in Europa e primo laboratorio accreditato dalla European Association of Echocardiography.

Il prof Fausto Pinto dell'Università di Lisbona e il prof Alan Fraser dell'Università di Cardiff (i primi due Presidenti della European Association of Echocardiography) mi hanno accolto nella Association, e mi hanno dato l'opportunità di farmi valere e dimostrare le mie capacità. Mi hanno inoltre difeso contro i veti delle gerarchie delle società scientifiche italiane aprendomi la porta, non solo alla Presidenza della Association, ma ad un esperienza professionale che mi ha portato a conoscere e stringere amicizia con i più grandi professionisti dell'imaging cardiovascolare nel mondo, e ad entrare in contatto con le istituzioni accademiche più famose. Il valore umano e professionale dei miei anni nella European Association of Echocardiography e nella European Society of Cardiology sono incommensurabili.

A quel punto della mia carriera, cosa potevo sognare di più? Di entrare a far parte dello staff di un'Università prestigiosa? Anche questo sogno si è avverato grazie ai proff.ri Sabino Iliceto e Gaetano Thiene.

Il prof Iliceto era uno dei miei modelli giovanili. Quando, appena laureato, frequentavo i Workshop di ecocardiografia a Bari, e vedevo questo giovane, brillante scienziato italiano, che parlava un inglese fluente, pubblicava sulle riviste più prestigiose e che si dava del tu con Jos Roelandt, Joe Kisslo, Nat Pandian e Harvey Feigenbaum (nomi che io leggevo solo sui libri!), mi dicevo, ecco è lì che devi arrivare. Vent'anni dopo, il prof. Iliceto mi ha offerto l'opportunità di venire all'Università di Padova e di rifondare l'ecocardiografia della Clinica Cardiologica. La sua amicizia, il suo supporto incondizionato e il suo continuo incoraggiamento, nonché la sua spinta continua ad andare avanti e ad innovare, sono stati la forza che ci ha permesso di creare in pochi anni uno dei laboratori di riferimento mondiale per l'ecocardiografia e le strutture per gestire gli studi che sono parte di questa tesi.

Se è dubbio che questa tesi sarebbe mai stata scritta senza l'incontro con il dott. Zanuttini, sicuramente non l'avrei mai scritta senza l'incontro con il prof Gaetano Thiene. Il prof Thiene mi ha insegnato l'orgoglio e gli oneri di far parte di un'Università prestigiosa con una grande tradizione accademica, l'amore per la Scienza (con la S maiuscola) ed il rigore metodologico, e i doveri verso gli studenti. La sua amicizia e i suoi apprezzamenti per il nostro lavoro sono stati un incredibile

stimolo per me e la dott.ssa Muraru a migliorare continuamente. Un ringraziamento particolare a Denisa che ha lasciato il suo Paese per condividere un progetto professionale e di ricerca in ecocardiografia. Senza il suo entusiasmo, la sua dedizione, la sua passione e intelligenza propositiva non sarei mai riuscito a realizzare il laboratorio di eco-ricerca a Padova ed a renderlo così produttivo dal punto di vista scientifico e divulgativo.

Senza saperlo, quando il prof Thiene mi offrì l'opportunità di entrare nella scuola di dottorato dell'Università di Padova, egli coronava il sogno di un giovane contadino e metteva il sigillo sul lavoro dei molti che ho ricordato in queste righe e dei moltissimi altri che mi hanno aiutato ed insegnato in tutti questi anni e che, per motivi di spazio, non ho potuto citare, ma a cui va il mio sentito ringraziamento.